An Offshore Wind Farm Featuring Differential Power Processing

by

Marten Pape

A thesis
presented to the University of Waterloo
in fulfillment of the
thesis requirement for the degree of
Doctor of Philosophy
in
Electrical and Computer Engineering

Waterloo, Ontario, Canada, 2021

Examining Committee Membership

The following served on the Examining Committee for this thesis. The decision of the Examining Committee is by majority vote.

External Examiner: Vijay Sood
Associate Professor, Dept. of Elec., Comp. and Software Eng., Ontario Tech University

Supervisor: Mehrdad Kazerani
Professor, Dept. of Elec. and Comp. Eng., University of Waterloo

Internal Member: Kankar Bhattacharya
Professor, Dept. of Elec. and Comp. Eng., University of Waterloo

Internal Member: Ramadan El Shatshat
Lecturer, Dept. of Elec. and Comp. Eng., University of Waterloo

Internal-External Member: Amir Khajepour
Professor, Dept. of Mech. and Mechatronics Eng., University of Waterloo

Author's Declaration

I hereby declare that I am the sole author of this thesis. This is a true copy of the thesis, including any required final revisions, as accepted by my examiners.

I understand that my thesis may be made electronically available to the public.

Abstract

Offshore wind farms are a rapidly growing technology used to harvest wind energy on the open seas where wind speeds are significantly higher and steadier than onshore. Current wind farms located far away from shore (e.g., 50 km or more) require a large amount of equipment to be deployed in order to transport generated energy to shore most cost-effectively. In these cases, energy is transmitted to shore using High-Voltage DC (HVDC) transmission connected to wind turbines with AC voltage output. During the past decade, research has studied alternate arrangements to reduce the amount of equipment deployed offshore and increase conversion efficiency. The redesign of offshore collection systems between wind turbines from AC to DC voltages is seen as a key tool to achieve the research objectives.

The presented research is focused on the design of offshore wind farms with DC collection system and series-connected wind turbines based on partial power processing converters (PPPCs). This wind farm configuration significantly improves conversion efficiency compared to AC wind farms with HVDC link, since PPPCs are only required to process output power differences among wind turbines in a wind farm to achieve maximum power point (MPP) operation, and other wind farm components are operated at variable operating points, improving low-load efficiency. Furthermore, PPPCs can be of reduced size to realize MPP operation. To find the best variable operating points, a loss minimizing HVDC link current scheduling scheme has been derived and a comprehensive sizing framework was developed to inform the best choice of PPPC ratings. The presented work addresses major design considerations at wind farm, wind turbine, and PPPC levels. An efficiency, size and economic evaluation has been conducted for a 450 MW wind farm located 100km from shore, confirming significant annual loss reductions and economic advantages compared to a conventional AC wind farm with HVDC link, as well as two other series-connected DC wind farm configurations. A generic converter sizing framework for single-string series-connected DC wind farms has been developed and applied to the 450 MW wind farm. Challenges in wind turbine startup with this configuration have been identified and schemes were developed to enable successful wind turbine startup without the need of significant adidtional hardware.

Acknowledgements

Dedication

"We did not inherit this world from our parents …
We are borrowing it from our children."

It is my fervent hope that the engineers, scientists, politicians, policy makers and ordinary people of today will dedicate themselves to the creation of a world where children and grandchildren will be left with air they can breathe and water they can drink, where humans and the rest of nature will nurture one another.

Based on Robert A. Messenger and Jerry Ventre – Photovoltaic Systems Engineering, Third Edition, CRC Press, 2010

To Heather, who has such an incredible sense for this air we breathe, the water we drink and our neighbours on earth; no matter how tiny or large.

To Leona, may you grow up in a world that supports your talents, lifts your spirit, offers you challenge and fulfillment, and leads you to a meaningful and joyful life.

To Laura, may your world be one in which humans and the rest of nature will nurture one another. May it lead you to a fulfulling and joyful journey on this planet we share.

Table of Contents

xi

List of Figures

List of Tables

List of Abbreviations

CSI/CSC	Current-Source Inverter / Current-Source Converter
DAB	Dual-active Bridge Converter
DD	Direct-Drive (wind turbine without gear box)
DFIG	Doubly-fed induction generator
DPP	Differential Power Processing
HVAC	High-Voltage Alternating Current
HVDC	High-Voltage Direct Current
LCC	Line-commutated Converter (Thyristor converter)
LCOE	Levelized cost of energy
MPP(T)	Maximum Power Point (Tracking)
PMSG	Permanent Magnet Synchronous Generator
PPPC	Partial Power Processing Converter
PWM	Pulse-width Modulation
SAB	Single-active Bridge Converter
TSR	Tip Speed Ratio $\left(TSR = \frac{Tip\ speed\ of\ turbine\ blade}{Wind\ speed} \right)$
VSI/VSC	Voltage-Source Inverter / Voltage-Source Converter
WECS	Wind Energy Conversion System (particularly: gearbox, generator, and all electric energy conversion equipment)
WRSG	Wound-Rotor Synchronous Generator
WTG	Wind turbine generator

Chapter 1

Introduction

1.1 Research Motivation

Over the last decade, electricity obtained from wind power has become one of the most affordable and available forms of renewable electricity generation in many countries around the world. The power rating of a single wind turbine allows harnessing wind power at a wide range of sites. Sites near population centres allow local deployment of wind turbines, reducing the need for long-distance transmission of obtained electrical energy. However, in many cases the amount of wind power available to potential wind project developments is higher on sites that are far away from load centers. Probably, one of the most extreme scenarios is the conversion of wind power offshore, with a distance to shore of several tens or even hundreds of kilometer from the point of connection on land. The advantages of offshore wind energy conversion compared to onshore are mainly higher average wind speeds, higher capacity factors, lower intrinsic turbulences, and lower wind shear [1]. Despite these advantages, the levelized cost of energy (LCOE) still tends to be higher than for onshore projects, due to difficult construction and general working conditions, as well as the need for additional, special equipment. The potential for offshore wind energy has been found to be significant and well distributed around the globe[1]. In order to transmit generated energy to the onshore

---

[1] The installed offshore wind power capacity in European waters has reached 25 GW in 2020 [2]. [3] has shown that the offshore wind energy potential is large with the most potential annual energy available to Russia, Canada, United States of America, United Kingdom, and China.

electricity grid, transmission systems based on AC or DC voltage are being used. As a result, current commercial wind farms rely on up to seven full-scale electric conversion stages from wind turbine to onshore grid connection. This can result in a significant amount of energy loss and large amounts of equipment deployed in a harsh environment. Through better integration of wind farm components, the number of conversion stages can be reduced.

The second motivation for this research originates from recent developments in a class of power electronic converters, called "Partial Power Processing Converters" (PPPCs), using the concept of "Differential Power Processing" (DPP). The application of such converters in each wind turbine of a wind farm promises to further reduce the amount of full-scale electric energy conversion equipment required to be deployed, as well as reduce energy conversion losses. Unique to other approaches, tighter integration would be achieved based on the correlation of instantaneous wind speed differences seen by neighbouring wind turbines.

Such schemes have been examined for applications in Photovoltaic Generators before, but not for Wind Power and its own intrinsic properties. Therefore, the objective of this work is to contribute to a better understanding of an optimal wind farm system configuration based on Partial Power Processing Converters and help to better quantify potential benefits compared to other market-ready and research-stage concepts.

1.2 Literature Survey

First, this literature review introduces and discusses different wind farm collection and transmission system configurations as proposed in literature. Then, comparative studies of these different proposed methods are presented.

1.2.1 Commercial Offshore Wind Farms with HVDC link

Most commercially-available, large-scale wind turbines for offshore application output AC power at 690V or at low medium-voltage level, before a transformer steps up the voltage to collection system level [4]. Output power from individual wind turbines is then collected locally in a local AC collection system operating at voltage levels of typically 33kV to 66kV [5]. For offshore wind farms with a large distance to shore, using High-Voltage DC (HVDC) transmission is more economical than using High-Voltage AC (HVAC) transmission (see Figure 1.1). This has been discussed extensively and quantified in [5], [6].

Using such a scheme maintains high levels of compatibility among products of different manufacturers, as well as subsystem compatibility among different product portfolios, such as onshore, offshore without HVDC link, and offshore with HVDC link. Furthermore, due to the lack of tight integration of wind farm and HVDC link it is comparably simple to use a single HVDC link for multiple wind farms, and to use a Multi-Terminal HVDC link. Some wind farm concepts discussed later do not exhibit this degree of flexibility.
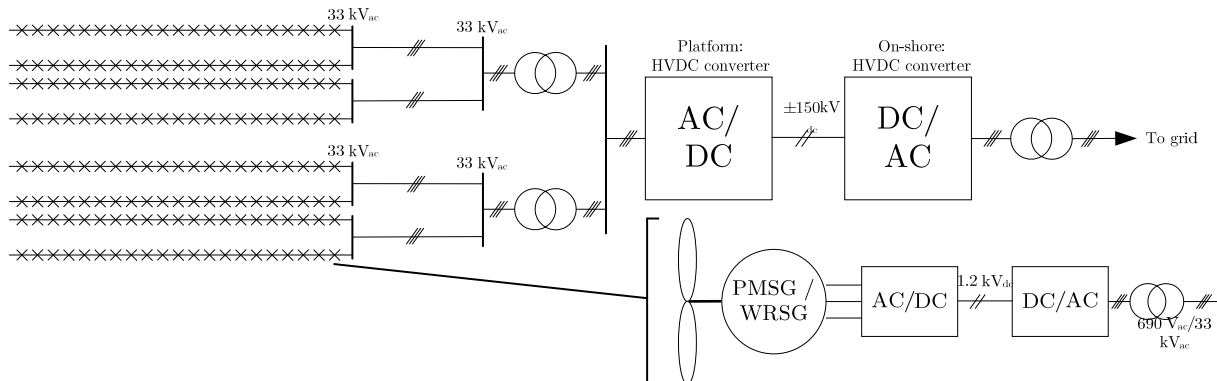
Figure 1.1 AC collection system layout with HVDC transmission [6]

As seen in the system layout in Figure 1.1, the number of electric energy conversion stages (including converters and transformers) is very high (up to 7 full-scale stages). This results in potentially unnecessary energy conversion losses, and additional weight and volume that need to be deployed and supported by offshore structures. Plenty of other research has been inspired by this limitation and is discussed next.

1.2.2 Offshore Wind Farms with parallel DC collection system

Since energy conversion systems of wind turbines with a full-scale power electronic converter configuration all include a rectification of generator voltages and currents, all such wind turbines already have a DC bus. Instead of converting this DC power back to AC power within the wind turbine, several research projects have focused on implementing a DC collection system from the already existing internal DC busses.

One approach is to connect the DC output of such a wind turbine in parallel with those of other wind turbines in a wind farm. Further step-up DC/DC converters have to be used at various stages in such a collection system in order to obtain the high voltage required for HVDC transmission. Since high step-up gains in a single DC/DC converter are difficult and costly to realize in terms of sizing and efficiency, multiple DC/DC converter stages are typically considered. This has been discussed in [7]. Basic

configurations are shown in Figure 1.2 and Figure 1.3. A third configuration is discussed in [7] which is identical to that in Figure 1.3, except that only one step-up converter is used that can provide the step-up from wind generator rectifier voltage to HVDC voltage (also referred to as "cluster step-up"). Note that voltage values in Figure 1.2 and Figure 1.3 are given for illustration purposes, only, and can vary with different wind farm designs.
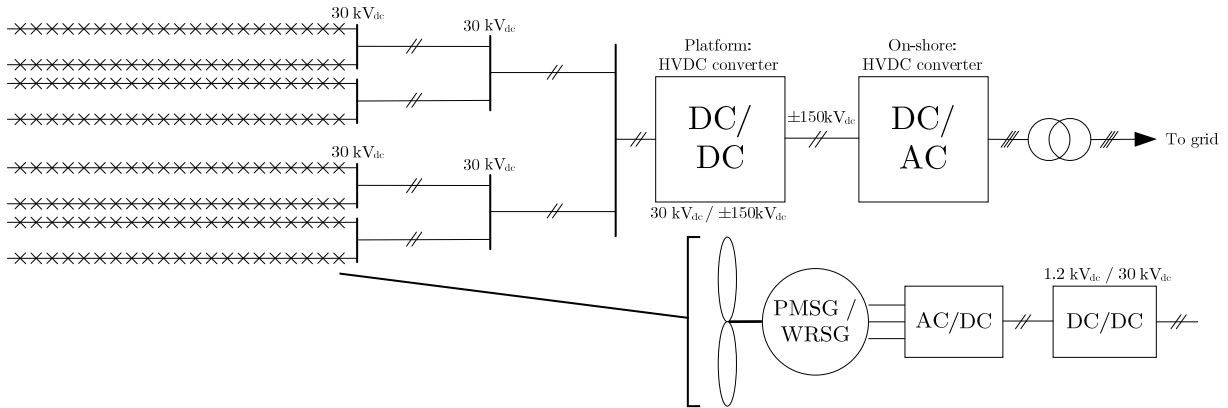
Figure 1.2 Parallel DC collection system with a DC/DC converter located in each wind turbine ("Turbine step-up") [7]
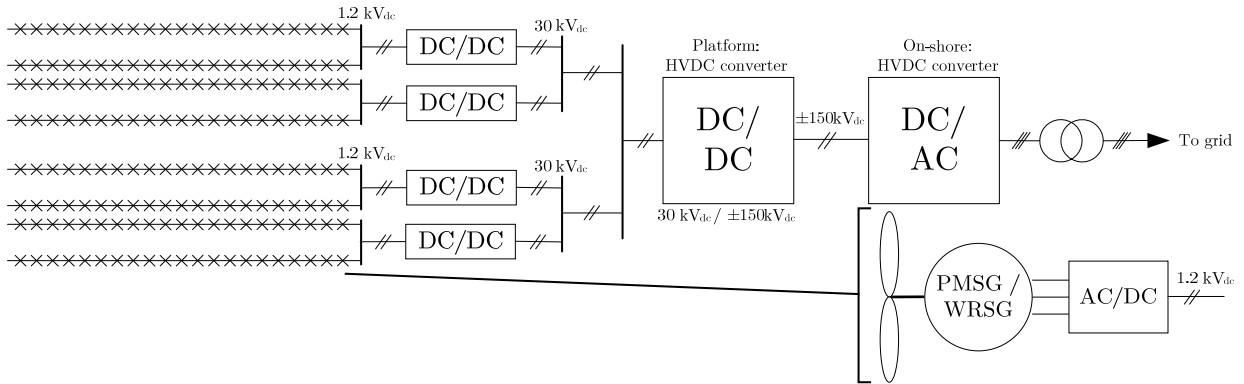
Figure 1.3 Parallel DC collection system with all DC/DC converters in collection system ("Two step-up") [7]

In [8] a parallel DC wind farm is described in which each wind turbine uses a three-level neutral-point clamped inverter for controlled rectification to DC voltage. A common DC bus is proposed as collection system. In order to step up the voltage to HVDC level, a combination of switch-mode DC/AC conversion, low-frequency step-up transformer and switch-mode AC/DC rectification is used. These converters have to be rated at the

full wind farm power rating (300MW). Compared to an AC wind farm with HVDC link, the authors claim that the number of DC/AC converters is reduced.

The authors in [9] examine a parallel DC wind farm. The assumed wind energy conversion system (WECS) consists of a 3MW, 4kV direct-drive generator, rectifier, and step-up DC/DC converter. Each wind turbine has a nominal DC output voltage of 40kV. One central DC/DC converter then provides a voltage step-up to 300kV for the entire wind farm. Thus, the proposed work relies on a two-step voltage boost. In particular, this work focuses on the integration of a novel resonant DC/DC converter as the first DC/DC converter stage using thyristors. This study demonstrates that diode-bridge rectifiers used with wind generators are significantly more efficient than voltage-source converters (VSC), especially at low-load conditions. *The proposed DC/DC converter reaches a maximum efficiency of approximately 95% with partial load efficiencies well below this level[2]. The system design evaluates the use of a diode-bridge rectifier compared to a VSC demonstrating superior efficiency for a diode rectifier; however, the chosen control strategy results in loss of these advantages: variable diode rectifier output voltage is compensated for with the local WECS DC/DC converter. Such a variable voltage operation of this converter causes additional losses which effectively render any diode rectifier efficiency gains void.* The main reason for this is a change in system sizing (a design for higher maximum step-up gains in the local DC/DC converter are required, compared to VSC rectification with constant DC voltage). Finally, the study finds that the proposed system has slightly higher losses (6.5% vs. 6% of the total energy produced). The main advantage is given as a reduction by a factor of thirteen in weight for required inductors and transformers in the wind farm.

In [10], the use of a parallel DC collection system in "small" (60MW) and "large" (160MW) wind farms is analyzed in terms of energy production cost with alternate AC and DC configurations for varying distance to shore. The study concludes that series DC collection systems are more favourable in terms of expected energy production cost, and thus devotes more analysis to series DC wind farms. Parallel DC wind farms are found to have a lower energy production cost than AC collection systems starting at distances from shore of about 90km. The parallel DC wind farm is constructed from

---

[2] For comparison: line-frequency AC step-up transformer efficiencies are assumed to peak at above 99% in this work. This is in line with the current NEMA Premium Efficiency Transformers Program (see https://www.nema.org/Policy/Energy/Efficiency/Documents/NEMA_Premium_Efficiency_Transformer_Product_Specifications.pdf).

wind turbines with a nominal output voltage of 5kV. Two step-up DC/DC converters are assumed, where a first stage performs the step-up for a subgroup of wind turbines (e.g., four) and the final step-up is performed with a single, central DC/DC converter. *The results of this study are a very useful indication of the economic feasibility of parallel DC wind farms. The assumed system sizing using 2MW wind turbines and a generator with rated voltage of 5kV ([11]) appears to be less common compared to commercially available wind generators at those power levels as indicated by* [4].

The authors of [7] discuss control issues of different parallel DC wind farms. However, in order to select a preferred collection system configuration, efficiency modeling is performed for a 500MW wind farm employing 5MW wind turbines and three-leg single-active-bridge (SAB) DC/DC converters. The considered parallel DC configurations are "turbine step-up", "two step-up", and "cluster-step-up" as outlined in the beginning of this section. The authors conclude that a cluster step-up configuration is the most preferable in terms of power losses for the chosen configuration. *A cluster step-up would require a DC/DC converter with a very large voltage transformation ratio ($\gg 10$).* According to the study, the next best configuration in terms of losses would be one in which each wind turbine comes with one DC/DC converter to step up to an intermediate voltage level, such as 30kV. This would help reducing power losses in the distribution network.

In [12] and [13], it is proposed to develop a parallel DC wind farm based on high-voltage, direct-drive *hybrid* generators. In this work, a hybrid generator consists of a synchronous generator that has both a permanent magnet-based excitation, and a wound-rotor-based excitation. This approach seeks to balance the efficiency advantage of PMSGs with controllability that a variable electrical excitation of a WRSG can provide. In this approach, each wind turbine would consist of a nine-phase hybrid synchronous generator without gearbox, and a diode-bridge rectifier. DC-voltage control and maximum power point tracking (MPPT) would be provided by the variable excitation of the WRSG part. The nominal output voltage of each wind turbine generator is assumed to be 38.1kV per phase. To each wind turbine rectifier, a DC/DC converter is connected to step up the voltage to 132kV for HVDC transmission. Due to the partial rating of the WRSG part, only a certain margin of wind speed differences can be tolerated in the wind farm while maintaining MPPT operation. In [13] a partial rating of 25% has been suggested based on wind speed measurements in a farm presented in [14]. The authors claim a reduction in size, as well as an increase in wind farm efficiency from 91.15% to 94.58% at full load for the $2 \times 183.6MW$ Walney wind farm

(U.K.). *However, since a constant HVDC voltage of 132kV is assumed, the DC/DC converter has to be able to provide a very large step-up ratio in order to support low-wind speed scenarios that result from a low rectified generator voltage. Typically, this will result in large transformer turns ratios of high-frequency step-up transformers in those DC/DC converters. This in turn may result in a lower DC/DC conversion efficiency because of large low-voltage side currents in the converter, as well as converter oversizing.*

1.2.3   Offshore Wind Farms with series DC collection system

Alternatively to parallel DC collection systems, it has been proposed to connect the outputs of wind turbines in series (see Figure 1.4). This would allow to obtain an HVDC link without the need of high-voltage, high-gain step-up DC/DC converter which could have a negative effect on system efficiency, cost, weight, and volume. Common challenges that have been stated in the work reviewed here are the requirement to isolate individual turbines against HVDC potential, and system protection, since wind turbines are now connected in a series string. In section 1.2.4 comparative studies are reviewed. In most of these studies a series DC system is seen as advantageous over all other wind farm collection system configurations (AC, AC+HVDC, parallel DC) in terms of system efficiency and/or energy production cost starting at a fairly close distance from shore (e.g., starting at 10km for some farm sizes [10]).
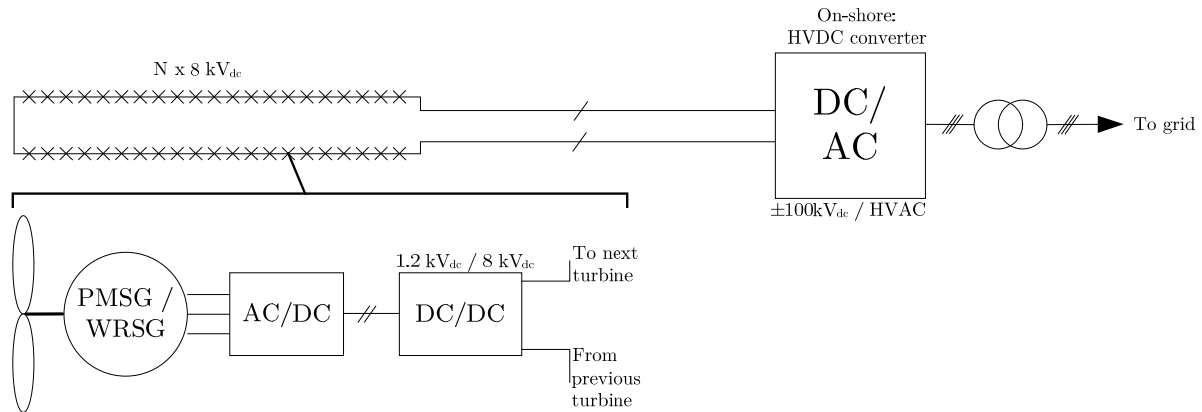
Figure 1.4 Series DC collection system with a single string (example)

Several of the works presented below also contain analysis and designs of controllers for the proposed schemes. Since the scope of this review is primarily focused on the design of a series DC collection system and related hardware components, control system designs are excluded from this literature review, unless necessary for context.

7

The author of [6], [10] describes and analyses a series DC wind farm where each wind turbine consists of an induction generator, gearbox, VSC as rectifier, and a full-bridge DC/DC converter with medium-frequency isolation transformer. It has been suggested to operate the wind farm with a single or with multiple parallel connected strings of series connected wind turbines. The onshore inverter station is selected to be a 2-level voltage-source converter (VSC). This work also contains a comparison of AC, parallel DC, and series DC configurations, as mentioned before. The authors conclude that a series DC configuration yields the lowest energy production cost among all configurations starting at about 10km distance from shore, depending on wind farm size. However, it is also noted that exact cost to realize an appropriate insulation against HVDC potential in the DC/DC converters is unknown. *This work sets a very useful baseline and provides a cost comparison with alternative wind farm configurations.*

The work in [15] discusses the design and optimization of a dual-active bridge and series-resonant converter with medium-frequency isolation transformer in detail. This can be seen as a potential specification to the system proposal made in [6]. The converter is rated at 1MVA, 1.2kV/12kV (input/output voltage level), and a switching frequency of 20kHz. *While this design does not take into consideration that operation at variable output voltages is unavoidable in a series string of wind turbines, each operating at MPP, it is shown that peak efficiencies of 98.6% can likely be achieved in a very compact design while achieving an insulation level sufficiently high to realize a bipolar HVDC link with series DC connected wind turbines (±100kV) involving dual-active bridge converters.*

In the simulation based study of [16], the use of a PMSG with a high gear ratio gearbox, insulation transformer, and 2-level VSC as rectifier is studied as WECS in a series DC wind farm. The system sizing (1.5MW generator with 1.5kV rated voltage) results in relatively low WECS output voltages of 2.8kV. As a result, the authors suggest that a series string should only be constructed up to a medium DC voltage, such as 40kV. Then, a central DC/DC converter is employed to provide the final step up to HVDC voltage for all wind turbines together. A wind farm can consist of a single or multiple parallel connected strings before the central DC/DC converter. Insulation against HVDC potential would be achieved using a low-frequency AC isolation transformer between generator and rectifier. The authors point out that due to the relatively constant generator voltage to frequency ratio at MPPT operation, transformer flux remains fairly constant over the entire operational range. *The presented analysis does not examine effects of output power differences in a string or between strings and resulting sizing considerations that need to be made for the central DC/DC converter.*

Furthermore, the existence of a central DC/DC converter diminishes the advantages of series DC collection systems over other configurations in that no offshore substation is required.

In [17] it is proposed to construct a series DC wind farm out of groups of multiple wind turbines connected to the same rectifier. The example given in this paper connects four wind turbines based on 2MW, 4kV PMSGs in parallel. A PWM current-source converter (CSC) then serves as rectifier for that group of wind turbines. All rectifiers are then connected in series to form the series string with a rated voltage of $\pm 60kV$ for a 200MW wind farm. The onshore converter station consists of a single, high-voltage, high-power PWM CSI converter. The means to provide insulation against HVDC potential in wind farms are suggested to be insulated generator windings, insulation of the nacelle, or the use of a transformer between generator and rectifier. In order to ensure stability within a group of generators, machine damper windings are required.

Another PWM CSC scheme is proposed in [18] suggesting to install a multi-phase PMSG in each wind turbine. For each set of three phases a PWM CSC is used as rectifier. All CSCs of a particular wind turbine are then connected in series. The authors claim that this allows to employ low voltage switches in the CSCs. Faulty CSCs would be bypassed by thyristors connected to the CSCs' DC sides. Insulation against HVDC potential is suggested to be realized using uprated generator winding insulation. The HVDC voltage would be set to several tens of kV. A test system is based on 1MW, 690V PMSGs.

A similar proposal has been made in [19]–[22]. There, PWM CSCs would also be used as rectifier to a medium-voltage, three-phase PMSG (3kV). Onshore conversion would be achieved through a series string of CSCs, as well. The wind turbine generator was chosen to have a low pole-pair count (8) thus requiring a gear box with high gear ratio. Insulation against HVDC potential would be achieved using a low-frequency transformer between generator and rectifier. Several additional aspects, such as DC link current control and fault ride-through capabilities have been studied for this configuration.

In [23], a wind farm configuration was proposed that features diode-bridge rectifiers as wind turbine converters, followed by stacked single-active bridge (SAB) converters in phase-shift operation. The onshore converter station is proposed to consist of a half-bridge modular multilevel converter; however, a simulation study is based on a conventional VSC. The authors consider a 4kV, 1MW PMSG and five SABs rated at 1 kV each. Insulation to ground for series-connected offshore wind turbines is achieved

through the SAB transformers. In [24], the authors study a similar system in which the onshore converter station consists of two CSCs and investigate the control of a bipolar HVDC link, taking into account the ground path in such a configuration. The simulated system considers a wind farm of two 1 MW wind turbines. In [25], the authors highlight the importance of considering appropriate circuit models for transmission lines for series-connected wind farms with current-controlled HVDC link. It is shown that a simple inductive, PI or T representation is insufficient for appropriate filter design, and that a distributed transmission cable model featuring multiple RLC cells should be considered. The control of a PWM CSC as onshore converter station is investigated in [26]. In particular, the authors simulate the PWM CSC controlled by a hierarchical approach that is supposed to reduce harmonic contents and offer a fast dynamic response. The current setpoint is derived from a non-linear programming model seeking to minimize transmission system losses to realize a desired wind farm power and subject to operational constraints, such as rated HVDC current.

Another approach to realize HVDC insulation in a wind turbine is to use a high-frequency transformer connected to an AC/AC frequency changing converter, followed by a rectifier. Such schemes have been proposed and examined in [27]–[30].

[27] proposes to use a three-phase AC to single-phase AC converter, medium-frequency transformer (operating at 10kHz), and AC/DC rectifier. The medium-frequency transformer is capable of withstanding HVDC potential to ground. A new switching pattern is proposed for the operation of the AC/AC converter. The wind turbine generator considered would be a medium-voltage PMSG with a gearbox.

The authors of [28] have focused on evaluating the appropriateness of matrix converters in wind turbine energy conversion systems. The chosen wind turbine topology consists of a 2MW or 10MW PMSG, connected to a frequency changing AC/AC converter, medium-frequency transformer for isolation operating at 5kHz, and a three-phase diode bridge rectifier. The AC/AC converter topologies that are compared are back-to-back VSC, conventional matrix converter (CMC) and indirect matrix converter (IMC). These setups are compared against the traditional parallel AC wind farm case for a 300MW, $150kV$ (V_{HVDC}) wind farm in terms of efficiency and reliability. The wind turbine sizes chosen are 2MW and 10MW, in order to study the state of the industry at that time and potential future wind turbines. The work concludes that a series DC wind farm using a conventional matrix converter can be operated with up to 6-15% less losses than the traditional parallel AC wind farm of equivalent size. It is also pointed out, that the choice of switching frequency for the matrix converter has a significant influence on

the exact loss profile. The system reliability is estimated to be better with the parallel AC wind farm concept. Furthermore this paper points out that larger-scale wind turbines in a series string contribute to a higher (better) Average System Availability Index (ASAI), because the length of required collection system cable is smaller. More detailed converter-focused studies have been continued in [29], [30]. A variant based on reduced matrix converter, high-frequency isolation transformer and full-bridge diode rectifier has been proposed in [31]. Wind turbine converter conversion losses have been estimated to range between 4-9% at rated operation with a 10 kHz switching frequency for a 2MW wind turbine in [32].

The authors of [33]–[35] describe a series DC wind farm based on medium-voltage, direct-drive PMSG[3], diode bridge rectifier and buck converter. HVDC insulation would be achieved using a transformer between generator and diode bridge rectifier, uprated generator insulation, or by using an insulated tower element. The onshore converter is chosen to be a line-commutated 12-pulse thyristor converter. The authors argue that while a diode rectifier has disadvantages in terms of generator current THD and lack of reactive power provision, the drawbacks are made up for by better efficiency[4], reliability, and lower cost. Various system protection cases and measures are discussed in [35]. *While a buck converter offers a compelling simplicity for the wind farm configuration, the choice of a buck converter as DC/DC converter unnecessarily limits freedom in system sizing, since the rated generator voltage has to be chosen relatively high only to be stepped down afterwards. The authors argue that the diode of a buck converter is the deciding factor for choosing this topology, as it can automatically serve as a bypass element, in case of faults. However, in* [35] *further bypass equipment is deemed necessary.*

In [36]–[41] a wind turbine for series DC wind farms is studied, that uses a thyristor converter as rectifier after the generator. Such a rectifier necessitates a synchronous generator which is chosen as PMSG or self-excited synchronous generator. The onshore converter station is also chosen as thyristor converter. A synchronous condenser is suggested at the onshore inverter station to compensate for reactive power consumption of the inverter station. *For the thyristor converters used as wind turbine rectifier, the*

---

[3] 5MW, 145 pole pairs, 2.89kV. This design appears to have been reverse engineered from the Multibrid M5000 design; however, it was omitted to incorporate the single-stage gearbox with a gear ratio of 1:10. Hence, the high number of generator pole pairs. According to [25] the actual pole-pair count is 14.

[4] This has been confirmed and quantified in [9].

thyristors' reactive power draw from the generator and low power quality pose significant challenges.

In [42], a voltage balancing system is proposed to be applied to wind turbine converters. This essentially features delta converters that have been discussed for PV application previously [43]. It appears that the wind turbine rectifier is based on a two-level VSC. Simulation studies for a 690V, 200kW generator are based on a fixed wind turbine VSC DC voltage of 1000V. To maintain such voltage during unequal wind speeds in the series string (with shared HVDC link current), the delta converters are used to facilitate such operating points. This configuration realizes an approach of differential power processing for series-connected offshore wind farms. Due to the nature of delta converters, this concept requires three conductors connnecting each wind turbine, instead of one for most other series-connected concepts.

Other converter topologies that have been studied for application in series-connected offshore wind farms as wind turbine converters are modular multilevel converters [44], VSC and biode-bridge rectifier-based power factor correction [45], voltage-source converter, dual-active bridge converter and storage [46], VSC, tap-changing transformer and diode-bridge rectifier [47], VSC and double full-bridge double-tapped inductor converter [48], and diode-bridge rectifier with synchronous generator excitation control [49].

The discussion of sizing of wind turbine converters in series string applications remains incomplete. For extreme operating conditions, such as a string with turbines operating near cut-in wind speed and near rated wind speed, the output voltages have to be very different, since all turbines see the same current in a string. In order to be able to withstand those, as well as transient conditions that can depend on interactions between local offshore and remote onshore converters, wind turbine converters might require to be oversized in their output voltage rating. Work and a further review on related literature are provided in Chapter 5.

1.2.4 Comparative evaluation of Offshore Wind Farm collection systems

The purpose of this section is to provide some background information on how different wind farm configurations compare based on published work. Typical criteria for comparison would include wind farm efficiency, reliability, energy production cost, market readiness, and unresolved research challenges. As partially confirmed in the

comparison of a small and a large wind farm in [10], wind farm parameters, such as total power rating, wind turbine power rating, distance from shore, wind farm layout, and site-specific wind characteristics can potentially have a significant influence on the comparison of different wind farm layouts.

The work of [6], [10] has already been discussed in previous sections. To summarize the results in here regarding the comparison of AC and DC wind farm configurations, one should have a look at Fig. 12 in [10]. There, the results of a comparison of energy production cost against distance from shore among pure AC, AC with HVDC link, parallel DC, and series DC wind farm configurations for a 160MW, 10m/s wind site are shown. For small wind farms (60MW), the energy production cost is more sensitive to distance from shore than for larger ones. For these small wind farms, a parallel DC configuration is found to be less economic than a pure AC configuration up to a transmission length of about 90km. For the larger wind farms (160MW), the pure AC configuration becomes less economical compared to AC wind farms with HVDC link, parallel DC and series DC configurations starting at 130km, 90km and 0km, respectively. The large DC series configuration is deemed more economic in all cases, except when compared to a small AC wind farm for distance from shore of 0-10km. *This study shows very clearly the structural differences between different wind farm configurations in terms of economic viability for a subset of varied system parameters (distance from shore and size of wind farm). However, it has to be noted that this study has been published in 2006 which was before the large-scale deployment of offshore wind parks in European Seas. It is therefore quite possible that some basic assumptions have shifted since then.*

In [50] a comparison of pure AC and AC wind farms with an HVDC link is made. The study compares wind farms of sizes 100-500MW in terms of economic assessment (investment, O&M, and energy loss costs). Farms with 150kVac, 400kVac, and VSC-based HVDC ($\pm 150kV_{dc}$) transmission systems have been studied. Several system parameters have been studied for their sensitivities with regard to system efficiency. For a 100MW wind farm, it has been found that starting at 90km distance from shore, an HVDC link becomes cost-effective for wind farms with AC collection system. *The methodology presented is very exhaustive and could potentially serve as base for comparative studies involving DC collection system configurations which have not been covered in this work.*

The authors of [11], [51] compare the efficiency of isolated full-bridge, SAB and series parallel resonant (SPR) converters for application in parallel DC wind farms with a two-

converter step-up configuration. The study compares these converters for a generator with 5kV rated output voltage (rectified). The rectifier is either a diode rectifier or a VSC. Different DC voltage control strategies (constant or variable with variable generator voltage as MPP varies) are studied, as well as losses at different wind speeds. The study shows that a SAB converter efficiency suffers significantly when operated under variable voltage conditions. It is found that the full-bridge and SPR converters handle these situations much better with the SPR having a better efficiency in most cases. Furthermore, it is shown, that a control strategy with variable voltage in the wind turbines' DC busses is advantageous in terms of DC/DC converter efficiency, compared to constant DC-bus voltage. *This is especially interesting for this PhD research, since the use of a diode-bridge rectifier as generator rectifier implies such variable voltage operation.*

The authors of [52] modeled wind farm losses, equipment cost and reliability for different AC and DC topologies. For AC wind farms, the wind turbine generators are assumed to be DFIGs *which nowadays are becoming less and less interesting for new developments* [4]. For DC configurations, a full-scale power electronic interface with VSC and isolating DC/DC converter has been chosen. The topologies examined are AC wind farms without HVDC link in radial and radial with loop collection system configurations, as well as parallel DC, series DC, and series DC with multiple strings configurations for a wind farm rating of 300MW. The authors conclude, that for the selected wind farm configurations and sizing, the series DC configuration is the only configuration with better overall efficiency than AC radial configurations. In terms of reliability the authors show that AC configurations currently have a higher reliability than DC configurations (for AC configurations, the electric energy not served is approximately halved while the availability is about 10 per cent points of ASAI). This difference mainly appears to originate from the higher failure rates of power electronic equipment compared to any other equipment. Furthermore, within the class of DC configurations, reliability is best with a multi-string series configuration, and worst for a parallel DC configuration (due to long collection system cables). The authors assume no cable redundancy for series DC connected wind farms. In terms of equipment cost, the authors conclude that the cheapest AC system is one with an AC radial configuration, while other AC configurations would be 7% more expensive. A series DC configuration would cost 85% of the cost of an AC radial configuration, and a multi-string series DC solution would be at 102%. Parallel DC configurations would be 55% more expensive. *This study shows potential for DC configurations; however, further research and development in*

components, system configuration, and system analysis might be required to find an optimal design.

In [53], an assessment of different collection systems in terms of losses and equipment cost has been performed for a 400MW wind farm. The examined collection system configurations are AC system with HVDC link, parallel DC with a turbine output voltage of 30kV (each wind turbine uses a PMSG, VSC and isolating DC/DC step-up converter) and central 30kV to 300kV step-up converter, and parallel DC with a turbine output voltage of 1.2kV (each wind turbine uses a PMSG and a VSC), step-up converters (1.2kV to 30kV) for a group of wind turbines and a central 30kV to 300kV step-up converter. These configurations were labelled 'AC', 'DC1', and 'DC2', respectively. Each wind turbine operates with a 5MW, 690V generator. The DC/DC converters are based on the full-bridge DC/DC topology with medium-frequency transformer operating at a switching frequency of 1kHz. The assumed wind site is characterized by Weibull parameters k=2 and c=9.5. Based on the calculation of yearly yield and energy losses, the wind farm efficiencies for 'AC', 'DC1', and 'DC2' are determined as 92.58%, 92.35%, and 92.46%, respectively, which are very close to one another. Slightly larger differences would be seen when only implementing a 200MW wind farm. Equipment cost of DC configurations is found to be larger than those of AC configurations (by 2% and 7%, respectively). For smaller wind farms (200MW), these differences remain similar. The authors attribute the cost increases of DC systems mainly to high cost of DC/DC converters and DC switch gear. *Both technologies are still under active research and development, so that future progress and economies of scale could potentially help reduce these cost components compared to other equipment typically used in (AC) wind farms.* Lastly, the authors point out, that DC farms might be able to improve their efficiency in the future, if generators with larger voltage ratings, or DC/DC converters with higher voltage transformation ratios become available on an economically feasible basis.

1.3   Research Objectives

The review has shown that wind farms with a series-connected DC collection system have potential to improve offshore wind generation. Different approaches have been taken with regard to selection of conversion topologies and system sizing. Some works have highlighted significant potentials in DC wind farms, but fail to completely take advantage of those potentials (such as efficiency gains with variable DC voltage operation in wind turbines in [9] and [42]). A closer examination of the operating points and

15

interdependencies of wind turbines in a series string reveals that there is a closer correlation between wind turbine output voltages and currents with the incoming wind conditions, than with conventional AC wind farms. The impact of real world operating conditions on wind turbine operating points and resulting converter sizing has not been studied extensively.

The thesis is focused on developing a wind farm configuration that can turn this correlation of wind speeds into an additional degree of freedom for system design and sizing, and exploit it for improvements in overall conversion efficiency, system availability, and amount of required offshore conversion equipment.

Thus, *the objective of the proposed work* is to perform an in-depth system study of an offshore wind farm with DC collection systems where each individual wind turbine uses a diode-bridge rectifier and partial power processing converter in order to take advantage of the correlation of wind speeds within a wind farm. By examining real-world, high-resolution data from offshore wind farms, and modeling expected operating conditions, the requirements on series-connected DC wind farms will become better understood. The overall goal of this thesis is to develop the fundamental wind turbine design, control and operational principles, develop a framework for determining preferable converter ratings, and provide a quantification of potential benefits achievable with this new configuration,

By using partial power processing converters with diode-bridge rectifiers, benefits in three aspects are realized:

- **Lower generation cost per kWh.** Resulting from a reduction in equipment and improvement of conversion efficiency, the production cost of electricity from offshore wind energy using the proposed wind farm configuration is expected to be lower than that using convetional technology (see Chapter 7).

- **Less power electronic equipment deployed**. This can lead to a reduction in equipment weight and volume in offshore wind turbines, and lower cost.

- **Reduced electric conversion losses.** Work presented in Chapters 3-5 and 7 shows that with a proper system sizing and HVDC link operation strategy, the power electronic converter equipment can run at operating points that incur less losses than those in conventional full-scale converter configurations.

1.4 Thesis Organization

The main content chapters of this thesis are Chapter 3 to Chapter 7. Necessary background for these is provided in Chapter 2. The proposed wind farm configuration is introduced in Chapter 3. Chapter 4 is dedicated to developing appropriate control algorithms for the wind turbine, wind turbine converters, and HVDC system, including for ancillary services. Furthermore, this chapter presents transient simulations of this wind farm configuration. Chapter 5 presents a framework for determining converter ratings in series-connected DC offshore wind farms. This framework is applied to the proposed wind farm configuration, as well as two further series-connected wind farm configurations for comparison. Since wind turbine startup is not available using conventional methods for the proposed configuration, a novel startup scheme is developed in Chapter 6. Finally, Chapter 7 presents a comparative economic assessment among all considered series-connected DC wind farm configurations, as well as a conventional AC wind farm featuring an HVDC link. A summary is provided in Chapter 8.

Chapter 2

Background review

2.1 Horizontal-Axis Wind Turbines
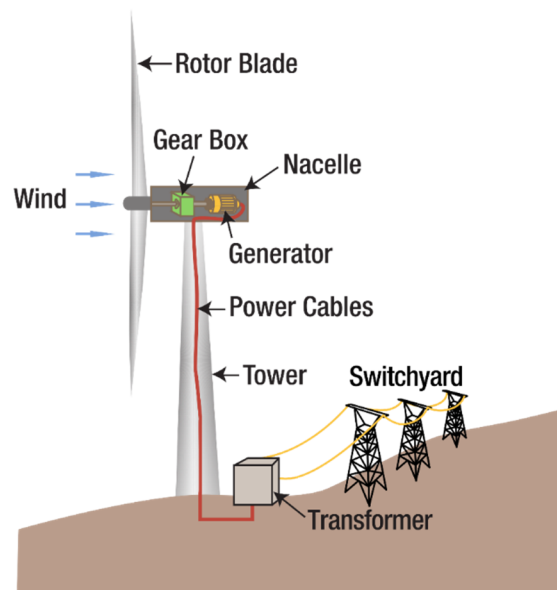
Figure 2.1 Basic Wind Turbine Components
(source: [54], Public Domain)

Modern large-scale wind turbines for electricity generation are usually classified as horizontal axis, upwind wind turbines with three blades, as illustrated in Figure 2.1. The amount of power available in the wind for conversion can be described as [55]:

$$P_U = \frac{1}{2}\rho A C_p U^3 \tag{2.1}$$

where ρ is the air density ($1.225\frac{\text{kg}}{\text{m}^3}$ at standard conditions), A the rotor swept area, U the wind speed, and C_p the power coefficient. According to the Betz limit, the maximum possible power coefficient is $\frac{16}{27} = 0.593$. Commercially available wind turbines usually operate at a maximum power coefficient of $0.4 - 0.5$. The power coefficient varies, as the ratio between speed at the tip of a blade and the wind speed (the so-called "Tip Speed Ratio", TSR, λ) varies and is a function of the turbine blade design. The tip speed ratio is defined as:

$$\lambda = \frac{\omega_T R}{U} \tag{2.2}$$

where ω_T is the rotational speed of the turbine, R the blade radius, and U the wind speed. At an optimal tip speed ratio λ_{opt}, which depends on the turbine blade design, the maximum power coefficient can be achieved. While the tip speed ratio is held at its optimal value, maximum power extraction can be achieved. The process of maintaining operating conditions to extract the maximum amount of power available at a given time is called maximum power point tracking (MPPT).

Ideally, the rotor blades always have to face the wind (rotor plane perpendicular to oncoming wind direction). Yaw drives built into the nacelle can turn the nacelle and rotors as needed to maintain optimal rotor orientation. Furthermore, most wind turbines deployed today convert wind energy based on the principle of lift. In order to maintain an optimal angle of attack, or to reduce power conversion (e.g., at wind speeds above rated wind speed), a so-called "pitching system" is installed to alter the rotor blade angle, and thus the angle of attack which results in a reduction of the power coefficient. Variable-speed wind turbines are usually controlled following MPPT from a minimum "cut-in" wind speed (wind turbine is off below cut-in wind speed) to rated wind speed by maintaining the tip speed ratio at its optimum value. From rated wind speed to a maximum "cut-out" wind speed, output power is held at rated value. In this range, the pitching system ensures that wind energy conversion does not exceed the rated power of the wind turbine. To turn off and halt a wind turbine at wind speeds above cut-out, a combination of pitching system, mechanical brake, and electrical brake can be applied.

Horizontal axis wind turbines (HAWT) have to be mounted high in the air to extract large amounts of wind power. Towers to facilitate this are usually tubular steel towers, concrete towers, or lattice towers. Supporting large masses in the nacelle and rotors

economically and at ever larger heights is one of the fundamental challenges in wind turbine tower construction.

2.2 Electromechanical energy conversion in wind turbines

The conversion of energy in the wind to electric energy relies on an aerodynamic, a mechanical, and an electric system. This section concerns the mechanical, and electric system types. Wind turbine generators (WTGs) interface the mechanical wind turbine system to the electricity grid by converting kinetic energy transported through the shaft into electric energy that is injected into the electricity grid. Five dominant general WTG topologies have formed over the past decades [56]. Type 1 (Figure 2.2) and Type 2 (Figure 2.3) WTG topologies are not of concern for the purpose of this research due to the limited ability to perform MPPT. The interested reader is referred to [56] for further background.

When the induction generator excitation of WTG type 1 and 2 is replaced by a power electronic back-to-back converter system fed from the grid connection point, the doubly-fed induction generator (DFIG) is obtained, WTG type 3 (Figure 2.4). The converters typically have a power rating of only 10-30% [56], [57] of full rated power. However, this arrangement allows the operation at sub- and super-synchronous speeds and fast reactive power control is available through the power electronic converter configuration. A gearbox is still required. This type is still a common configuration in some existing applications, followed by type 4 [58]. For new developments, type 4 is dominating [4].

In order to allow a fully variable-speed wind turbine operation that can always operate at its aerodynamic optimum, in type 4 WTGs the electrical frequency is fully decoupled from the mechanical speed using a power electronic converter system in a back-to-back configuration (Figure 2.5). The power electronic converters have to be rated to the full power rating of the turbine. This configuration allows fast-responding four-quadrant operation; however, active power is unidirectional. If a large reactive power capacity is required at high active power output, the converter system has to be oversized accordingly. Depending on the individual design, a gearbox might not be necessary, improving reliability, and reducing volume and maintenance cost. However, the generators have to be purpose-designed for such applications, as these generators tend to require a high pole-count and operate at low-speed, and high-torque. This gearbox-

less concept is referred to as 'direct-drive (DD) wind turbine'. To improve generator efficiency, permanent-magnet excited synchronous generators have become the dominating technology in new large-scale wind turbine designs [4].

[56] also describes a type 5 WTG topology. Here, a synchronous generator interfaces the grid. A variable-speed wind turbine is realized by using a speed/torque converter (for example, a continuously variable transmission, CVT) that decouples turbine rotational speed from generator rotor speed. Effectively, this system forms an electrical interface that is very similar to that of conventional steam power plants. Reactive power control is achieved through controllable excitation (automatic voltage regulator, AVR). DeWind D8.2 2MW, AMSC-Windtex SuperGear 2MW, and Wikov W2000 2MW wind turbines are rare examples of such a configuration deployed commercially [4].

This thesis document focuses on wind turbines of type 4 from now on, unless stated otherwise.
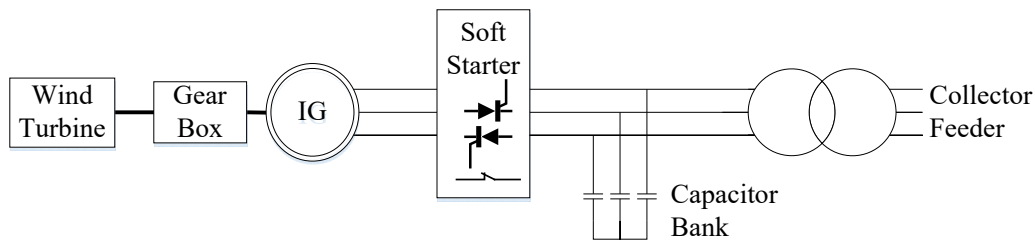
Figure 2.2 Typical Configuration of a type 1 WTG
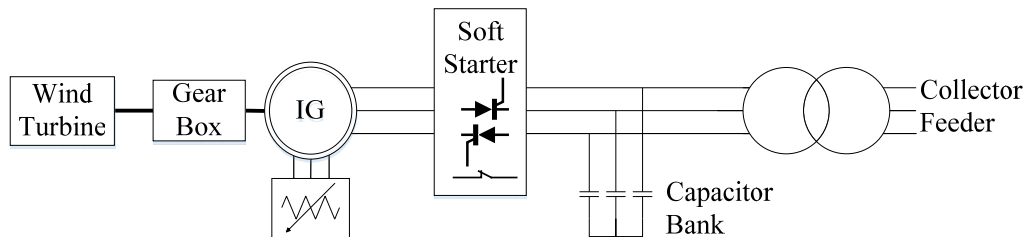
Figure 2.3 Typical Configuration of a type 2 WTG
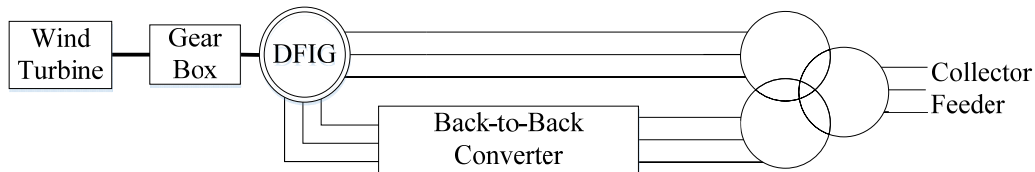
Figure 2.4 Typical Configuration of a type 3 WTG

Figure 2.5 Typical Configuration of a type 4 WTG

2.3 Offshore Wind Farms

Wind farms are constructed by locating a large number of wind turbines in close proximity within one project. In particular, wind farms located at sea (offshore) have become a common way of implementation. Wind farms can consist of only a few or up to hundreds of wind turbines. Large-scale wind farms are attractive at sea due to the benefits of economies of scale, higher average wind speeds and capacity factors, lower intrinsic turbulences and wind shear, less resulting visual intrusion, the lack of natural and human-made obstacles impacting wind flow, and existence of fewer other restrictions, such as infrastructure, environmentally sensitive areas, and competing land use [1], [59]. One significant issue in wind farms is wakes. The air flow behind a turbine becomes turbulent and its speed is reduced temporarily. If another wind turbine is located closely behind, its maximum power output will be reduced. Therefore, proper wind farm array design needs to take wake effects into account [59]. A collection system within the wind farm concentrates the power of all wind turbines at a small number of points within the farm (e.g., one, two, or three). At these points, an offshore substation is placed to condition the power for transmission to shore [59]. Typical collection system voltages are 33kV_{AC} to 66kV_{AC} [60].

Depending on the distance to shore, AC or DC transmission systems are being implemented. AC transmission systems typically operate in the range of 150kV_{AC} to 220kV_{AC} and only require line-frequency transformers on both ends [59]. For short distances, this scheme is more cost-effective, since the cost of transformers is relatively low. However, the line losses are higher than with an equivalent DC transmission system. For this reason, DC transmission systems are more cost-effective for wind farms located farther away from shore (starting at around 90km distance [50]). DC transmission systems use line-frequency step-up transformers and power electronic converters on either side to interface AC and DC systems. Typical transmission voltages in DC transmission systems for offshore wind farms are in the range of $\pm150\text{kV}$ to $\pm320\text{kV}$ [61]. Thus, these transmission systems are called 'High-Voltage DC (HVDC) transmission'.

2.4   High-Voltage DC Transmission

HVDC Transmission can be realized using Line-Commutated Converters (LCCs) based on Thyristors, or Voltage-Sourced Converters (VSCs) based on IGBTs [62]. A typical LCC-HVDC configuration is shown in Figure 2.6 and a typical VSC-HVDC configuration is shown in Figure 2.7. In both figures, a bipolar configuration has been depicted. This configuration is the most flexible, but also the most expensive configuration. Alternate arrangements are monopolar configurations in which the neutral return conductor is omitted or replaced by earth returns. A symmetrical monopolar configuration has the positive and negative DC conductor, whereas an unsymmetrical monopolar configuration only consists of one conductor and earth return. A high-level comparison between LCC-HVDC and VSC-HVDC transmission systems is provided in Table 3.2.
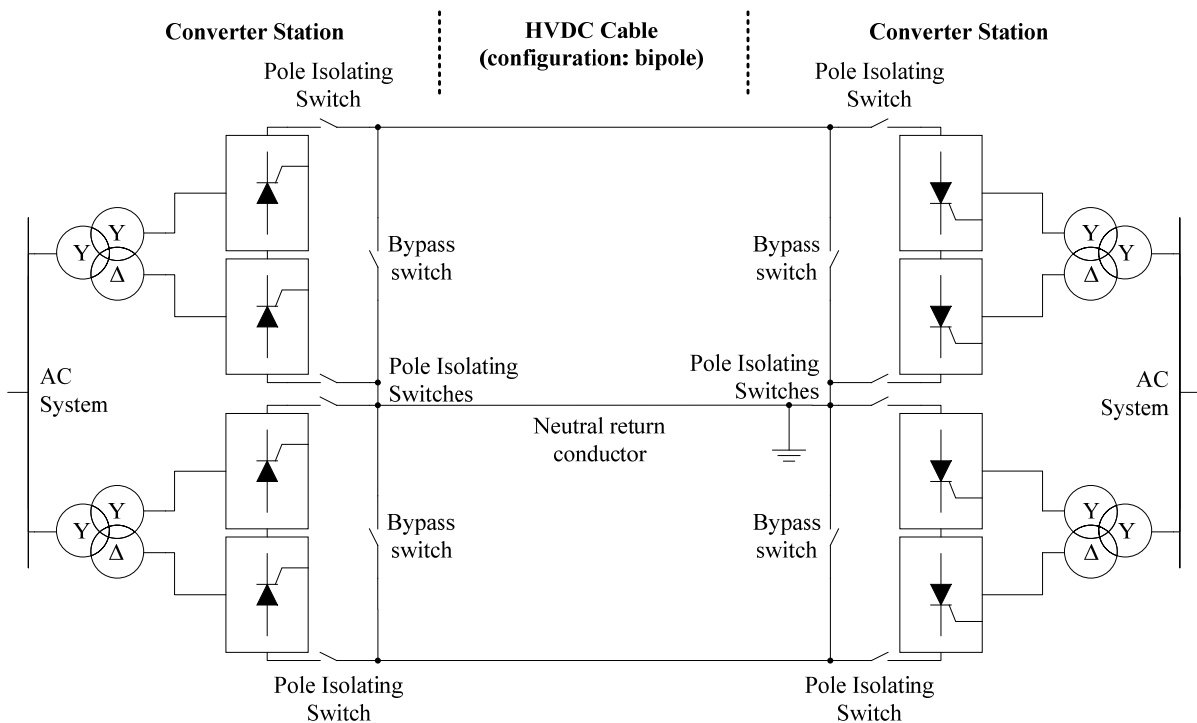
Figure 2.6 LCC-HVDC Transmission system with bipolar cable configuration. [63]–[65]
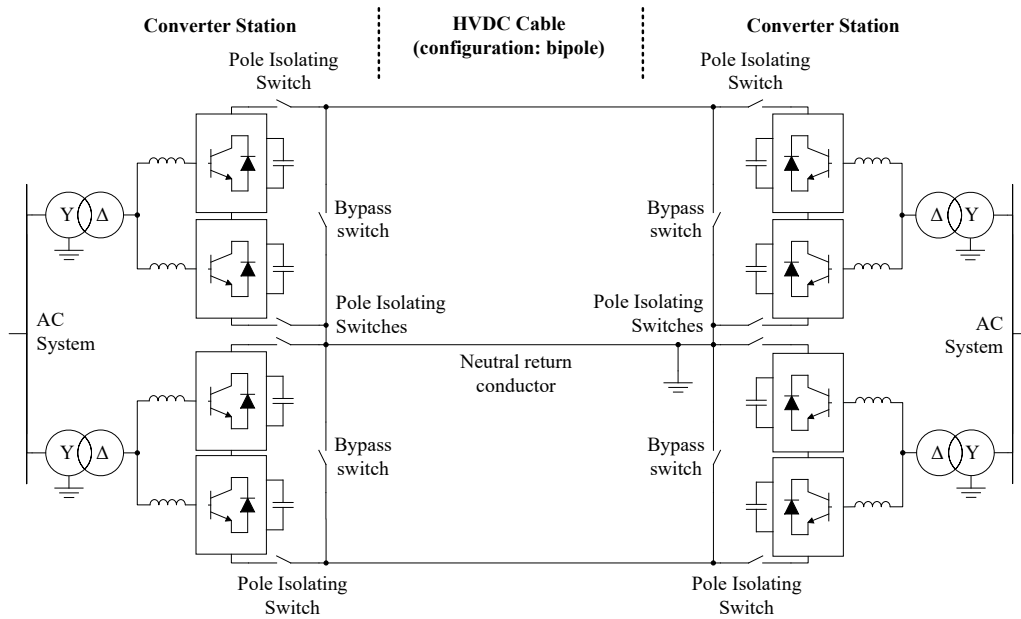
Figure 2.7 Bipolar VSC-HVDC transmission system [64], [65].

Table 2.1 Comparison of HVDC technologies [61], [64], [65]

LCC-HVDC TRANSMISSION	VSC-HVDC TRANSMISSION
Mature	Rapid growth
Most cost-effective solution for long-distance bulk power transmission	
Usually requires strong AC system	Can support weak AC systems, can form islands or realize black starts
Lower losses	Higher losses
DC current can be controlled, down to zero	DC current cannot be controlled directly
DC voltage flexible (positive, zero and negative)	DC voltage mostly fixed, always positive
Needs reactive power (compensation). Capacitor-commutated conversion eliminates this requirement.	Independent active and reactive power control
Multi-terminal operation challenging	Multi-terminal operation possible
Large harmonic filters required	Lower harmonic filter requirements
Higher reliability and DC fault tolerance	DC line faults difficult to handle
Large footprint of converter stations	Smaller footprint of converter stations
Large installations: Itaipu1&Itaipu2, Brazil, 3150MW, $\pm$600kV$_{dc}$, 796km	Large installations: SylWin1, Germany, 864MW, $\pm$320kV$_{dc}$, 204.5km

2.5 Partial and Differential Power Processing

Partial and differential power processing converters are classes of converter configurations in which only a fraction of the total power flow is processed by a power electronic converter whereas the remaining power flow bypasses most of the converter components. Their rating can be at a fraction of total power capacity [66], [67]. When input and output voltages are in close proximity, reductions in conversion losses, weight, and volume can be achieved [66]. Based on the style of connection of the converter and the bypass path, common PPPC connections are referred to as input-series, output-parallel (ISOP), and input-parallel, output-series (IPOS), as shown in Figure 2.8. According to [66], positive power flow in the converter will result in an output voltage boost for an IPOS configuration and a buck operation for ISOP configuration. If the direction of converter power flow is reversed, the output voltage mode (buck or boost) is also reversed while maintaining overall positive power flow. PPPCs have been evaluated for use in low-voltage power supplies [66], [68], cell balancing [69], electric vehicle DC/DC conversion [70], and photovoltaic systems for the mitigation of partial shading losses [43], [67].
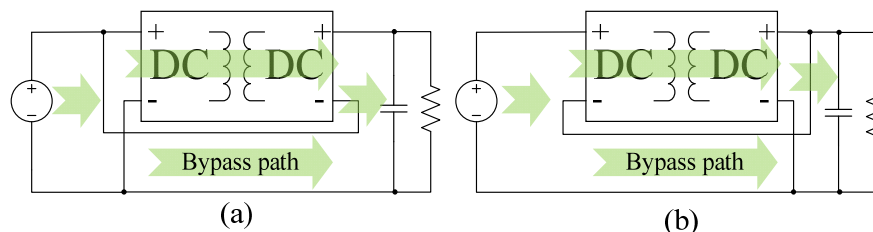
Figure 2.8 Partial power processing converter connections.
(a) Input-parallel, output-series (IPOS); (b) Input-series, output-parallel (ISOP)

When applying the PPPC concept to a series string of converters at their outputs, differential power processing (DPP) can be obtained [43], [67]. In DPP, individual converters only process the difference of power flow between a natural power flow imposed by the string current and converter input voltage, and the amount of actually desired power flow. This concept has been studied for application in photovoltaic plants [43], [67].

2.6 Thesis Scope and Assumptions

In this thesis, a series-connected DC wind farm is constructed from individual strings, only. While DC wind farms with parallel connections of series strings ("series-parallel") have been studied in literature, the commonly found challenges around string protection and the lack of an economic case have lead to the work in this thesis to focus on single-string, series-connected wind farms.

Simulations in this thesis have been performed in ways that are designed to capture the dynamics of interest while reducing the computational complexity. Due to the large size of offshore wind farms (80-90 wind turbines), full dynamic simulations of the entire wind farm and its HVDC system are computationally infeasible with modern computers. For this reason, full-order dynamic simulations have been performed for 5 wind turbine models and upscaled to represent a string of 30 series-connected wind turbines. Simulations capturing long term operation have been performed for the entire wind farm with longer durations using steady-state models for electrical systems and dynamic models for the aero-mechanic systems. This approach is appropriate since electrical time constants can be assumed to be much shorter than those of the aerodynamic and mechanical systems that are of interest, and under regular operation electrical systems can be assumed to function with stable and normal operation.

Lastly, this thesis focuses on using a dedicated HVDC system per wind farm. It does not consider the use of HVDC systems shared between multiple wind farms, as it can be implemented in large clusters of offshore wind farms. This assumption is a result from the variable HVDC voltage and current that the proposed wind farm operates with. Using one HVDC system for multiple wind farms could be considered an interesting potential future research direction.

2.7 Summary

This chapter reviewed basic components of offshore wind farms. The most commonly applied wind turbine concept is the horizontal-axis, three-blade upwind wind turbine that usually operates with a maximum power coefficient of about 0.4 to 0.5. At sea, wind turbines can be deployed in large quantities, forming offshore wind farms. When the distance to shore is large, it may be more economical to use HVDC transmission to deliver generated energy to shore over AC voltage transmission. The traditional HVDC

converter topology at the shore connection is a thyristor-based line-commutated converter, whereas competing concepts are the voltage-source and modular multi-level converter-based stations. Series-connected DC wind farms are a research-stage concept to deliver tighter integration of offshore wind turbines and onshore converter stations to derive benefits in terms of converter equipment needed, conversion efficiency, and generation cost. Differential power processing can be leveraged to reduce converter capacity in systems with many individual conversion stages that operate at similar operating points, such that only differences in operating points require processing by a power electronic converter. One approach to implement such concept is through the use of partial power processing converters, where each converter processes only a fraction of power.

Chapter 3

An Offshore Wind Farm Featuring Differential Power Processing

3.1 Output Power Differences in Offshore Wind Farms

Offshore wind farms are known to be exposed to steadier and higher winds, leading to higher capacity factors [55]. Winds can move fairly evenly across the open sea and are not as obstructed as on land in the presence of hills, valleys, forests, cities and other surface features. As a result, output power differences witin an offshore wind farm may well be dominated by wake effects [55]. To investigate the magnitude of output power differences within a typical offshore wind farm, operational data was retrieved from the Danish Wind Farm 'Horns Rev 1'.

The Horns Rev 1 wind farm is located 14km from the west coast of Denmark as shown in Figure 3.2. It consists of 80 Vestas V80 2MW wind turbines arranged in an array of 8 by 10 turbines [71]. 1 Hz output power measurement data from each turbine has been obtained for the period of February 16th, 2005 to December 21st, 2005. After removing data rows with invalid or missing data points, non-operational wind turbines, as well as wind turbine start-up/shutdown transitions, 109 days, 1 hour, and 22 minutes of data remained to compute each wind turbine's output power deviation from the average wind
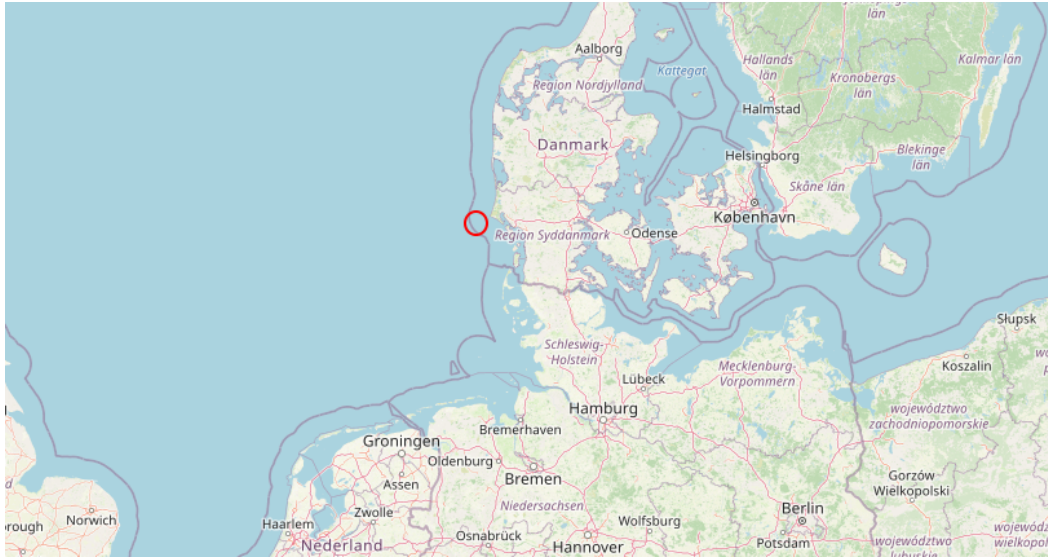
Figure 3.2 Location of Horns Rev 1 offshore wind farm in Denmark (red circle).
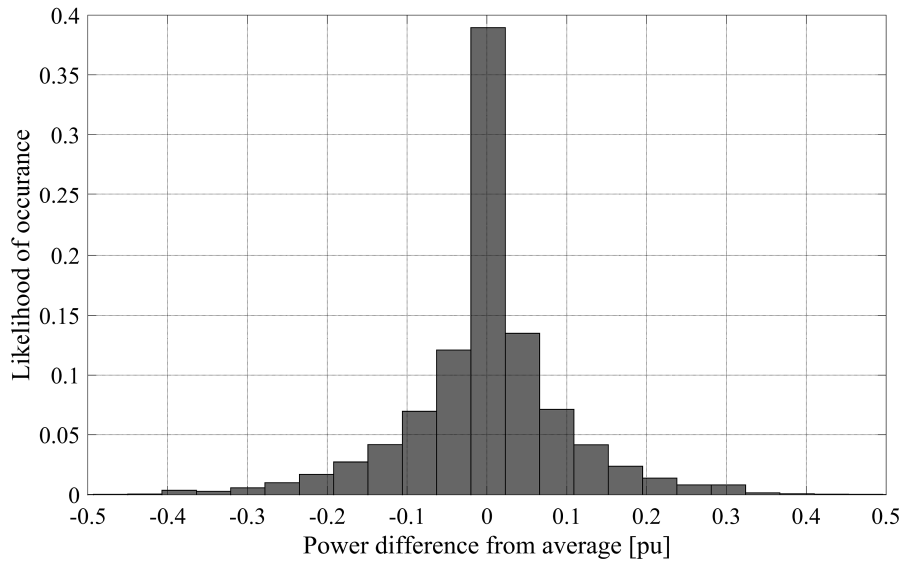
Figure 3.1 Histogram of wind turbine output power differences from average wind turbine output power within Horns Rev 1 Offshore Wind Farm (1Hz data).

turbine output power in the farm for each second. As it can be seen in Figure 3.2, there is a very significant likelihood for all wind turbines to operate at a similar output power. The likelihood of wind turbines' output powers to deviate by more than 30% of rated power from the farm average is less than 1.3%. Similarly, in 90% of the cases, wind turbines' output powers deviate less than 17.5% of rated power from the average output power. The particularly high likelihood of zero output power deviations in the farm

29

mainly stems from long periods at which incoming wind speed is high enough to operate all wind turbines at rated power.

Differential power processing is based on the principle to only use converters to process power deviations from a common 'average' level of power flow. Past PMSG-based wind farm designs rely on full-scale, full power processing converters for all wind turbine converter stages. While wind farms with a series-connected DC collection system exhibit sensitivities to local output power differences in all wind turbine converters of a series string [72], none of them exploit the opportunity of differential power processing in the wind turbine converter stage becomes apparent in this data analysis of the Horns Rev 1 wind farm data.

To explore this opportunity, a DC wind farm design featuring partial power processing converters is presented in this chapter.

3.2   Proposed Wind Farm Overview

The proposed wind farm configuration is shown in Figure 3.3. Each wind turbine consists of a medium-voltage PMSG, a three-phase diode-bridge rectifier, and an IPOS-connected, bidirectional PPPC that ensures MPP operation. The PPPC can be realized using one or multiple isolated DC/DC converters. The PPPC design is discussed further in section 3.5.
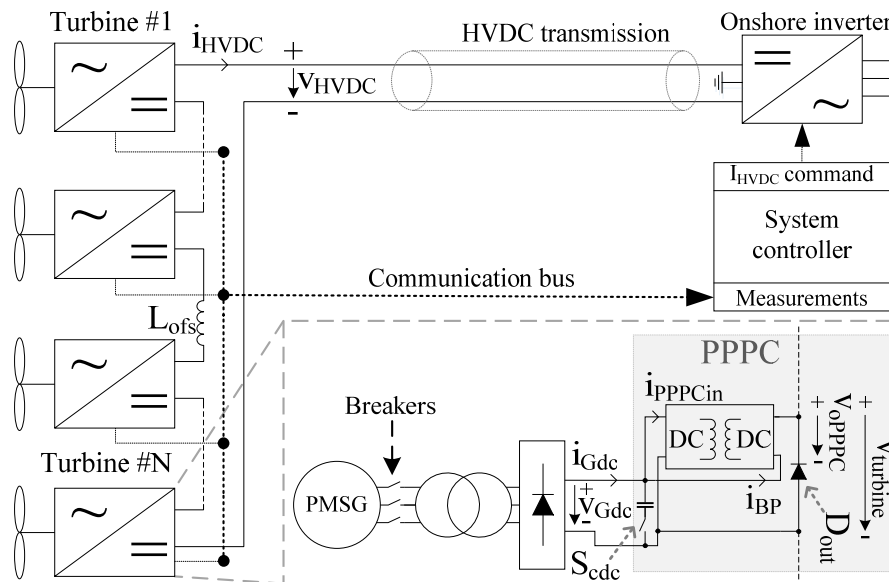
Figure 3.3 Proposed system configuration.

All wind turbines are connected in a single series string in order to obtain an HVDC link without the need for a dedicated offshore HVDC converter station. This HVDC link is realized in a bipolar configuration in order to keep the required insulation levels low. The on-shore inverter station converts HVDC power to AC power to be absorbed by the grid. Its converter topology is of current-sourced type, such that the HVDC-link current I_{HVDC} can be controlled by the on-shore converter station. For such station the twelve-pulse thyristor converter, as shown in Figure 3.4, is a mature technological option [64]. However, other converter topologies with the ability to control the DC-side current can also be compatible.

A highly reliable communication link enables a system controller to determine the optimum HVDC current to be scheduled depending on the state of all wind turbines. To address potential short-term interruptions in the communication link, a fallback HVDC-link current scheduling law is presented in chapter 4.5 that only relies on local measurements at the onshore converter station. Communication delays do not affect the HVDC-link current control due to a very low bandwidth of current reference calculation of the chosen onshore converter, and the fact that the communication channel is not part of a feedback control loop. Instead, it is merely used in the process of deriving a reference value for local feedback control of the HVDC-link current I_{HVDC}.
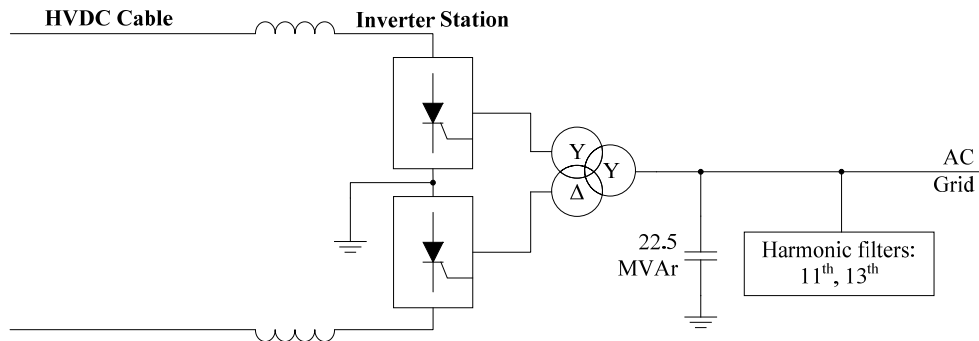
Figure 3.4 Basic schematic of an onshore thyristor-based inverter station

3.3   Steady-State Model

The basic operating principle of the proposed wind farm configuration is outlined in this section through the definition of a high-level steady-state model of the wind farm.

3.3.1 System operation below rated wind speed

As outlined in section 2.1, the maximum mechanical power P_{mech} captured by a wind turbine can be expressed as [1]:

$$P_{mech} = \frac{1}{2}\rho A c_p(\lambda, \beta)U_w^3 \tag{3.1}$$

where ρ is the air density, A the area swept by the wind turbine blades, c_p the power coefficient as a function of tip speed ratio λ and pitch angle β, and U_w the wind speed.

While wind speed is between cut-in and rated values, a conventional speed controller to maintain near-optimal tip speed ratio is used. The objective of this control loop is to operate the turbine at or near the maximum power coefficient $c_{p,max}$ by regulating the rotor speed ω_r. A simplified illustration of this controller is shown in Figure 3.5. This controller generates a power reference P_{dc}^* for the control loops of the electrical system. Below rated power, P_{dc}^* is obtained by deriving the set of values for ω_r and P_{dc} for which
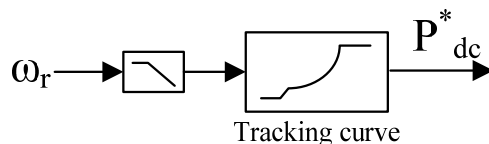
Figure 3.5 Simplified wind turbine speed control diagram.

$c_{p,max}$ is obtained by maintaining optimal tip speed ratio. P_{dc}^* is limited to the rated wind turbine power.

Deriving the relationship between DC-side voltage (V_{Gdc}) and current (I_{Gdc}) of a three-phase diode-bridge rectifier connected to the PMSG with DC-side capacitor, and including the generator inductance, following analytical procedures, is complicated as reported in [73]. Therefore, for the purpose of steady-state analysis, an empirical, rather than analytical approach using steady-state simulations in MATLAB/Simulink can be followed to describe the relationship between $V_{Gdc} = f(P_{mech})$ and $I_{Gdc} = g(P_{mech})$. Figure 3.6 shows V_{Gdc} and I_{Gdc} for the entire MPP operating range using system parameters provided in section 3.6 (on page 41).

Without a PPPC, the HVDC link would absorb a fixed amount of power determined by V_{Gdc} and I_{HVDC} and MPP operation could not be guaranteed. In order to be able to set I_{Gdc} different from I_{HVDC} for the purpose of MPP operation, the PPPC can draw/return additional power from/to the diode-bridge rectifier by adding/subtracting current to/from the bypass current I_{BP}. I_{BP} is equal to I_{HVDC} due to the series connection of the PPPC output stage. As a result, the PPPC input current can be expressed as a function of rectifier DC current I_{Gdc} and HVDC-link current I_{HVDC}:

$$I_{PPPC_{in}} = I_{Gdc} - I_{BP} = I_{Gdc} - I_{HVDC} \tag{3.2}$$

Assuming lossless operation, the amount of power processed by the PPPC and its output voltage in order to achieve MPP operation (P_{PPPC} & V_{oPPPC}) are given as:

$$P_{PPPC} = V_{Gdc}I_{PPPC_{in}} = V_{Gdc}(I_{Gdc} - I_{HVDC}) \tag{3.3}$$

$$V_{oPPPC} = \frac{P_{PPPC}}{I_{HVDC}} = \frac{P_{dc}}{I_{HVDC}} - V_{Gdc} \tag{3.4}$$

The wind turbine output voltage, $V_{turbine}$, can be written as:

$$V_{turbine} = V_{oPPPC} + V_{Gdc} = \frac{P_{PPPC}}{I_{HVDC}} + V_{Gdc} \tag{3.5}$$
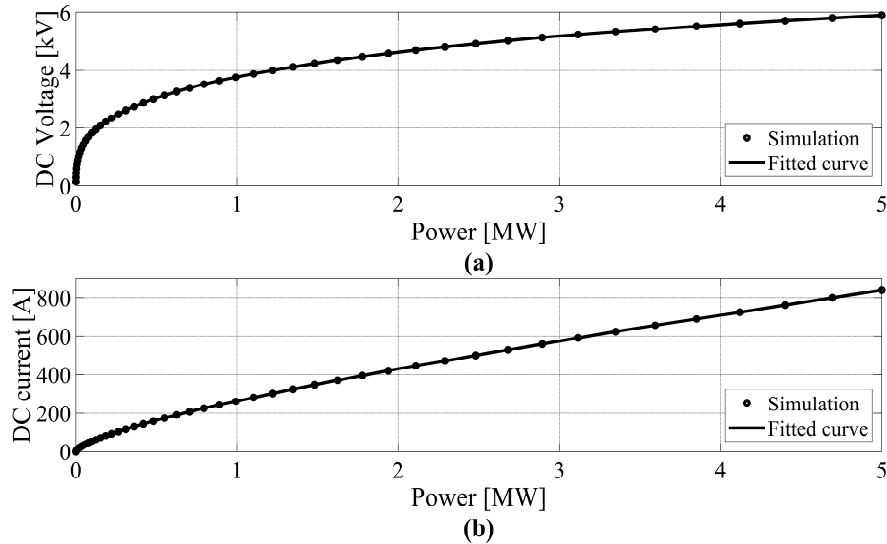
Figure 3.6 Voltages and currents on DC-side of rectifier for entire operation range at MPP (simulation and curve fitting of simulation results). (a) V_{Gdc} versus P_{mech} (obtained from simulation), (b) I_{Gdc} versus P_{mech}

33

While I_{Gdc} is equal to I_{HVDC} for a given wind turbine, all switching operation of the PPPC converter can be deactivated, so that no switching, primary-side switch conduction, and medium-frequency transformer losses are incurred. Then, the converter output stage incurs conduction losses, only.

Due to the series connection of all wind turbines, the HVDC-link voltage becomes:

$$V_{HVDC} = \sum_{n=1}^{N} V_{turbine,n} = \sum_{n=1}^{N} \left(\frac{P_{PPPC,n}}{I_{HVDC}} + V_{Gdc,n} \right) \tag{3.6}$$

where the suffix n denotes a quantity relating to the nth turbine in a series string of N wind turbines.

3.3.2 System operation between rated and cut-out wind speed

While wind speed is between the rated and the cut-out wind speed, it is being assumed that the wind turbine's pitch angle is adjusted by a pitch controller and rated output power and rotor speed are maintained. As a result, electrical system modeling for rated wind speed applies in this operating range. The turbine is deactivated for wind speeds below cut-in or above cut-out values. A control scheme to start up and shut down wind turbines is presented in Chapter 6 on page 117.

3.4 Considerations on Wind Farm Components

The proposed wind farm configuration differs from established norms and conventions in multiple aspects. This section outlines some of these deviations and discusses their rationale, importance and impacts.

3.4.1 PPPCs and HVDC-link operation

A proper HVDC current scheduling scheme has a significant influence on the total amount of power processed by all PPPCs. The amounts of power processed by the PPPCs are not entirely tied to the absolute level of power generation or average wind speed in a wind farm, as PPPCs only need to process a power deviation from a common level of power absorption set by the HVDC-link current-scheduling scheme (see eq. (3.4)). This highlights that even partially-sized PPPCs will not by themselves result in a limitation of variable-speed operation. Instead, the PPPCs are used to only process the power differences between power reference P_{dc}^* and the power draw that would occur in the absence of a PPPC (equal to $V_{Gdc}I_{HVDC}$). As a consequence, both HVDC-link

current and voltage are variable quantities, unlike with the conventional parallel AC wind farms with a fixed-voltage HVDC link.

3.4.2 Generator voltage level

The use of medium-voltage generators reduces resistive losses compared to low-voltage generators (e.g., 690V), and renders use of boost converters with large voltage gains unnecessary. Commercially deployed medium-voltage wind turbine generators operate at voltages as high as 3300 to 4000V [9]; further related designs have been reported in [33] and [74]. Due to the elimination of a boost converter and controlled rectifier in the proposed scheme, the choice of generator voltage directly influences the rated output voltage of a wind turbine, and thus affects the minimum number of wind turbines required in a series string to obtain a sufficiently high HVDC-link voltage.

3.4.3 Diode-Bridge Rectifiers

The choice of a diode-bridge rectifier over a VSC results in lower cost, lower losses, control equipment elimination, and higher robustness. However, it introduces two drawbacks, namely an increased level of generator current harmonics, and the inability to provide compensation for reactive power consumed by the generator inductance [73]. These can lead to increased losses in the generator, increased excitation requirements and the need to design a more robust drivetrain [75]. Possible measures to dampen the negative impacts can be introduction of small parallel-connected capacitors between generator and rectifier to provide reactive power support [76] or potential use of an elastic coupling between wind turbine rotor and generator. For the sake of simplicity, these measures have not been adopted in this work.

3.4.4 Offshore HVDC converter station and system operation

Compared to conventional AC wind farms with HVDC link, the proposed scheme can offer lower mass and volume of offshore-deployed electric conversion equipment; especially as power electronic converters in wind turbines would be smaller in deployed capacity, and a central offshore HVDC converter station would no longer be required. Conversion efficiency increases can be achieved through reduction of number of conversion stages involved, the replacement of full-scale power processing with partial power processing, and optimization of operating points for remaining conversion equipment.

3.4.5 HVDC insulation

The challenge of insulation against HVDC potential is common to all concepts based on series-connected wind turbines, and has been discussed in this context, for example in [17], [19], and [33]. Among the most commonly chosen solutions is the use of low-frequency AC transformers with increased insulation level to ground between generator and rectifier. This solution has been adopted for the proposed wind farm configuration, as shown in Figure 3.3. In the interest of limiting transformer weight and size, a Multibrid wind turbine concept [77] could be adopted to maintain a higher level of electrical generator frequency, compared to direct-drive PMSGs. However, particularly with the increasing diameter of direct-drive PMSGs for increasingly large wind turbines, a direct-drive generator may also be feasible. Due to the existing uncertainties in maximum economically feasible insulation level, this study assumes a maximum HVDC voltage-to-ground potential of $\pm 100kV$ for the proposed scheme as it closely relates to the peak voltage value of 66kV AC transformers used in collection systems of conventional AC wind farms.

3.5 Partial Power Processing Converter Design

The selection of a suitable PPPC is dominated by two main aspects: (i) proper PPPC connection (IPOS or ISOP connection) and (ii) a suitable converter topology and modulation scheme.

3.5.1 PPPC connection

The choice of partial power processing converter connection affects its sizing and the losses incurred in a wind farm. The work in [66] points out that in order to achieve a particular voltage boost, IPOS connections require less converter capacity than ISOP connections operated with reversed PPPC power flow. In particular, for the IPOS connection, the required PPPC capacity is always smaller than that of an equivalent full-scale converter. For that reason, an IPOS connection was found to be more appropriate for the proposed wind farm configuration.

3.5.2 PPPC topology

The choice of converter topology and unidirectional or bidirectional PPPC power flow capability have significant consequences on the HVDC link operation strategy, PPPC converter sizing, and resulting conversion losses. A PPPC with unidirectional power flow

capability results in $I_{PPPC_{in}}$ being zero or positive at any time. A bidirectional PPPC can produce negative, zero or positive $I_{PPPC_{in}}$. This means that the point of lowest losses ($P_{PPPC} = 0$) is in the center of its operational range for a bidirectional PPPC, whereas it is at the lower operational range limit for a unidirectional PPPC. For a bidirectional PPPC, control action can be taken in both directions around the point of lowest power processed with respect to changing $I_{PPPC_{in}}$. This makes a reduction in PPPC size and losses more likely, as unidirectional PPPCs would have the point of lowest power processed at a limit for $I_{PPPC_{in}}$, resulting in the need for addition of a control margin. For this reason, a PPPC topology with bidirectional power flow capability is considered in this study.

Based on the design of high-efficiency dual-active bridge (DAB) converters for wind turbine application in [15], a DAB converter, shown in Figure 3.7, is considered. For the sake of simplicity, a single phase-shift (SPS) modulation has been adopted as discussed in [78]. However, more sophisticated modulation schemes could potentially be used to decrease current flow in the DAB medium-frequency transformer and increase zero-voltage switching ranges under a wide range of operating points. For the chosen modulation scheme, the power output for the dual-active bridge converter is a function of terminal voltages V_{Gdc} and V_{oDAB}, and phase shift ϕ [79]:

$$P_{DAB} = \frac{V_{Gdc}V_{oDAB}N_{ps}}{2\pi f_s L_t} \phi \left(1 - \frac{|\phi|}{\pi}\right) \tag{3.7}$$

where N_{ps} and L_t are the transformer turns ratio and leakage inductance (see Figure 3.7), f_s is the converter switching frequency, and ϕ the phase shift of the DAB-SPS modulation.
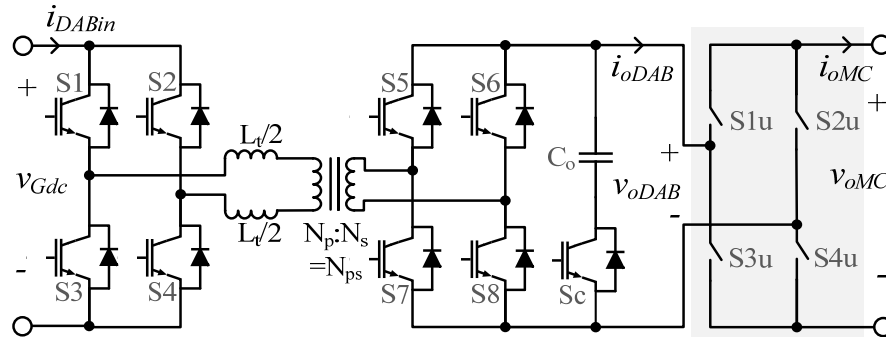
Figure 3.7 Dual-active bridge converter with unfolder circuit.

The PPPC can be realized in a multi-converter configuration, which is further addressed in section 3.5.5 below. In the absence of such multi-converter configuration,

the unfolder output voltage V_{oMC} and current I_{oMC} can be regarded as the PPPC output voltage V_{oPPPC} and current I_{HVDC}, as denoted in Figure 3.3 on page 30. Furthermore, the DAB output power P_{DAB} is equal to the PPPC output power P_{PPPC}.

The insulation of the DAB's medium-frequency transformer is only required to withstand the maximum wind turbine output voltage to avoid internal short circuits due to the IPOS connection [66], not the full HVDC potential to ground. This results from the connection of the bypass path within the PPPC converter. Insulation against full HVDC potential to ground is provided by the low-frequency transformer and has been discussed in section 3.4.5.

In order to enable bidirectional power flow with an IPOS-connected PPPC, an unfolder circuit has to be added to the output stage of the DAB [80], as shown in Figure 3.7. Positive PPPC power flow implies positive output voltage V_{oMC} and output current I_{oMC}. In this case, only switches S1u and S4u are on, denominated as unfolder polarity $UF = 1$. For reverse power flow operation of the PPPC (resulting in negative V_{oMC} and $UF = -1$), the DAB converter is operated in reverse power flow mode and the unfolder circuit only operates with switches S2u and S3u activated. As a result, the unfolder terminal characteristics can be described as:

$$V_{oMC} = UF \times V_{oDAB} \; ; V_{oDAB} \geq 0 \tag{3.8}$$

$$I_{oDAB} = UF \times I_{HVDC} \; ; I_{HVDC} \geq 0 \tag{3.9}$$

where V_{oDAB} and I_{oDAB} are the DAB output voltage and current before unfolder circuit, as shown in Figure 3.7. Since the PPPC output is connected in series, I_{oMC} is equal to I_{HVDC}, thus I_{HVDC} is used in equation (3.9) in place of I_{oMC}.

The capacitor disconnect switch S_c is normally on and only required to be operated during wind turbine start ups (as discussed further in Chapter 6 on page 119).

3.5.3   Unfolder circuit operation

To reduce conduction losses and cost, and increase robustness, it is meaningful to realize the unfolder switches S1u-S4u using contactors. This is possible, as S1u-S4u assume static positions, do not participate in converter modulation, and are never required to break load current without an alternate low-impedance path available. To ensure a successful transition between positive and negative PPPC power flow, unfolder switches must always be operated following the sequence shown in Figure 3.8. During

the transition, the DAB control loop must be halted, switches S1-S8 deactivated and the DAB phase-shift ϕ held at zero.

P_{DAB}: Positive to negative transition:	P_{DAB}: Negative to positive transition:
Initial condition: S1u & S4u on	Initial condition: S2u & S3u on
↓	↓
Close S2u & S3u	Close S1u & S4u
↓	↓
Open S1u & S4u	Open S2u & S3u
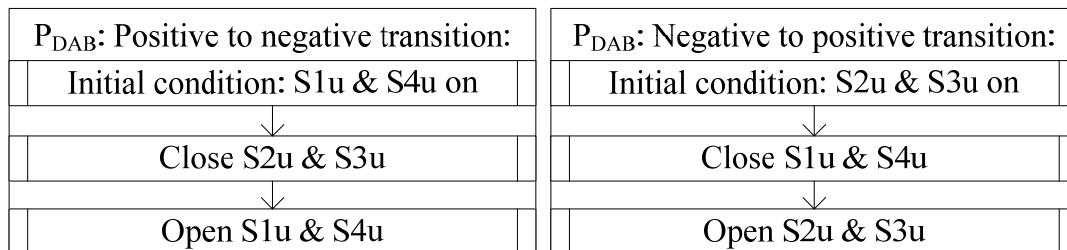
Figure 3.8 Unfolder switch states during P_{DAB} power polarity transitions.

3.5.4 Unfolder circuit control

The unfolder circuit switch states decide over the polarity of DAB power and voltage. As a polarity change in the output voltage reference V^*_{oMC} (derived from a control loop) is detected, the unfolder switch states need to be changed eventually to allow V_{oMC} to be set to a value with that new polarity. In order to avoid surge currents from the DAB output capacitor C_o, such transitions should only be initiated, once V_{oMC} has reached a sufficiently small absolute voltage threshold $V_{oMCThres}$. The resulting unfolder control logic is described in Figure 3.9. Here, $UF_{desired}$ refers to the desired polarity based on the polarity of V^*_{oMC}.

$$V^*_{oMC} \rightarrow \boxed{\diagdown} \rightarrow V_{oMC} \rightarrow$$

$V_{oMCThres} = 0.01 \times V_{DcBase}$
$UF_{desired} = sign(V^*_{oMC})$
If $V^*_{oMC} == 0$ then: $UF_{desired} = UF$

If $UF_{desired} \neq UF$ then: {
    if $((UF_{desired} == 1)$ AND $(V_{oMC} > -V_{oMCThres}))$ then: $UF = 1$
    if $((UF_{desired} == -1)$ AND $(V_{oMC} < V_{oMCThres}))$ then: $UF = -1$
}
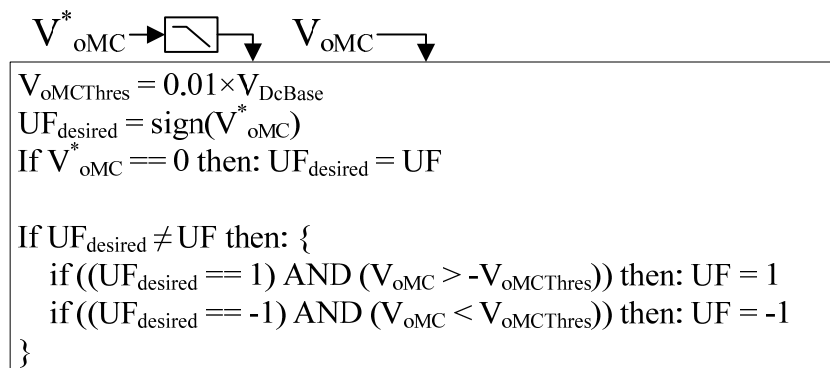
Figure 3.9 Unfolder control logic. V_{DcBase} is the DC voltage per unit base.

3.5.5 Multi-converter configuration

Differential power processing is based on the notion that individual converters only process a power differential from a common 'average' power draw. In this wind farm configuration, PPPCs the common power draw is equal to $V_{Gdc}I_{HVDC}$. The difference between that common power draw and the power reference P^*_{dc} is processed by the PPPC (i.e., P_{PPPC}). As a result, the PPPC's loading P_{PPPC}, output voltage V_{oPPPC}, and input

current I_{PPPCin} is a function of differences between common power draw ($V_{Gdc}I_{HVDC}$) and power reference P_{dc}^*. In times when the differences are low, only small values for P_{PPPC}, I_{PPPCin} and V_{oPPPC} are needed.

Secondly, it is known that DAB converters' zero voltage switching (ZVS) regions are maximized when the DAB operates near or at unity voltage gain m [79]:

$$m = N_{ps}V_{oDAB}/V_{Gdc} \tag{3.10}$$

When implementing a multi-converter configuration as shown in Figure 3.10, it becomes possible to reduce conversion losses during operation with low differential power processing requirements, and increase converter redundancy.
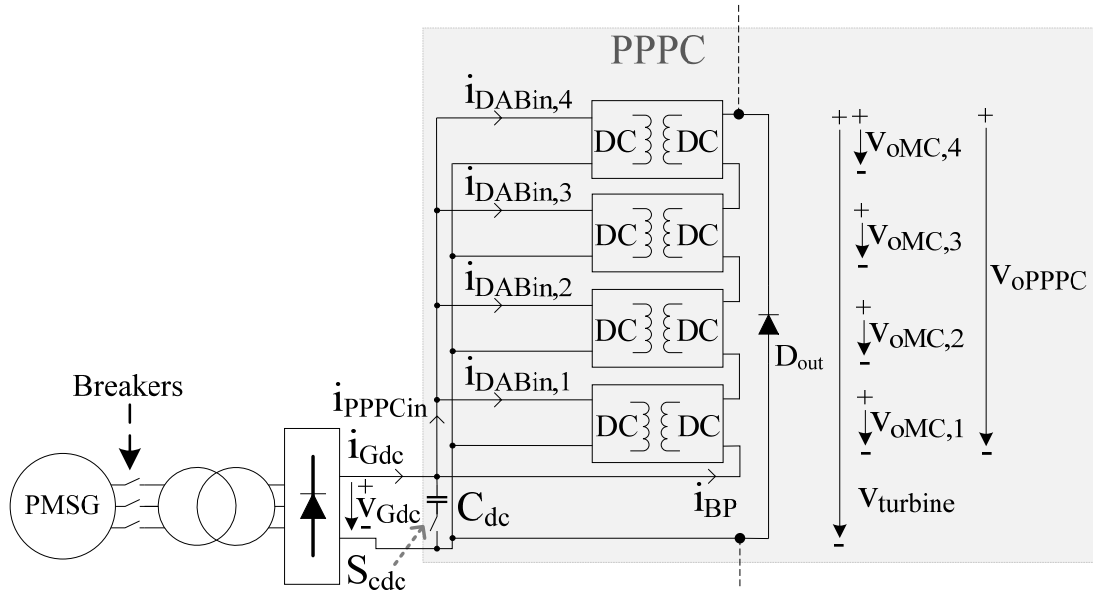
Figure 3.10 PPPC multi-converter configuration (4 IPOS-connected DABs, $K = 4$).

In this scheme, one large DAB is replaced by K smaller DABs. The sum of terminal ratings of the smaller DABs is equal to those of the large DAB assumed previously. With this configuration, it becomes possible to deactivate some DABs when the required total PPPC output power is low, reducing conduction and switching losses. Additionally, the assignment of DAB voltage references can be altered in such a way to maximize the likelihood of ZVS operation in as many DABs as possible. Related control algorithms are discussed in Chapter 4. Additionally, wind turbine availability can possibly be increased during the outage of a single DAB, since other DABs may still be available to operate in the wind turbine.

With a multi-converter PPPC configuration, the terminal quantities between overall PPPC and individual DABs are related as follows. The primary bridges of all DABs in a wind turbine are parallel connected. Hence:

$$I_{PPPCin} = \sum_{k=1}^{K} I_{DABin,k}$$ (3.11)

where the index k denotes the k'th DAB of K DABs in a PPPC. Similarly, the PPPC output voltage and power is the sum of individual DAB output voltages and powers after their respective unfolder circuits:

$$V_{oPPPC} = \sum_{k=1}^{K} V_{oMC,k}$$ (3.12)

$$P_{PPPC} = \sum_{k=1}^{K} P_{DAB,k}$$ (3.13)

For all inactive DABs, $I_{DABin,k}$, $V_{oMC,k}$ and $P_{DAB,k}$ are equal to zero.

3.5.6 Inactive wind turbines

During planned outages, very low or very high wind speed conditions, and some faults within the PPPC or generator, the wind farm must be operated with some wind turbines deactivated. A deactivated wind turbine can be bypassed by opening the breaker between generator and diode-bridge rectifier (see Figure 3.3), the DC-bus capacitor switch S_{Cdc}, and activating all four unfolder switches. In the event of a fault in the collection or transmission system, the fault must be isolated by disconnecting all AC systems: each wind turbine breaker and the AC breakers of the onshore station must open.

3.6 A 450MW Reference Wind Farm Design

To support numerical analyses, and component or subsystem design considerations on the proposed as well as other wind farm configurations, a reference wind farm design is presented in this section. This reference wind farm is derived from multiple reference designs in literature and close to some commercial designs, where data was available. In particular, the wind turbine structures, aerodynamics and drivetrain are adopted from the NREL 5MW reference wind turbine design [81]. Since the NREL 5MW design lacks a complete definition of a generator, it has been replaced by a gearbox and generator

design that is close to that of the Areva M5000-135 5MW wind turbine model which features a so-called Multibrid drivetrain concept [77][35]. This drivetrain features a single-stage gearbox (instead of conventional two to three-stage gearboxes), and a medium-speed, medium-voltage generator. For wind turbines of higher power ratings, the use of medium-voltage, direct-drive generators is a popular option, as well [82][83]. A 5MW design has been adopted in this thesis, due to the richness of available component data in literature, as well as computational models leveraging these designs, such as SimWindFarm [84].

The reference wind farm is assumed to be located at the site of the FINO3 meteorological mast in the European North Sea, approximately 80km off the German island Sylt, as shown in Figure 3.11.
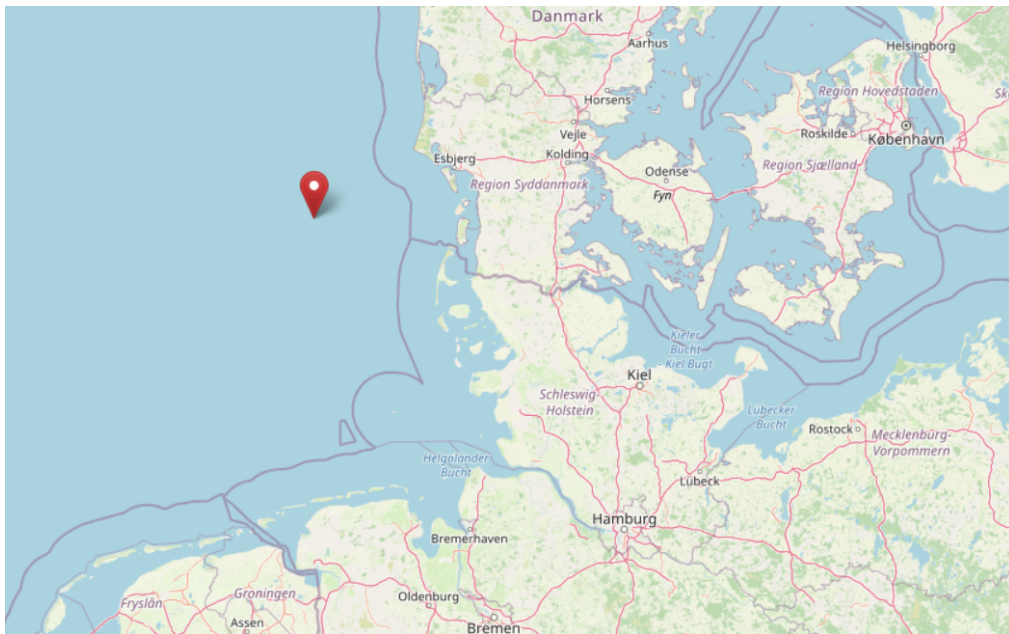
Figure 3.11 Location of FINO3 meteorological mast
© 2021 OpenStreetMap, www.openstreetmap.org
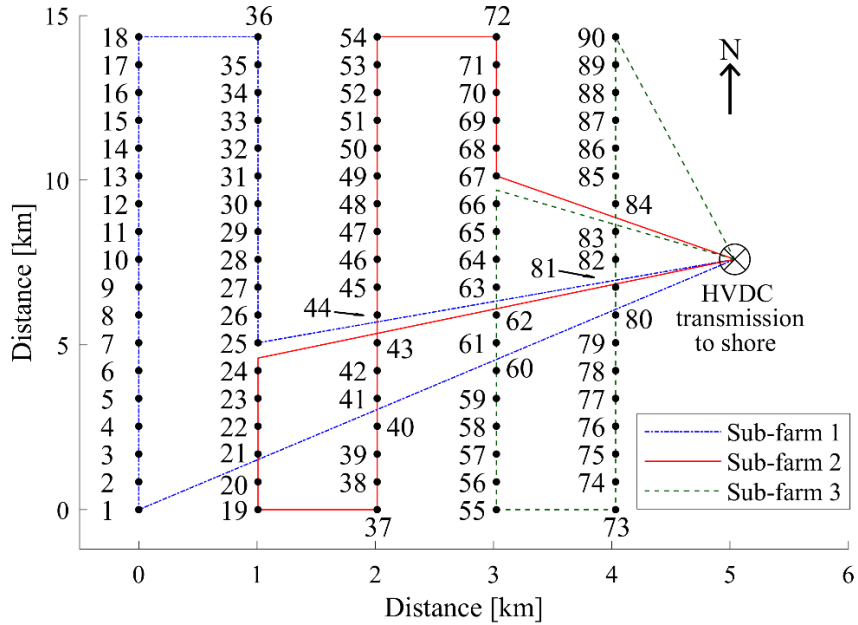
Figure 3.12 Reference wind farm layout and cabling for 90 wind.

The wind farm layout is adapted from the rectangular 800MW reference wind farm design derived for the same location and discussed in [85]. In contrast, this reference wind farm design assumes the use of 90 5MW wind turbines to come to a 450MW wind farm, instead of 80 10MW wind turbines. This is to better accommodate unique properties of series-connected wind farm designs, where groups of wind turbines are assigned to three subfarms. The wind farm layout and cabling for this reference wind farm is shown in Figure 3.12. Wind turbines are arranged in 5 rows of 18 wind turbines. The spacing between rows was set to 8 rotor diameters, while wind turbines within a row are set 6.7 rotor diameters apart. The wind farm is split into three subfarms that are interconnected at the onshore inverter station's AC terminals. In this thesis, assignment of wind turbines to subfarms was chosen to be sequential without further optimization.

In the following, parameters for the wind turbines' aerodynamics, drivetrain, generators and electrical systems are defined. The definition of some parameters may be given in later chapters when parameters are employed in models and analyses.

Table 3.1 defines per unit base values and fundamental quantities for each wind turbine. Fundamental aerodynamic characteristics are given in Table 3.2. These values are largely derived from the NREL 5MW wind turbine design [81]. The presented wind

turbine design has been adapted in a few ways to accommodate a Multibrid single-stage gearbox design and medium-voltage generator, following designs discussed in [35] and [77]. Drivetrain and generator parameters are given in Table 3.3 and Table 3.4 which are adopted from [84]. The wind turbine generator design follows that of [35] with the exception of incorporating a single-stage gearbox. This is consistent the Areva M5000-135 wind turbine drivetrain and generator design. The gear ratio has been adjusted slightly to mate NREL 5MW blade designs with the drivetrain and generator specifications of the Areva M5000-135 wind turbine. Wind turbine control parameters are taken from [84] and listed in Table 3.5. This does not include PPPC control, which is discussed in Chapter 4. Table 3.6 lists baseline electrical parameters for the proposed wind farm configuration. The resulting wind turbine power curve is shown in Figure 3.13. Finally, Table 3.7 shows key parameters for the HVDC system and onshore inverter station. This design largely follows the CIGRE HVDC benchmark system as adapted in [35] for the use in single-string, series-connected DC wind farms.

Table 3.1 Wind Turbine Base Values

PARAMETER	SYMBOL	DEFAULT VALUE	SOURCE
Rated Wind Speed	$U_{w,rated}$	11.25m/s	[81] [1]
Cut-in Wind Speed	$U_{w,cut-in}$	3.5m/s	[81] [1]
Cut-out Wind Speed	$U_{w,cut-out}$	25m/s	[81]
Rated Rotor Speed	$\omega_{rot,rated}$	12.96RPM	[81] [1]
Rated Generator Speed	$\omega_{gen,rated}$	148.5RPM	[35] [1]
Rated Electric Output Power	P_{Base}	5.0MW	[81]
Rated Rotor Power	$P_{rot,rated}$	5.282MW	-
DC Voltage Base	V_{dcBase}	5,800V	-
DC Current Base	I_{dcBase}	862A	-

[1]With adaptations.

Table 3.2 Wind Turbine Aerodynamic Parameters

PARAMETER	SYMBOL	DEFAULT VALUE	SOURCE
Rotor diameter	d_{rot}	126m	[81]
Swept area	A_{rot}	12,469m^2	[81]
Air density	ρ	1.223kg/m^3	[84]

Optimal Tip Speed Ratio	λ_{opt}	7.6	[81][84]
Rotor Power and Thrust coefficients according to rotor design of [81][84]			
Power Coefficient at λ_{opt} and zero pitching angle	$C_{p,max}$	0.4865	[81][84]
Hub Height		90m	[81]
Pitch Actuator Delay Time		50ms	[84]
Pitch Actuator Hydraulic Time Constant		50ms	[84]

Table 3.3 Wind Turbine Drivetrain Parameters

PARAMETER	SYMBOL	DEFAULT VALUE	SOURCE
Rotor Moment of Inertia	J_{rot}	35,444,067kg/m^2	[84]
Main Shaft Spring Constant		867,637,000Nm/rad	[84]
Main Shaft Viscous Friction		6,215,000Nms/rad	[84]
Gearbox Gear Ratio	n_{GB}	11.4585	-
Braking Torque (High-Speed Shaft)		23,801Nm	[81] [1]
Nacelle Mass		350t	[84]
Tower Eigenfrequency		0.321Hz	[84]
Tower Damping Coefficient		0.08	[84]

[1]With adaptations.

Table 3.4 Wind Turbine Generator Parameters

PARAMETER	SYMBOL	DEFAULT VALUE	SOURCE
Rated Generator power	$P_{gen,rated}$	5.176MW	-
Rated Generator Voltage	$V_{Gen,rated}$	5,000V	[35]
Generator Pole Pair Count	n_{PP}	14	[35][1]
Generator Moment of Inertia	J_{rot}	3,828kg/m^2	[84]
Generator D & Q Inductances	L_S	0.1885pu	-
Rated Voltage Line-to-Line	$V_{Gen,rated}$	5,000V	[35]

[1]With adaptations.

Table 3.5 Wind Turbine Control Parameters

PARAMETER	DEFAULT VALUE	SOURCE
Pitch Control Proportional Gain	246.08°s/rad	[84]

Pitch Control Integral Gain	105.46°/rad	[84]
Pitch Control Rate Limit	8°/s	[84]
Pitch Actuator Control Gain	10°/s^2	[84]
Power Controller Torque Ramp Limit	15,000Nm/s	[84]

Table 3.6 Wind Turbine Electrical Parameters

PARAMETER	SYMBOL	DEFAULT VALUE
Diode-Bridge Rectifier Diodes	Infineon D2601NH, 9000V, 2810A	
Main DC Bus Capacitance	C_{dc}	4.5mF
Number of Multi Converters	N_{MC}	4
DAB Primary Bridge IGBTs	Hitachi MBN500H65E2, 6.5kV, 500A	
DAB Secondary Bridge IGBTs	Hitachi MBN500H65E2, 1.7kV, 3600A	
DAB output capacitor	C_o	2.2mF
DAB switching frequency	f_s	7.5kHz
DAB transformer turns ratio	N_{ps}	8
DAB transformer leakage inductance (referred to primary side)[2]	L_t	185μH
DAB transformer ESR	R_{Lt}	45.5mΩ

[2] This value changes for evaluations done in Chapter 7.
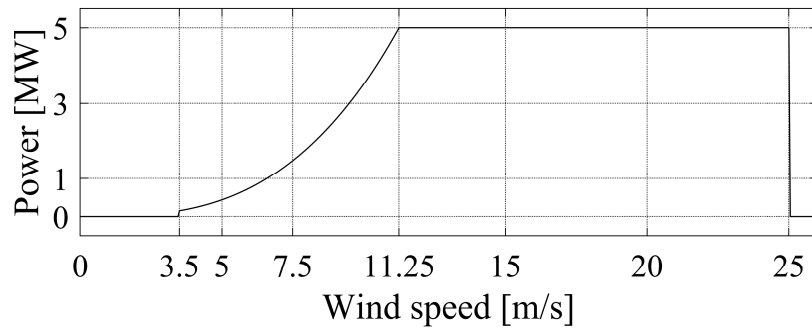
Figure 3.13 Wind Turbine Power Curve

Table 3.7 HVDC System Electrical Parameters

PARAMETER	DEFAULT VALUE	SOURCE
Collection/Transmission System Cable	Nexans 800 mm^2, 187kV, 898A, 22.1mΩ/km, 197nF/km, 401µH/km	
Thyristor Converter Rated Power	3×150MW	-
Maximum DC voltage	2×113kV	
Maximum DC current	1200A	[35]
Thyristor devices	Mitsubishi FT1500AU-240 12kV, 1500A Thyristors	
Onshore DC filter inductance L_{dc}	500mH	
Offshore DC filter inductance L_{ofs}	50mH	
Transformer Grid-side Rated Voltage	230kV	
Transformer Thyristor-side Rated Voltage	103kV	
Transformer Leackage Inductance	19.3mH	[35]

3.7   Discussions

The presented wind farm configuration is designed to provide a range of benefits by exploiting system-level optimization opportunities:

- Removal of a costly and bulky offshore HVDC converter station,
- Reduction of conversion stages needed to transmit power to shore through series connection of DC output wind turbines, and
- Improvements of electric operating points in wind turbine and HVDC system to reduce wind turbine converter loading, ratings, and losses through HVDC system operation strategies and differential power processing.

The resulting variable-voltage and variable-current HVDC link suggests that the proposed wind farm configuration may be particularly well suited for wind farms that are directly connected to shore without a dedicated offshore HVDC backbone network. However, during the development of multiple neighbouring wind farms, transmission cables could be laid at once for all wind farms to reduce cost overhead due to an offshore backbone network being infeasible for this configuration. Alternatively, future research

could focus on the interconnection of the proposed wind farm to fixed-voltage or limited variable-voltage HVDC links using high-power DC/DC converters.

Furthermore, the implementation of wind farms with multiple strings of wind turbines ("series-parallel DC wind farms") are expected to result in more challenges relating to extreme operating points, wind turbine startup, and system protection. Future research should explore this configuration, as it promises a potential reduction of transmission cables and consolidation of onshore converter stations.

Lastly, the choice of thyristor converters for the onshore inverter station is merely based on their technical maturity. However, there are significant limitations to this technology when used in this context: (1) inferior harmonic performance and need for bulky harmonic filters, (2) need for reactive power compensation and limited reactive power control, (3) black start capabilities are challenging, and (4) operation with weak grids is limited. An emerging alternative technology are modular multilevel converter (MMC) based HVDC inverter stations. In particular, full-bridge MMCs might be capable of providing the necessary DC current control, as explored in [86]. This would overcome most limitations of the thyristor technology.

3.8 Summary

In this chapter, a novel wind farm configuration was introduced that leverages differential power processing to improve overall system efficiency, amount and ratings of offshore-deployed equipment, and support energy production cost reductions. Firstly, a data analysis from the Horns Rev 1 wind farm has shown that there is a significant likelihood for wind turbines in a wind farm to be operating at or near the same output powers most of the time. Based on this observation, a wind farm configuration was proposed that uses highly-efficient and robust diode-bridge rectifiers in each wind turbine for bulk power rectification, combined with partial-scale, partial power processing converters to facilitate differential power processing and enable maximum power point tracking. This wind farm is based on a series-connected DC collection system to remove the need for a bulky and costly offshore HVDC converter station, as well as wind turbine inverters and step-up transformers. The resulting transmission system is operated with variable currents and voltages to closely align with natural operating points of the wind turbines and their rectifiers. It will be shown in Chapter 7, that this supports a favourable economic case, compared to similar wind farm configurations not operating

as closely at the wind turbines' natural operating points (e.g. [35]). Differential power processing is implemented using PPPCs that are realized with multiple dual-active bridge converters per wind turbine. Such configuration allows to optimize zero-voltage switching in dual-active bridge converters, and potentially increase wind turbine availability during some PPPC outages. Lastly, a 450MW reference wind farm design has been presented that is used throughout this thesis for transient simulations, and studies on losses, component ratings, and economic assessments.

Chapter 4

Wind Farm Control

This chapter discusses the control of individual wind turbines, as well as the wind farm overall. This entails wind turbine controls to facilitate maximum power point tracking and operation at rated power, control of wind turbine PPPCs and the operation of the HVDC link. Various additional operational modes are treated, including operation without communication link, low-voltage ride-through (LVRT), power curtailment, and inertial response. Finally, time-transient simulations for a 150MW wind farm demonstrate each of the features discussed in this chapter.

4.1   Wind Turbine Speed and Pitch Control

Wind turbine conventional variable speed and pitch control is adopted in the proposed wind farm configuration to: (1) operate the wind turbine at optimal tip speed ratio below rated wind speed, (2) operate the wind turbine at rated speed and output power between rated and cut-out wind speed, and (3) facilitate wind turbine startup and shutdown. In particular, the controls implemented in [84] are used as foundation and altered slightly. The general control diagram is shown in Figure 4.1. In this control scheme, the low pass-filtered generator rotational speed ω_{gen} is used to derive an electric power reference P_{ref}, as well as a reference pitching angle β_{ref}. A tracking curve between generator reference torque and rotational speed is used for speed control. Below cut-in wind speed, the reference generator torque $\tau_{gen,ref}$ is set to zero. Between generator speeds corresponding to cut-in and rated wind speeds, the reference generator torque is set such that the wind turbine operates at optimal tip speed ratio.

For generator speeds at or above rated value, $\tau_{gen,ref}$ is held at its torque value for rated power operation. The rated generator torque value is then used to compute the electric power reference P_{ref} through multiplication with the filtered generator speed $\omega_{gen,f}$.
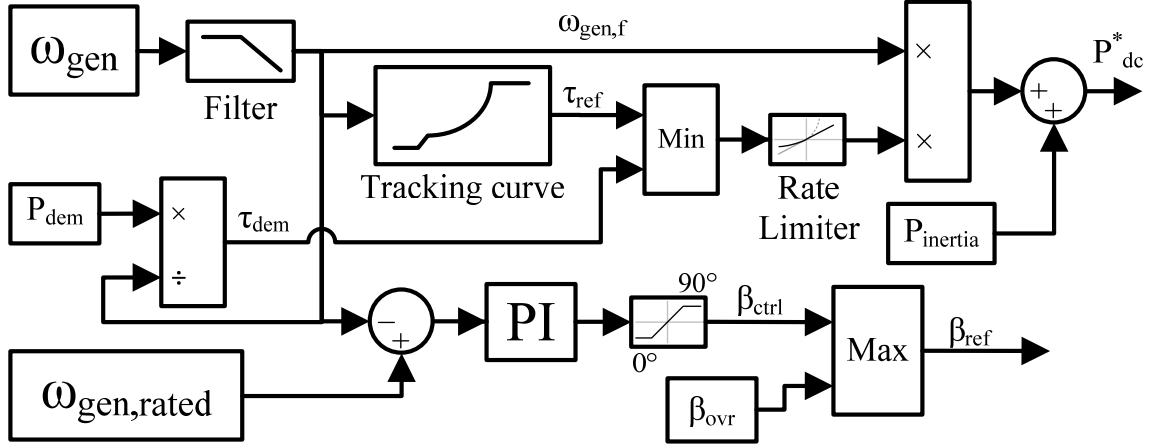
Figure 4.1 Wind turbine speed and pitch control scheme for the proposed wind farm configuration

Pitch control is implemented as in [84], where a PI controller is employed to use blade pitch to prevent generator speeds above its rated value $\omega_{gen,rated}$. While generator speed is below its rated value, the control pitching angle β_{ctrl} is held at zero and wind-up of the PI controller is suppressed. [84] employs gain scheduling for the PI controller gains for improved controller performance, which has also been adopted for this wind farm configuration. To enable additional operational modes, such as those during wind turbine startup and shutdown, an additional pitching reference override signal β_{ovr} has been added. The final pitching angle reference signal β_{ref} then becomes the maximum value of β_{ctrl} and β_{ovr}. To implement power curtailment capabilities, a maximum power demand signal P_{dem} is included. Finally, the reference power P_{dc}^* can be biased using the signal $P_{intertia}$ to provide the ability to implement farm-wide inertial response. These additional operational modes are discussed in following subsections, as well as in Chapter 6.

4.2 Operational Limits with Dual-Active Bridge Converters as PPPCs

The presented wind farm configuration employs PPPCs to realize differential power processing. As a result, the operating points of PPPCs are related to the output power differences within a wind farm. Each DAB within the PPPC is realized with finite component ratings. To ensure that DABs are operated within their ratings, wind turbine converter control presented in section 4.3 includes a model predictive component to limit controller reference and output variables. Furthermore, the determination of DAB component ratings itself is discussed in Chapter 5. For both control and determination of converter ratings, relations are needed to predict at which operating points given DAB converter ratings are violated. This section discusses the basic relations. Further derivations are presented in later chapters for the purpose of converter sizing and wind turbine startup considerations.

For a IPOS-connected DAB in this wind farm configuration, there are a number of parameters which are affected by the differential power processing operation. Some other parameters are solely influenced by the absolute output power of each wind turbine. Most notably, the following ratings are dominantly related to the absolute wind turbine output power:

- DAB primary bridge IGBT voltage rating (determined from V_{Gdc} at rated output power)
- DAB secondary bridge IGBT current rating (determined from DAB operation at 90° phase shift, rated wind turbine power, zero DAB output voltage, and rated HVDC-link current)

However, other parameters are determined based on the differential power processing nature of operation, such as:

- DAB transformer turns ratio N_{ps} and leackage inductance L_t, as it relates to:
  - Maximum DAB power
  - DAB primary bridge IGBT current rating
- DAB secondary bridge IGBT and output capacitor C_o voltage rating

4.2.1 DAB power limit

In the following, relations relating to the latter set of parameters will be derived. As stated in equation (3.7) the DAB output power is given as:

$$P_{MC} = \frac{V_{Gdc}V_{oMC}N_{ps}}{2\pi f_s L_t} \phi \left(1 - \frac{|\phi|}{\pi}\right) \tag{4.1}$$

Maximum power values are obtained for a phase shift ϕ at $\pm\frac{\pi}{2}$ [79]. Hence, ϕ must be constrained to the interval $[-\frac{\pi}{2}; \frac{\pi}{2}]$.

4.2.2 DAB current limit

The peak transformer current on its primary side $I_{L,pk}$ can be calculated for SPS modulation as [79]:

$$i_{L,pk} = \max(|i_{L0}| \quad |i_{L1}|) \frac{V_{Gdc}}{2\pi f_s L_t} \tag{4.2}$$

where i_{L0} and i_{L1} mark characteristic saddle or extremum points of the transformer current waveform, as defined in Figure 4.2.
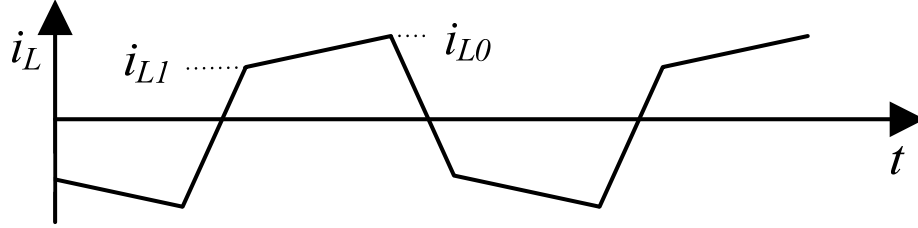
Figure 4.2 Definition of DAB transformer current points i_{L0} and i_{L1}

According to [79], these points can be calculated for SPS modulation as follows:

$$i_{L0} = \begin{cases} \dfrac{(1+m)\phi}{2} + \dfrac{(1-m)(\pi-\phi)}{2}, & \phi > 0 \\ 0.5[-2m\phi + (1-m)\pi], & \phi < 0 \wedge m < 1 \\ 0.5[-(m-1)\pi], & \phi < 0 \wedge m > 1 \end{cases} \tag{4.3}$$

$$i_{L1} = \begin{cases} \dfrac{(1+m)\phi}{2} - \dfrac{(1-m)(\pi-\phi)}{2}, & \phi > 0 \\ 0.5[-(m-1)\pi], & \phi < 0 \wedge m < 1 \\ 0.5[2\phi - (m-1)\pi], & \phi < 0 \wedge m > 1 \end{cases} \tag{4.4}$$

For improved clarity, these functions can be rewritten to highlight their linear nature:

$$i_{L0} = \begin{cases} m\phi + \dfrac{1-m}{2}\pi, & \phi > 0 \\[2mm] -m\phi + \dfrac{1-m}{2}\pi, & \phi < 0 \wedge m < 1 \\[2mm] \dfrac{1-m}{2}\pi & \phi < 0 \wedge m > 1 \end{cases} \tag{4.5}$$

$$i_{L1} = \begin{cases} m\phi - \dfrac{1-m}{2}\pi, & \phi > 0 \\[2mm] \dfrac{1-m}{2}\pi, & \phi < 0 \wedge m < 1 \\[2mm] \phi - \dfrac{m-1}{2}\pi, & \phi < 0 \wedge m > 1 \end{cases} \tag{4.6}$$

In (4.3)-(4.6), m is the DAB converter gain and ϕ is the phase shift in radians of the SPS modulation. m is given as:

$$m = N_{ps}V_{oMC}/V_{Gdc} \tag{4.7}$$

To predict the violation of DAB switch current ratings, $\overline{i_{L,pk}}$ can be calculated and compared to component current ratings on the DAB's primary side. To examine component current ratings on the secondary side, $\overline{i_{L,pk}}$ is multiplied by N_{ps} prior to evaluation of component ratings.

Conversely, in order to limit ϕ to values such that a particular transformer peak current is not exceeded during control loop execution, equations (4.3) and (4.4) can be solved for ϕ, using rated values for the transformer peak current:

$$\phi_{L0} = \begin{cases} \dfrac{2i_{L0} - (1-m)\pi}{2m}, & 2i_{L0} > (1-m)\pi \\[2mm] \dfrac{(1-m)\pi - 2i_{L0}}{2m}, & i_{L0} > \dfrac{1-m}{2}\pi \wedge m < 1 \end{cases} \tag{4.8}$$

$$\phi_{L1} = \begin{cases} \dfrac{2i_{L1} + (1-m)\pi}{2}, & i_{L1} > \dfrac{m-1}{2}\pi \\[2mm] \dfrac{2i_{L1} + (m-1)\pi}{2}, & i_{L1} < \dfrac{1-m}{2} \wedge m > 1 \end{cases} \tag{4.9}$$

where ϕ_{L0} and ϕ_{L1} represent the phase angles that correspond to a particular i_{L0} and i_{L1} current, respectively. In this reformulation, the conditions on ϕ from (4.3) and (4.4) have been rewritten in terms of i_{L0} and i_{L1}. In order to estimate the maximum and minimum allowable phase angles, ϕ_{max} and ϕ_{min}, to not exceed a maximum peak current rating $\overline{i_{L,pk}}$, variables i_{L0} and i_{L1} can be substituted by $\overline{i_{L,pk}}$. It is important to note, that $\overline{i_{L,pk}}$ is normed to $\frac{V_{Gdc}}{2\pi f_s L_t}$ just as i_{L0} and i_{L1} are in (4.2). While a current rating $\overline{i_{L,pk}}$ would be defined as a strictly positive value, i_{L0} and i_{L1} can be non-positive under

certain operating conditions. Therefore, it is important to consider $\pm\overline{i_{L,pk}}$ such that conditions in (4.3) and (4.4) are fulfilled in the equations derived from it. In the following, $\pm\overline{i_{L,pk}}$ are considered for each line in (4.8) and (4.9) individually, such that the sign of $\pm\overline{i_{L,pk}}$ matches the signs of i_{L0} and i_{L1}, respectively.

Regarding the first line in (4.5):

$$i_{L0,0} = m\phi_{L0,0} + \frac{1-m}{2}\pi, \qquad \phi_{L0,0} > 0 \wedge m > 0 \tag{4.10}$$

In this equation, the postfix ',0' refers to the first line in the equation for i_{L0}. ϕ_{L0} denotes the phase angle ϕ corresponding to i_{L0}. In the following, the same principle will be applied to all lines in (4.5) and (4.6).

In (4.10):

$$i_{L0,0} \geq 0, if: \quad \phi_{L0,0} \geq \frac{m-1}{2m}\pi \tag{4.11}$$

$$i_{L0,0} < 0, if: \quad \phi_{L0,0} < \frac{m-1}{2m}\pi \tag{4.12}$$

It should be noted, that $m > 0$ and $\phi_{L0,0} > 0$ in this case. Therefore, substituting $\pm\overline{i_{L,pk}}$ for i_{L0} in the first line of (4.8) yields a maximum phase shift $\phi_{L0,0,max}$:

$$\phi_{L0,0}(m) = \begin{cases} \dfrac{2\overline{i_{L,pk}} - (1-m)\pi}{2m}, & \overline{i_{L,pk}} > \dfrac{(1-m)\pi}{2} \wedge \phi_{L0,0} \geq \dfrac{m-1}{2m}\pi \\ \dfrac{-2\overline{i_{L,pk}} - (1-m)\pi}{2m}, & -\overline{i_{L,pk}} > \dfrac{(1-m)\pi}{2} \wedge \phi_{L0,0} < \dfrac{m-1}{2m}\pi \\ \dfrac{\pi}{2} & otherwise \end{cases} \tag{4.13}$$

In (4.13), it should be noted that the conditions are self referencing in terms of $\phi_{L0,0}$. For the purpose of implementation, all possible solutions for $\phi_{L0,0}$ should be computed and those not fulfilling the stated conditions should be discarded. As (4.8) and (4.9) represent a set of linear functions, only one line in (4.13) will be valid at a time. This is also indicated in Figure 4.3. For any discarded values, $\phi_{L0,0}$ is assigned the value $\frac{\pi}{2}$ which, in practical application, is equivalent to discarding its value.
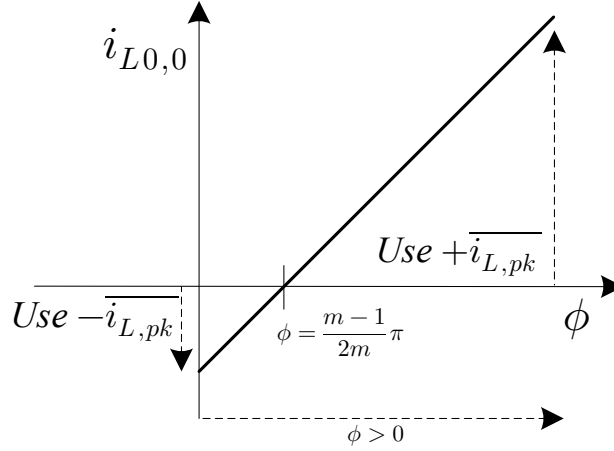
Figure 4.3 Relationship between $i_{L0,0}$ and ϕ, and polarity of $\overline{i_{L,pk}}$

Regarding the second line in (4.5):

$$i_{L0,1} = -m\phi_{L0,1} + \frac{1-m}{2}\pi, \qquad \phi_{L0,1} < 0 \wedge 0 < m < 1 \tag{4.14}$$

In this equation, the postfix ',1' refers to the second line in the equation for i_{L0}. ϕ_{L0} denotes the phase angle ϕ corresponding to i_{L0}. In the following, the same principle will be applied to all lines in (4.5) and (4.6).

In (4.14):

$$i_{L0,1} \geq 0, if: \quad \phi_{L0,1} \leq \frac{1-m}{2m}\pi \tag{4.15}$$

$$i_{L0,1} < 0, if: \quad \phi_{L0,1} > \frac{1-m}{2m}\pi \tag{4.16}$$

It should be noted, that $0 \leq m < 1$ and $\phi_{L0,1} < 0$ in this case. As a result, the term $\frac{1-m}{2m}\pi$ is always non-negative, resulting in $i_{L0,1}$ to always be non-negative according to the conditions in (4.15) and (4.16). Therefore, substituting $-\overline{i_{L,pk}}$ for i_{L0} in the second line of (4.8) yields a minimum phase shift $\phi_{L0,1,min}$:

$$\phi_{L0,1,min}(m) = \begin{cases} \dfrac{-2\overline{i_{L,pk}} + (1-m)\pi}{2m}, & -\overline{i_{L,pk}} > \dfrac{(1-m)\pi}{2} \wedge 0 < m < 1 \\ -\dfrac{\pi}{2} & otherwise \end{cases} \tag{4.17}$$

For the purpose of implementation, solutions for $\phi_{L0,1}$ not fulfilling the stated conditions should be discarded. Equation (4.17) is also illustrated in Figure 4.4. For any discarded values, $\phi_{L0,1}$ is assigned the value $-\frac{\pi}{2}$ which, in practical application, is equivalent to discarding its value.

56
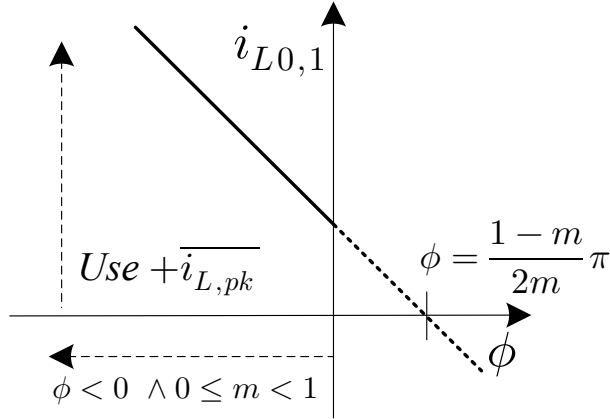
Figure 4.4 Relationship between $i_{L0,1}$ and ϕ, and polarity of $\overline{i_{L,pk}}$

Regarding the first line in (4.6):

$$i_{L1,0} = m\phi_{L1,0} - \frac{1-m}{2}\pi, \qquad \phi_{L1,0} > 0 \wedge m > 0 \tag{4.18}$$

In (4.18):

$$i_{L1,0} \geq 0, if: \quad \phi_{L1,0} \geq \frac{1-m}{2m}\pi \tag{4.19}$$

$$i_{L1,0} < 0, if: \quad \phi_{L1,0} < \frac{1-m}{2m}\pi \tag{4.20}$$

It should be noted, that $m > 0$ and $\phi_{L1,0} > 0$ in this case. Therefore, substituting $\pm\overline{i_{L,pk}}$ for i_{L1} in the first line of (4.9) yields a maximum phase shift $\phi_{L1,0,max}$:

$$\phi_{L1,0}(m) = \begin{cases} \dfrac{2\overline{i_{L,pk}} + (1-m)\pi}{2m}, & \overline{i_{L,pk}} > \dfrac{(m-1)\pi}{2} \wedge \phi_{L1,0} \geq \dfrac{1-m}{2m}\pi \\ \dfrac{-2\overline{i_{L,pk}} + (1-m)\pi}{2m}, & -\overline{i_{L,pk}} > \dfrac{(m-1)\pi}{2} \wedge \phi_{L1,0} < \dfrac{1-m}{2m}\pi \\ \dfrac{\pi}{2} & otherwise \end{cases} \tag{4.21}$$

In (4.21) it should be noted that the conditions are self referencing in terms of $\phi_{L1,0}$. For the purpose of implementation, all possible solutions for $\phi_{L1,0}$ should be computed and those not fulfilling the stated conditions should be discarded. As (4.8) and (4.9) represent a set of linear functions, only one line in (4.21) will be valid at a time. This is also indicated in Figure 4.5. For any discarded values, $\phi_{L1,0}$ is assigned the value $\frac{\pi}{2}$ which, in practical application, is equivalent to discarding its value.
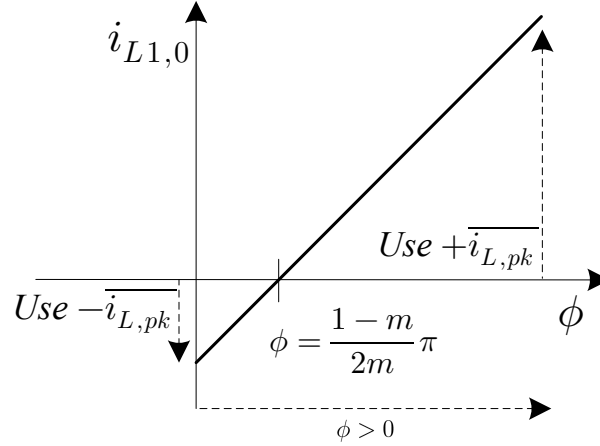
Figure 4.5 Relationship between $i_{L1,0}$ and ϕ, and polarity of $\overline{i_{L,pk}}$

Regarding the second line in (4.6):

$$i_{L1,1} = \phi_{L1,1} - \frac{m-1}{2}\pi, \qquad \phi_{L1,1} < 0 \wedge m > 1 \tag{4.22}$$

In (4.22):

$$i_{L1,1} \geq 0, if: \quad \phi_{L1,1} \geq \frac{m-1}{2}\pi \tag{4.23}$$

$$i_{L1,1} < 0, if: \quad \phi_{L1,1} < \frac{m-1}{2}\pi \tag{4.24}$$

It should be noted, that $m > 1$ and $\phi_{1,1} < 0$ in this case. As a result, the term $\frac{m-1}{2}\pi$ is always non-negative, resulting in $i_{L1,1}$ to always be negative according to the conditions in (4.23) and (4.24). Therefore, substituting $-\overline{i_{L,pk}}$ for i_{L1} in the second line of (4.8) yields a minimum phase shift $\phi_{L1,1,min}$:

$$\phi_{L1,1,min}(m) = \begin{cases} -\overline{i_{L,pk}} + \dfrac{(m-1)\pi}{2}, & -\overline{i_{L,pk}} < \dfrac{(1-m)\pi}{2} \ \wedge \ m > 1 \\ -\dfrac{\pi}{2} & otherwise \end{cases} \tag{4.25}$$

For the purpose of implementation, solutions for $\phi_{L1,1}$ not fulfilling the stated conditions should be discarded. Equation (4.25) is also illustrated in Figure 4.6. For any discarded values, $\phi_{L1,1}$ is assigned the value $-\frac{\pi}{2}$ which, in practical application, is equivalent to discarding its value.

58
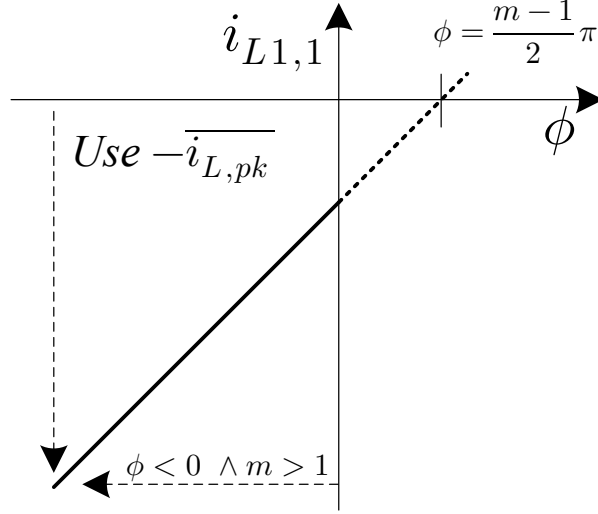
Figure 4.6 Relationship between $i_{L1,1}$ and ϕ, and polarity of $\overline{i_{L,pk}}$

As a result, the maximum and minimum allowable phase angles $\phi_{max}(m)$ and $\phi_{min}(m)$ to prevent primary current rating $\overline{i_{L,pk}}$ violations are derived as the maximum of $\phi_{L0,0,max}(m)$, and $\phi_{L1,0,max}(m)$ and minimum of $\phi_{L0,1,min}(m)$ and $\phi_{L1,1,min}(m)$:

$$\phi_{max}(m) = \min\{\phi_{L0,0,max}(m), \phi_{L1,0,max}(m)\} \qquad (4.26)$$

$$\phi_{min}(m) = \max\{\phi_{L0,1,min}(m), \phi_{L1,1,min}(m)\} \qquad (4.27)$$

As mentioned before, conditions (4.26) and (4.27) were derived for the primary side DAB transformer current. In order to consider secondary side peak transformer currents, the peak current limit $\overline{i_{L,pk}}$ for the secondary side needs to be referred to the primary side by dividing the secondary-side rating by the transformer turns ratio N_{ps}.

4.2.3 DAB output voltage limit

The maximum and minimum values of output voltage of the PPPC are determined by the voltage ratings of switches S5-S8 and S1u-S4u. From (3.4) the HVDC-link current can be related to the PPPC output voltage as:

$$I_{HVDC} = \frac{P_{dc}}{V_{oPPPC} + V_{Gdc}} \qquad (4.28)$$

As a result, to not violate the maximum and minimum PPPC output voltage limits $\overline{V_{oPPPC}}$ and $\underline{V_{oPPPC}}$, the minimum and maximum HVDC-link current values are defined as:

$$\frac{P_{dc}}{\overline{V_{oPPPC}} + V_{Gdc}} < I_{HVDC} < \frac{P_{dc}}{\underline{V_{oPPPC}} + V_{Gdc}} \tag{4.29}$$

Assuming all DABs of a PPPC being designed with the same output voltage limits $\overline{V_{oMC}}$ and $\underline{V_{oMC}}$, $\overline{V_{oPPPC}}$ and $\underline{V_{oPPPC}}$ are equal to the number of multi converters times their respective DAB limits.

To limit the DAB output voltage to its rated value during execution, respective reference values in the DAB control loops for V_{oMC} and/or V_{oPPPC} can be limited to rated values. Assuming a stable control loop with negligible overshoot, this will result in an effective output voltage limitation during regular operation.

4.3   Wind Turbine Converter Control

Each wind turbine contains a control system to control the operation of its PPPC. The primary objective of the PPPC is to realize the electric power reference P_{dc}^* that was obtained from the wind turbine speed control loops discussed in section 4.1.

The control objective is achieved by actively regulating the PPPC output voltage in such a way, that the wind turbine reference power is delivered to the HVDC system. A feedback control loop for the PPPC output voltage was chosen to support stable HVDC link operation, as the onshore station is operating with a feedback control loop for the HVDC link current.

The PPPC control system shown in Figure 4.7 is implemented in three subsystems. In a first subsystem (shown at the top in Figure 4.7), the wind turbine power reference P_{dc}^* is recomputed to a PPPC output voltage reference V_{oPPPC}^*. Following equation (3.4):

$$V_{oPPPC}^* = \frac{P_{dc}^*}{I_{HVDC}} - V_{Gdc} \tag{4.30}$$

Since these relations are derived as DC average values, it is meaningful to low pass-filter the I_{HVDC} measurement to prevent harmonics in I_{HVDC} from being passed on into the PPPC voltage reference calculation. Using the PPPC output voltage reference, an overall PPPC voltage gain reference M_{PPPC}^* is the calculated:

$$M_{PPPC}^* = \frac{|V_{oPPPC}^*|}{V_{Gdc}} N_{PS} \tag{4.31}$$

The PPPC voltage gain reference is used for the determination of number of active DABs within a PPPC and allocation of PPPC output voltage reference to individual DABs.

V^*_{oMC} **calcuation:**

If $M^*_{PPPC} \leq N_{DAB}$:

    For $m=1 \dots floor(M^*_{PPPC})$:

        $V_{*oMC,m} = sign(V^*_{oPPPC}) \times V_{Gdc}/N_{ps}$

    For $m=floor(M^*_{PPPC})+1 \dots N_a$:

        $V_{*oMC,m} = sign(V^*_{oPPPC}) \times V_{Gdc}/N_{ps} \times (M^*_{PPPC} \bmod 1)$

    For $m=N_a+1 \dots N_{DAB}$:

        $V_{*oMC,m} = 0$; *(DAB deactivated)*

 else:

    For $m=1 \dots N_{DAB}$:

        $V_{*oMC,m} = V^*_{oPPPC}/N_{DAB}$
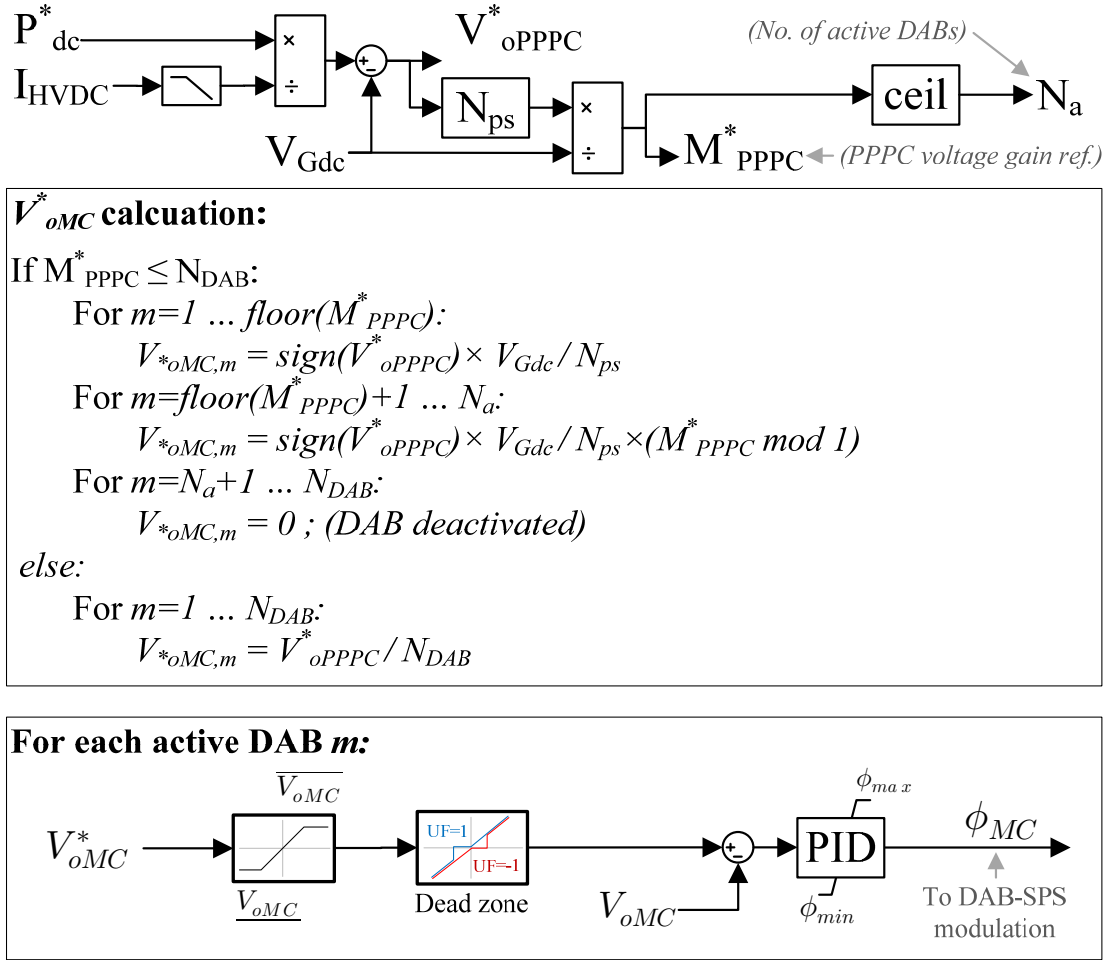
Figure 4.7 Control diagram for PPPCs and each of its DABs

The second subsystem (shown in the center block of Figure 4.7) is used to derive output voltage references V^*_{oMC} for each DAB/multi converter from the PPPC output voltage reference V^*_{oPPPC}. This allocation algorithm is based on two considerations:

1. Maximize number of DABs operating at unity voltage gain

2. Deactivate DABs that are not needed

It is known that for a conventional DAB with SPS modulation, the ZVS operating region is largest at or near a unity voltage gain m [79]. Consequently, it is expected that maximizing the number of DABs operating at unity voltage gain is likely to result

individual DABs operating at high conversion efficiency. Similarly, when the PPPC output voltage is low, only using a fraction of all available DABs may be sufficient with respect to the component ratings of those DABs. This allows to deactivate switching of some DABs and reduces conversion losses further. As a result, the algorithm to allocate the PPPC output voltage reference V_{oPPPC}^* to its DABs as $V_{oMC,m}^*$ is implemented as follows:

- If the PPPC voltage gain M_{PPPC}^* is less or equal than the total number of DABs available, operate $ceil(M_{PPPC}^*)$ DABs at unity gain and allocate the remaining output voltage reference to one other DAB. All other DABs are to be deactivated.

- If the PPPC voltage gain M_{PPPC}^* is larger than the total number of DABs available, the PPPC output voltage reference V_{oPPPC}^* is allocated proportionally to all DABs available

- If the PPPC voltage gain M_{PPPC}^* is zero, all DABs are deactivated.

The third and last subsystem is implemented for each DAB in a PPPC. In this subsystem, the DAB output voltage is regulated to its reference value $V_{oMC,m}^*$ using a closed-loop feedback control loop. In addition, the control loop features measures to ensure that converter component ratings are not exceeded during operation, and that excessive unfolder operations due to undesired harmonics in the voltage reference are avoided. In particular, the converter output voltage rating is enforced by limiting the reference V_{oMC}^* to rated values $\overline{V_{oMC}}$ and $\underline{V_{oMC}}$. Excessive unfolder operations due to noise in the reference value that originates from harmonics in I_{HVDC} are limited by the dead zone that is implemented unfolder polarity-dependent as shown in Figure 4.7. The PPPC output power limitation and current ratings are respected through saturating the PI controller output phase shift at $\phi_{max}(m)$ and $\phi_{min}(m)$ as computed in equations (4.26) and (4.27). In addition to those equations, $\phi_{max}(m)$ and $\phi_{min}(m)$ are computed to respect secondary side current ratings, as well. This has been outlined in section 4.2.2.

4.4 HVDC-Link Current Scheduling with Converter Limits

As outlined in Chapter 3, the scheduling of the HVDC current sets the baseline for the overall wind farm operation, and can be used to minimize power processed by the

PPPCs. In conjunction with variable wind farm output voltage, an HVDC onshore converter topology is required that can handle wider variations of HVDC-link voltage and HVDC-link current without significantly oversizing the converter, and that can actively control the link current. Due to these requirements, a voltage-source converter topology is deemed inappropriate and a current-source converter topology is selected, instead. For the purpose of this study, a twelve-pulse thyristor converter-based onshore station has been chosen.

4.4.1 Derivation of an HVDC-link current scheduling scheme for PPPC power minimization

In this section, a scheduling strategy for a bidirectional IPOS-connected PPPC is derived. The primary objective of the HVDC-link operation strategy has been chosen to minimize the total amount of power processed by all PPPCs in the wind farm. The expectation is that this is likely to improve conversion efficiency, as the amount of DABs incurring switch-mode conversion power losses will be low. The index "n" denominates the n-th out of a total of N operating wind turbines in a series string. Non-operational wind turbines in the series string are simply bypassed as outlined in Chapter 3 and disregarded for this analysis. For all calculations, the assumption of lossless wind turbine operation has been made.

When using a bidirectional PPPC, $P_{PPPC,n}$ can be negative, zero or positive. The minimization of total power processed in the PPPCs and thus maximization of total wind turbine power in the bypass paths can be expressed as a function of I_{HVDC}:

$$\min F(I_{HVDC}) = \min \sum_{n=1}^{N} \left| P_{PPPC,n} \right| \tag{4.32}$$

where F is the total amount of power processed in all PPPCs. Using (3.3) the objective can be rewritten as:

$$\min F(I_{HVDC}) = \min \sum_{n=1}^{N} \sqrt{\left(V_{Gdc,n}(I_{Gdc,n} - I_{HVDC}) \right)^2} \tag{4.33}$$

In general, the condition for minimality is:

$$\frac{dF(I_{HVDC})}{dI_{HVDC}} = 0 \tag{4.34}$$

With given operating conditions, expressed here as $V_{Gdc,n}$ and $I_{Gdc,n}$, the condition for minimality is derived as:

$$\sum_{n=1}^{N} -V_{Gdc,n} \frac{I_{Gdc,n} - I_{HVDC}}{\sqrt{(I_{Gdc,n} - I_{HVDC})^2}} = 0 \tag{4.35}$$

For the purpose of HVDC-link scheduling, (4.33) and/or (4.35) can be used to solve for the optimum I_{HVDC} using algorithms, such as Newton-Raphson, or those discussed in [87] (implemented in MATLAB as '*fzero*' and used in this thesis).

This scheme can be used to derive a reference value I_{HVDC}^* for the current control feedback loop at the onshore station. This reference value has been low pass-filtered with a cutoff frequency of 2Hz to suppress interactions between faster offshore wind turbine controls and the slower I_{HVDC}^* scheduling. This also results in a significantly relaxed performance (bandwidth and delay) requirement on the communication system transmitting wind turbine measurements ($V_{Gdc,n}$, $I_{Gdc,n}$ and I_{HVDC}) to the onshore station.

4.4.2 Derivation of an HVDC-link current scheduling scheme respecting wind turbine converter ratings

The previous scheme was derived without any consideration of wind turbine converter ratings. During operating conditions causing larger deviations of operating poins among wind turbines, it is possible that wind turbine converters would be required to operate beyond their component ratings. As the control loop presented in section 4.3 would prevent individual wind turbines operating beyond their ratings, curtailment of wind energy production would be the consequence. In order to minimize the curtailment of energy production and maximize the available operational range for given wind turbine converter ratings and HVDC system specifications, the previously derived HVDC-link current scheduling scheme is augmented with modes that respect wind turbine converter ratings.

In the following, additional modes for the scheduling scheme will be derived. These modes will be enacted when a previous, higher-priority mode cannot be used due to violation of component ratings. The operating priority of these modes is as follows (1=highest priority, 4=lowest priority):

1. Minimize total PPPC power processed

2. Reduce I_{HVDC} when it is scheduled above a maximum I_{HVDC} to remain within PPPC ratings

3. Increase I_{HVDC} when it is scheduled below a minimum I_{HVDC} to remain within PPPC ratings

4. Increase I_{HVDC} when it is scheduled in such a way that V_{HVDC} is expected to exceed its rated value.

In addition, during inertial response, the HVDC-link current value is being held at its previous value until inertial response is deactivated again.

Modes 2 and 3 require a prediction of which HVDC-link current will cause one or more wind turbine converters to start curtailment due to component ratings being exceeded. For the purpose of this scheme, it is suggested to precompute a 3D lookup table:

$$atLimitCache = f(P_{Gdc} = V_{Gdc}I_{Gdc}, V_{Gdc}, I_{HVDC}) \qquad (4.36)$$

atLimitCache can be precomputed numerically during wind turbine design for all possible operating conditions defined by P_{Gdc}, V_{Gdc} and I_{HVDC} to indicate if such operating condition will cause the violation of a PPPC rating. When there is no violation, *atLimitCache* is equal to zero, while it is equal to one otherwise. To precompute this lookup table, it is important to observe DAB power, current and voltage limits that relate to component ratings within the DABs. This can be achieved using relations discussed previously:

1. DAB power can be calculated using equation (3.3) and multi-converter assignment (Figure 4.7). The required phase shift ϕ can be derived using equation (4.1). This phase shift is required to be within the range of $[-\frac{\pi}{2}; +\frac{\pi}{2}]$.

2. Primary and secondary transformer peak currents can be estimated using relations (4.2)-(4.4). These can be compared against current ratings of adjacent device ratings, such as IGBT peak current ratings.

3. Equation (4.29) can be used to predict a violation of the PPPC output voltage rating.

During realtime execution, *atLimitCache* will be queried for minimum and maximum I_{HVDC} values at which no converter limits are exceeded for each wind turbine. The final minimum and maximum I_{HVDC} values, $\underline{I_{HVDC}}$ and $\overline{I_{HVDC}}$, are the maximum and minimum values of I_{HVDC} limits for each wind turbine.

a. Mode 2: Reduce I_{HVDC} when it is scheduled above a maximum I_{HVDC} to remain within PPPC ratings

If mode 1 results in an I_{HVDC}^* value that exceeds $\overline{I_{HVDC}}$ obtained through the evaluation of *atLimitCache* for each wind turbine in the series string, the maximum value $\overline{I_{HVDC}}$ is used as I_{HVDC}^* instead. As a result, PPPCs with the tightest limits on I_{HVDC} will operate at their limits without energy curtailment, instead of curtailing energy production.

To account for the impact of harmonics in I_{HVDC} measurements, $\overline{I_{HVDC}}$ is being reduced by a safety margin of 0.07 pu in the simulations provided in this chapter.

b. Mode 3: Increase I_{HVDC} when it is scheduled below a minimum I_{HVDC} to remain within PPPC ratings

If modes 1 and/or 2 result in an I_{HVDC}^* value that is below $\underline{I_{HVDC}}$ obtained through the evaluation of *atLimitCache* for each wind turbine in the series string, the minimum value $\underline{I_{HVDC}}$ is used as I_{HVDC}^* instead. As a result, PPPCs with the tightest limits on I_{HVDC} will operate at their limits without energy curtailment, instead of curtailing energy production.

To account for the impact of harmonics in I_{HVDC} measurements, $\underline{I_{HVDC}}$ is being increased by a safety margin of 0.07 pu in the simulations provided in this chapter.

It is worth noting that with mode 3, there is a potential for energy curtailment: if $\overline{I_{HVDC}}$ is less than $\underline{I_{HVDC}}$, there is no solution for which all PPPCs in the series string can operate within their limits. As a result, it is required to operate some PPPCs at their limits and with power curtailment. In this scheduling scheme, a priority has been set for respecting $\underline{I_{HVDC}}$ over $\overline{I_{HVDC}}$. As a result, low-power wind turbines will be kept in operation, while high-power wind turbines will curtail some energy production.

c. Mode 4: Increase I_{HVDC} when it is scheduled in such a way that V_{HVDC} is expected to exceed its rated value.

Since HVDC-link voltage and current are variable in the proposed system, there is a possibility that I_{HVDC} is chosen, such that the resulting V_{HVDC} for a particular operating condition exceeds the rated voltage of the HVDC system, $\overline{V_{HVDC}}$. The estimated HVDC-link voltage based on the I_{HVDC}^* value chosen in modes 1, 2 and/or 3 can be calculated as:

$$V_{HVDC,est} = \frac{1}{I^*_{HVDC}} \sum_{n=1}^{N} P_{Gdc,n} \qquad (4.37)$$

where N is the number of wind turbines in the series string. If $V_{HVDC,est} > \overline{V_{HVDC}}$, the HVDC-link current reference I^*_{HVDC} is altered to:

$$I^*_{HVDC} = \frac{1}{\overline{V_{HVDC}}} \sum_{n=1}^{N} P_{Gdc,n} \qquad (4.38)$$

4.5 HVDC-link Current Scheduling during Loss of Communication

In the event of a temporary communication system outage, the previously discussed HVDC-link current scheduling scheme cannot be applied due to its reliance on P_{Gdc} and V_{Gdc} measurements. To enable the continuation of power production in such circumstances, a fallback HVDC-link current scheduling scheme can be implemented. The presented scheme is derived from the $V_{Gdc} = f(P_{mech})$ and $I_{Gdc} = g(P_{mech})$ relations presented in Figure 3.6. An I_{HVDC}/V_{HVDC} characteristic is derived by solving the set of equations f and g for I_{Gdc}/V_{Gdc} and upscaling V_{Gdc} by the number of series-connected wind turbines. For extreme voltages, I_{HVDC} is held constant. The resulting HVDC-link current scheduling law is shown in Figure 4.8 for the wind farm parameters discussed in section 3.6.
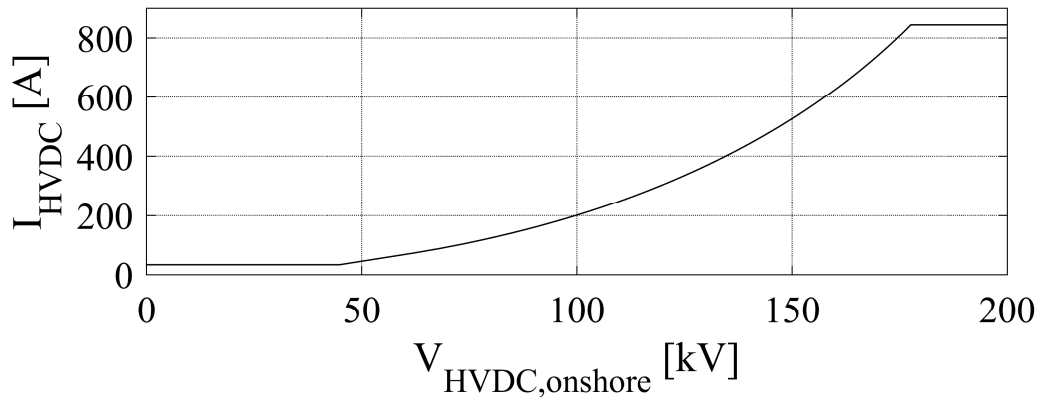
Figure 4.8 HVDC-link current scheduling scheme during communication outages

While this scheme only relies on local measurements at the onshore station, it is impossible to optimize wind farm operation for a particular objective (e.g., minimize total power processed by all PPPCs). During extreme operating conditions, this scheme may result in premature energy curtailment. However, because local wind turbine converter controls prevent exceeding converter ratings, this operation is safe for wind turbine converters. However, the presented scheme does not prevent excessive HVDC-link voltages. For this reason, it would be necessary to add a simple protection scheme at the wind farm site that monitors the HVDC-link voltage and triggers wind turbine curtailment or deactivation during excessive HVDC-link voltages.

4.6 Ancillary Services

In this section, the provision of key ancillary services is discussed. These encompass low voltage ride through (LVRT), active power control and inertia response. Reactive power and AC voltage control services would be implemented equivalently to those in thyristor-based HVDC systems, using STATCOMs, switched capacitors and/or synchronous condensers, or would be implemented through the use of an MMC-based onshore station [86]. For this reason, reactive power and AC voltage control services are not discussed further in this thesis.

4.6.1 Low-Voltage Ride-Through

During low AC voltage, limited ability by the grid to absorb active power requires alternate means of dissipating or reducing wind power production. Current offshore wind farms rely on braking resistors at the onshore station to dissipate wind energy during the fault [88] while all offshore systems continue normal operation. This solution has been adapted for the proposed system and is shown in Figure 4.9. A series string of braking chopper modules is inserted into the HVDC link to support I_{HVDC} control during low voltage ride during conditions. Under normal operating conditions, switch S_{bp} is closed to avoid braking chopper switch conduction losses. During an LVRT event, the braking chopper elements are controlled in such a way to maintain tight HVDC-link current control.
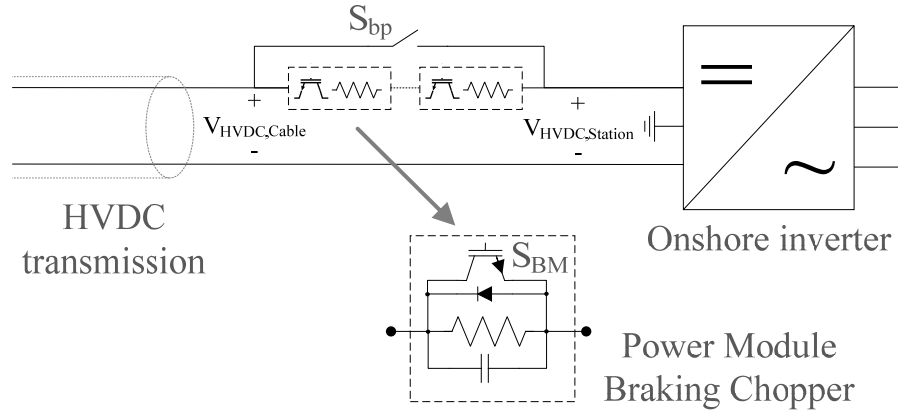
Figure 4.9 HVDC braking chopper to support low voltage ride through.

The HVDC braking chopper is activated ($B_{active} = 1$) when a low AC voltage level is detected, if the HVDC-link current significantly exceeds its reference value by a threshold $I_{b,err,Thres}$, or when the maximum HVDC-link current $I_{HVDC,max}$ is exceeded. This is shown in the block diagram of Figure 4.10
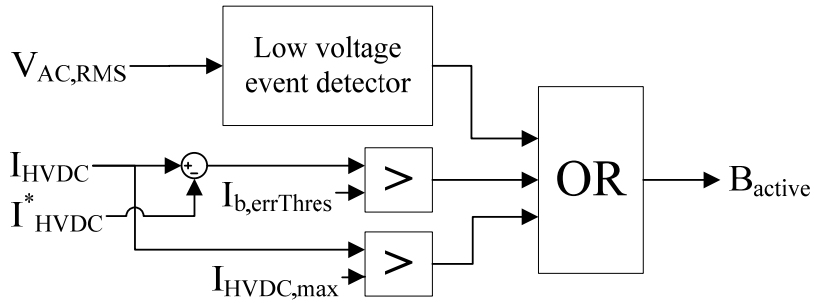
Figure 4.10 LVRT braking chopper activation logic

While the HVDC braking chopper has been activated, a series string of braking modules (as shown in Figure 4.9) is used to maintain a tight control of the HVDC-link current according to its reference value. The control scheme is shown in Figure 4.11.
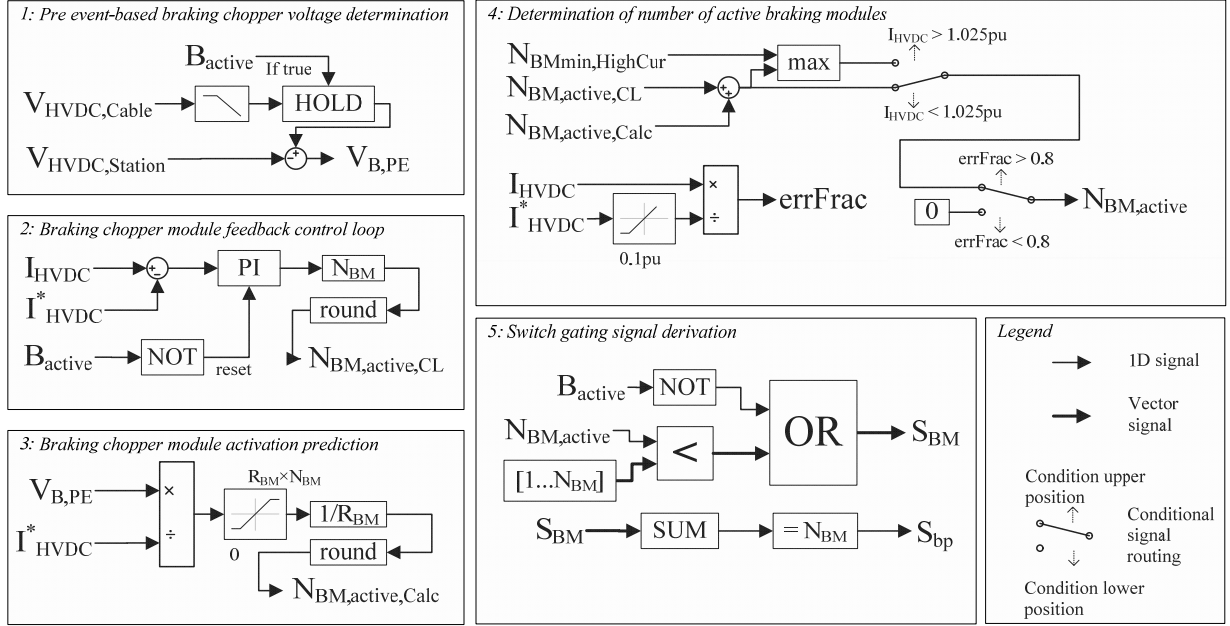
Figure 4.11 LVRT braking chopper control logic

In this control scheme, the number of activated braking modules (S_{BM} signal for such module is equal to zero and switch S_{BM} is off) is determined from a combination of calculation of required braking resistance, and a feedback control loop. The objective of this control is to maintain offshore operating conditions during an LVRT event (i.e., maintain I_{HVDC} at its reference value). For this reason, the cable-side onshore HVDC-link voltage is assumed to be reasonably constant during the time-limited LVRT event (step 1 in Figure 4.11). Based on this assumption, a required braking resistance and number of active braking modules is derived in step 3. To compensate for any deviations and errors, such as in the assumption of step 1, a feedback control loop is added (step 2). In step 4, the number of active braking modules derived from steps 2 and 3 are added. In addition, to ensure timely limitation of excessive HVDC-link currents, a minimum braking resistance is enforced for HVDC-link currents above 1.025pu ($N_{BMmin,HighCur}$). If the HVDC-link current is significantly below its reference value, the braking chopper is deactivated to support the recovery of HVDC-link current ($errFrac < 0.8$). Lastly, to reduce conduction losses during normal operation, the braking chopper bypass switch S_{bp} is activated in step 5, when all braking modules are configured to be bypassed. For the wind farm design presented in section 3.6, the HVDC braking chopper parameters are given in Table 4.1.

70

Table 4.1 HVDC Braking Chopper Parameters

PARAMETER	SYMBOL	DEFAULT VALUE
Number of braking modules	N_{BM}	45
Braking module resistance	R_{BM}	20Ω
Minimum number of active braking modules during high HVDC-link current event	$N_{BM,HighCur}$	20

4.6.2 Power Curtailment / Active Power Control

Active power control allows to reduce wind power production below the maximum power available. The implementation of active power control has been adapted from [89][84]. In [89][84], wind farm power reductions are allocated to individual wind turbines proportionally to the power available, which is obtained from online estimations using nacelle wind speed. In the proposed system, wind power reductions are allocated to the high-power wind turbines first, to reduce output power differences and total PPPC power processed within the series string during power curtailment. The P_{dem} signal of Figure 4.1 on page 51 is leveraged in order to command a certain reference power to each wind turbine. In addition, the pitch control system is used to maintain a rotor speed slightly above that equal to the regular MPP operational speed at demanded power.

4.6.3 Inertial Response

There are several methods to implement an inertia response [90]. The adopted method (Fig. 7 in [90]) is provided in Figure 4.12. During a frequency excursion event, a power reference offset is computed and added to each individual wind turbine's power reference P_{dc}^*. Hence, there are little differences in operation for the proposed electrical system compared to active power control. For the purpose of demonstrating inertial response, the virtual inertia constant H_v has been chosen to be equal to three times the wind turbine's inertia constant ($H_v = 14.82s$).
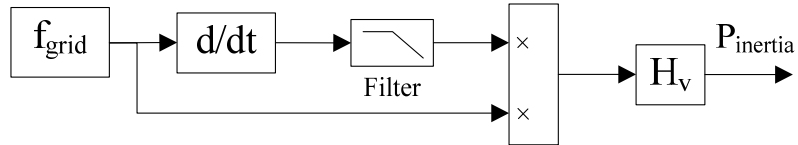
Figure 4.12 Inertia response emulation. H_v is the virtual inertia constant. All other quantities are treated as per-unit values.

4.7 Case Study: a 150MW Offshore Wind Farm

The complete wind farm system has been simulated using a dynamic wind farm model implemented with the Simscape Power Systems toolbox of MATLAB/Simulink. To limit the simulation complexity, a wind farm consisting of 30 wind turbines is modelled using five wind turbine models, each representing six wind turbines. To maintain correct dynamics, the output voltages of each wind turbine model are scaled accordingly. The distance to shore is 100km. The aerodynamic and mechanical sub-system models have been adopted from the NREL 5MW reference wind turbine [81] as implemented in the SimWindFarm toolbox [89][84]. It has been assumed, that a single-stage gearbox is used in conjunction with a 14-pole pair medium-voltage generator, adapted from [33]. Dual-active bridge converters have been simulated using their generalized average model as discussed in [91]. Wind farm parameters are those given in section 3.6. Two scenarios have been chosen to demonstrate the fundamental system operation; wind speed profiles for a staggered step change of wind speeds, and those measured by the five wind turbines of the Wind Energy Institute of Canada (WEICan), located in North Cape, Prince Edward Island, Canada. Further test cases are presented to demonstrate operation near converter ratings, ancillary service performance (LVRT, active power control and inertia response), as well as wind farm operation during a temporary communication system outage.

4.7.1 Normal operation

a. Simulation of wind speed step changes

In this scenario, all wind turbines are first subjected to a rated wind speed of 11.25m/s, followed by staggered step changes to 8.25m/s for six wind turbines at a time. The results, shown in Figure 4.13, demonstrate the stable operation of the wind farm under these conditions. Starting at t=10s, output powers of wind turbines start to differ. As a result, PPPCs are required to start processing power. However, as it can be seen, the maximum amount of power processed by a PPPC in this condition is about 2.5MW ($50\%P_{Base}$) at a maximum V_{oPPPC} of less than 6kV (see Figure 4.13 (e) and Figure 4.13 (f)).

As wind turbine output powers drop, the rectifier currents I_{Gdc} drop, eventually resulting in the scheduling of a lower HVDC-link current. In this particular case, I_{HVDC} follows the I_{Gdc} values of wind turbines 13-18 in order to minimize total PPPC power. As a result, the PPPCs of wind turbines 13-18 do not process any significant power,

except during brief unfolder transitions (see Figure 4.13 (f)). All other PPPCs process the difference in power between their power reference P_{dc}^* and the power absorbed by the HVDC link (equal to $V_{Gdc,n}I_{HVDC}$). As I_{HVDC} drops after t=30s (Figure 4.13 (b)), the PPPC output voltages V_{oPPPC} in Figure 4.13 (e) are required to increase in order to process a similar amount of absolute power difference. This is reflected in the higher positive V_{oPPPC} magnitude of wind turbines 19-30, compared to the negative values of wind turbines 1-12 at earlier times in the simulation. The HVDC-link voltage V_{HVDC} is the sum of all wind turbine output voltages $V_{turbine}$ (shown in Figure 4.13 (c)). The wind turbine output voltage is the sum of V_{Gdc} and V_{oPPPC} for each turbine. Starting at t=10, PPPC output voltages are zero or negative, contributing to a lowering of $V_{turbine}$ and V_{HVDC} (see Figure 4.13 (c) and Figure 4.13 (d)). Starting at t=30s, the HVDC-link current is scheduled to drop in accordance with the scheduling strategy described in section 4.4. This causes active PPPCs to adopt more positive output voltages, resulting in an overall increase of V_{HVDC}. Once I_{HVDC} has settled at the new steady-state operating point near t=40s, V_{HVDC} starts to fall again, as the output power of wind turbines 19-30 continues to fall until t=70s, when the new steady-state operating point has been reached for all turbines.

The operation of DAB converters of wind turbine 1 is shown in Figure 4.14 highlighting the operation of multiple IPOS-connected DABs forming a PPPC. In Figure 4.14 (a) and (c), it can be seen how the PPPC output voltage V_{oPPPC} is synthesized from the output voltages of its four DAB converters, $V_{oC,m}$. While V_{oPPPC} is of low absolute value, only few DAB converters are active and process power to create a non-zero output voltage V_{oC}. Near t=30s, V_{oPPPC} reaches its largest absolute value, which is obtained from the operation of all four DAB converters. As evident from Figure 4.14(e), the DAB output voltage references are set in such a way that as many DAB converters as possible operate at a DAB reference voltage gain M_{DAB}^* equal to one. Unfolder operations, related control loop execution interruptions during unfolder transitions and control loop dead zones (compare to Figure 4.7) can be identified from small transients in the V_{oPPPC} waveform that can be observed in the intervals of t=10s to t=20s and t=30s to t=40s. As it can be seen, the controller is adequate to limit these transients sufficiently. The peak value of the primary-side DAB transformer current for each DAB converter of wind turbine 1 is shown in Figure 4.14 (d). From Figure 4.14 (c) and (d) it can be seen that the PPPC output voltage and input current loading follows the differential power demand of the wind turbine. DAB converters not required for the requested PPPC power are deactivated and associated conversion losses are avoided.

The dominating source of harmonics in the PPPC quantities are the harmonics in the HVDC-link current, resulting from the operation of the onshore thyristor converter.
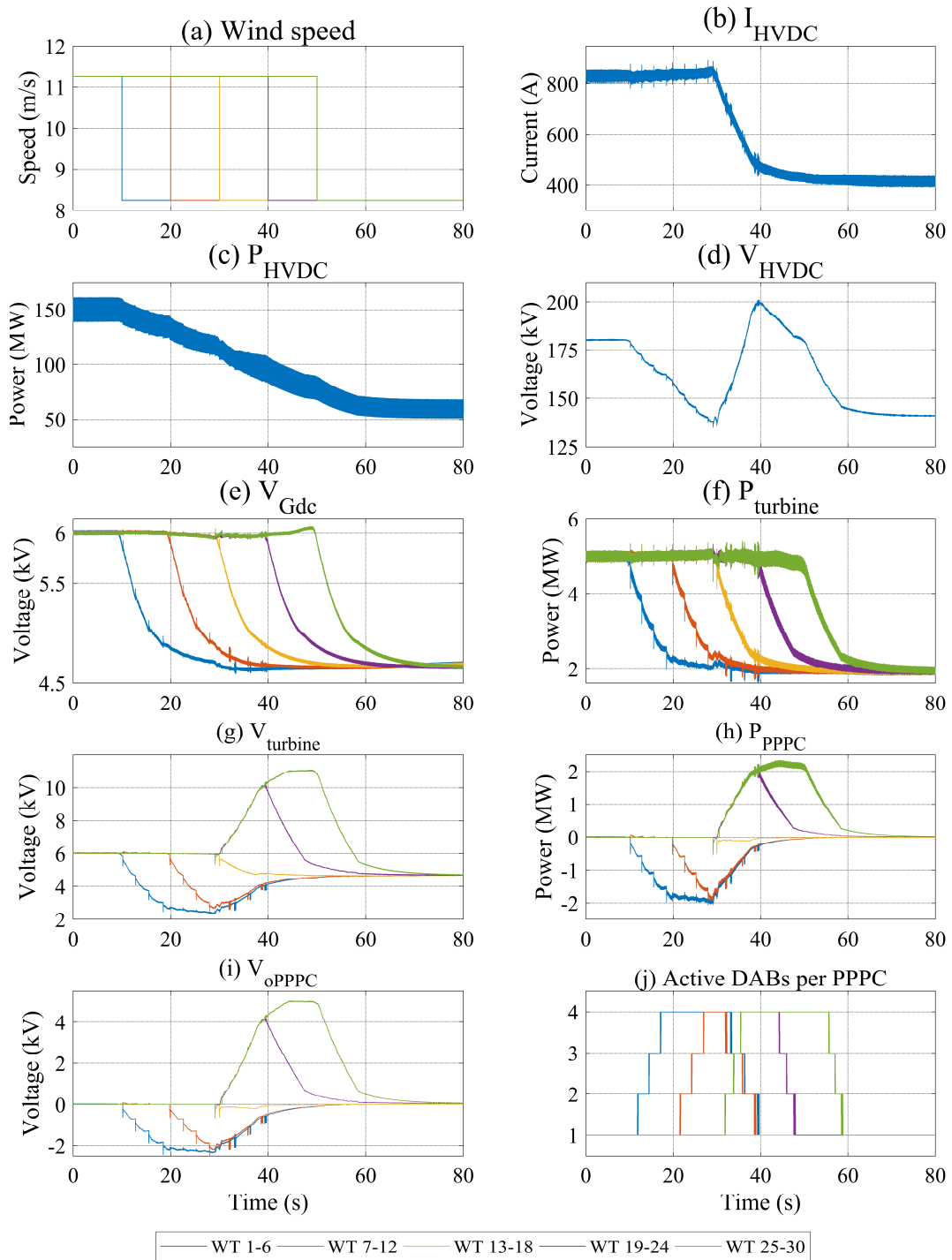
Figure 4.13 Simulation results for 'high wind' profile. "WT" = Wind turbine.

74
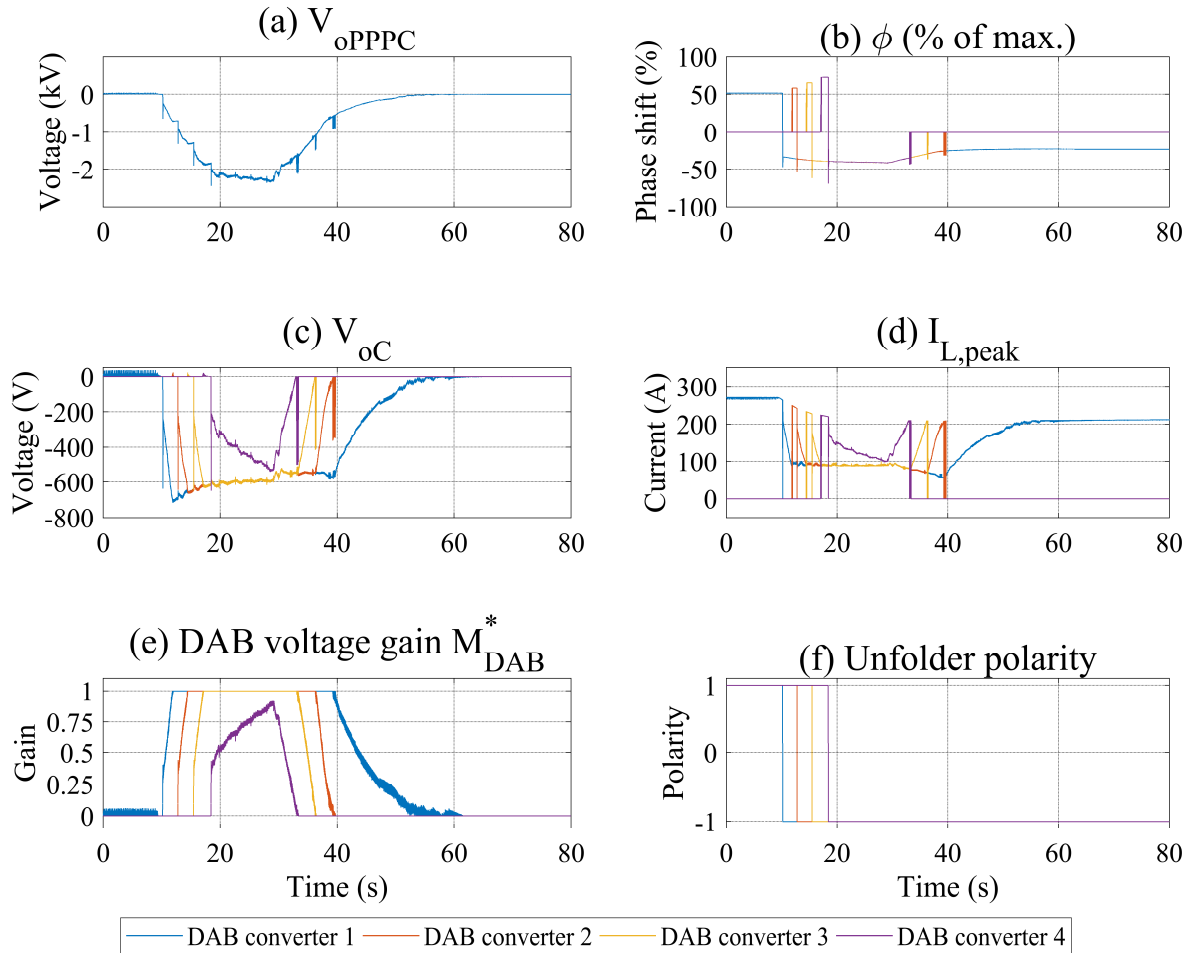
Figure 4.14 Simulation results for 'high wind' profile. Displaying DAB converter quantities for PPPC of wind turbine 1.

b. WEICan wind speed measurements

In a second scenario, 1Hz wind speed measurements from the ultrasonic sensors mounted on the nacelles of the five WEICan wind turbines have been used as inputs to the wind turbine models of this wind farm. A 10 minute profile has been selected in which the wind speeds are above cut-in and below rated wind speed. As can be seen in Figure 4.15 (a), one wind speed signal (WT 7-12) is consistently below that of others. This introduces larger output power differences in the wind farm, similar to those that can be observed due to wake effects. The simulation results shown in Figure 4.15 demonstrate a stable wind farm operation for all wind turbines operating at their MPPs. It can be seen that the PPPC output powers and voltages are well below rated values for wind turbine power (5MW), or rectifier output voltage V_{Gdc} (5.8kV) and are well

below those values obtained from the artificial wind profile considered at first. The most extreme operating points for this scenario are given in Table 4.2. Upon close observation of V_{oPPPC} in Figure 4.15 (i), it can be seen that at any time at least one V_{oPPPC} value is equal to zero. This is a result from the HVDC-link current scheduling algorithm that tends to schedule I_{HVDC} in such a way that at least one PPPC operates with zero power and output voltage to achieve a minimal overall PPPC power. Figure 4.15 (j) shows the number of active DAB converters per PPPC. As V_{oPPPC} for wind turbines 19-24 (purple) tends to be low for the majority of the wind profile, the number of active DAB converters for these wind turbines is also low. In contrast, the low-power wind turbines 7-12 (red) exhibit the largest output power differences with respect to the natural power absorption defined by the scheduled I_{HVDC}. As a result, these wind turbines operate with the largest V_{oPPPC} magnitudes and highest numbers of DAB converters per PPPC for most of the wind profile.

Figure 4.16 shows the DAB converter operation of wind turbine 7 that is operating the most heavily loaded PPPCs. In Figure 4.16 (a) and (c), the relation between PPPC output voltage V_{oPPPC} and individual DAB converter output voltages $V_{oC,m}$ becomes apparent. For most of the simulation, $M_{DAB,m}$ is larger than one. For this reason, all DAB converters operate with the same output voltage. Around t=400s and after t=550s, the magnitude of V_{oPPPC} is low enough, such that selected DAB converters can temporarily operate at lower loading or be deactivated entirely.

Table 4.2 Extreme PPPC and DAB Operating Points for WEICAN Scenario

QUANTITY	MAXIMUM VALUE	MINIMUM VALUE
P_{PPPC}	1.42 MW	-1.95 MW
V_{oPPPC}	3 kV	-2.77 kV
$V_{oC,m}$	810 V	-693 V
$I_{L,peak}$	267 A	
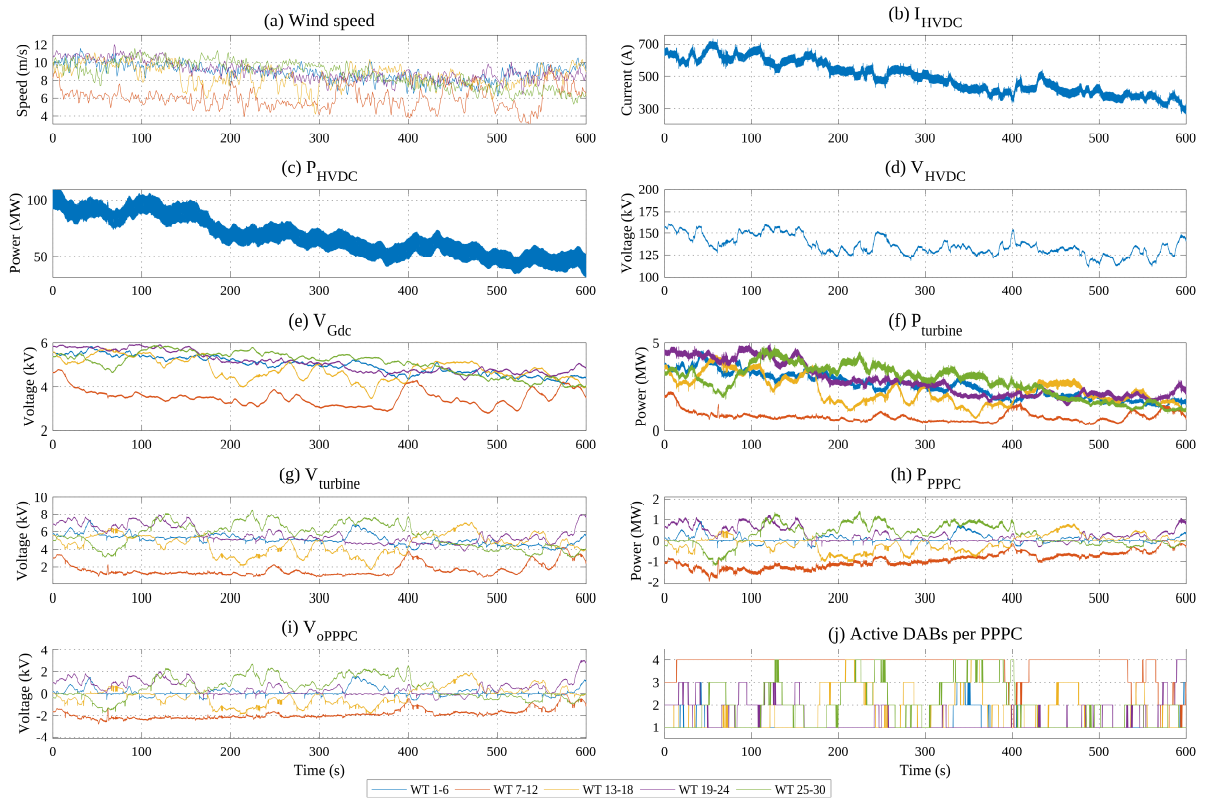
Figure 4.15 Simulation results for the WEICan wind profile. "WT" = Wind turbine.
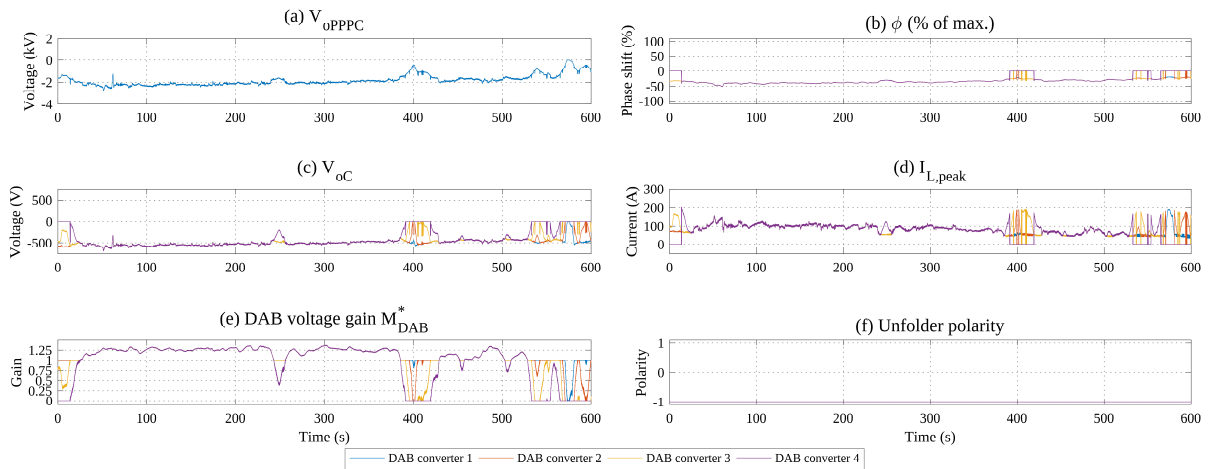
Figure 4.16 Simulation results for the WEICan wind profile. Displaying DAB converter operation for wind turbine 7.

4.7.2 Operation near Converter Ratings

The objective of this section is to verify the proper operation of the wind farm in scenarios in which converter limits might be violated, if not protected against. The expected behaviour would be that PPPC control loops limit DAB operating points in such a way that no rating (current, voltage or power transfer) is violated. Further impacts to the wind farm system may occur as a result that may reduce the amount of energy produced, but no component will operate beyond its limits. To test this, two test cases have been designed. In the first test case, wind turbines operate at rated power while one set of wind turbines experiences a ramp change of wind speed towards cut-in wind speed. In the second test case, wind turbines operate near cut-in wind speed, while one set of wind turbines experiences a wind speed ramp towards rated wind speed (full power operation). PPPC ratings have been chosen such that converter ratings will be violated well before the final steady-state operation is reached.

For simulations in this section, each PPPC has been realized with two DABs, each rated at 0.215pu output voltage, 0.36pu input current, and the transformer leackage inductance is 740μH. All other parameters remain the same as before.

The simulation results of the first test case are shown in Figure 4.17. As seen in Figure 4.17 (a), wind speeds for wind turbines 7-30 are constant at 11.25 m/s, the rated wind speed. Wind speed for wind turbines 1-6 start at 10m/s and ramp down towards cut-in wind speed. Since the events of interest happen before cut-in wind speed is reached, the simulation has been ended after 70 seconds. Figure 4.17 (b) shows the HVDC link current values: the reference value $I_{HVDC,ref}$ is shown in red, the actual HVDC-link current I_{HVDC} is shown in blue, the maximum possible HVDC-link current to not violate any converter limits of active wind turbines, $I_{HVDC,max}$, is shown in yellow, and the minimum possible HVDC-link current to not violate any converter limits of active wind turbines, $I_{HVDC,min}$, is shown in purple. The HVDC scheduler mode is shown in Figure 4.17 (j). The scheduler modes are denominated as follows, similar to the presentation in section 4.4.2:

1. Minimize total PPPC power processed

2. Reduce I_{HVDC} when it is scheduled above a maximum I_{HVDC} to remain within PPPC ratings

3. Increase I_{HVDC} when it is scheduled below a minimum I_{HVDC} to remain within PPPC ratings
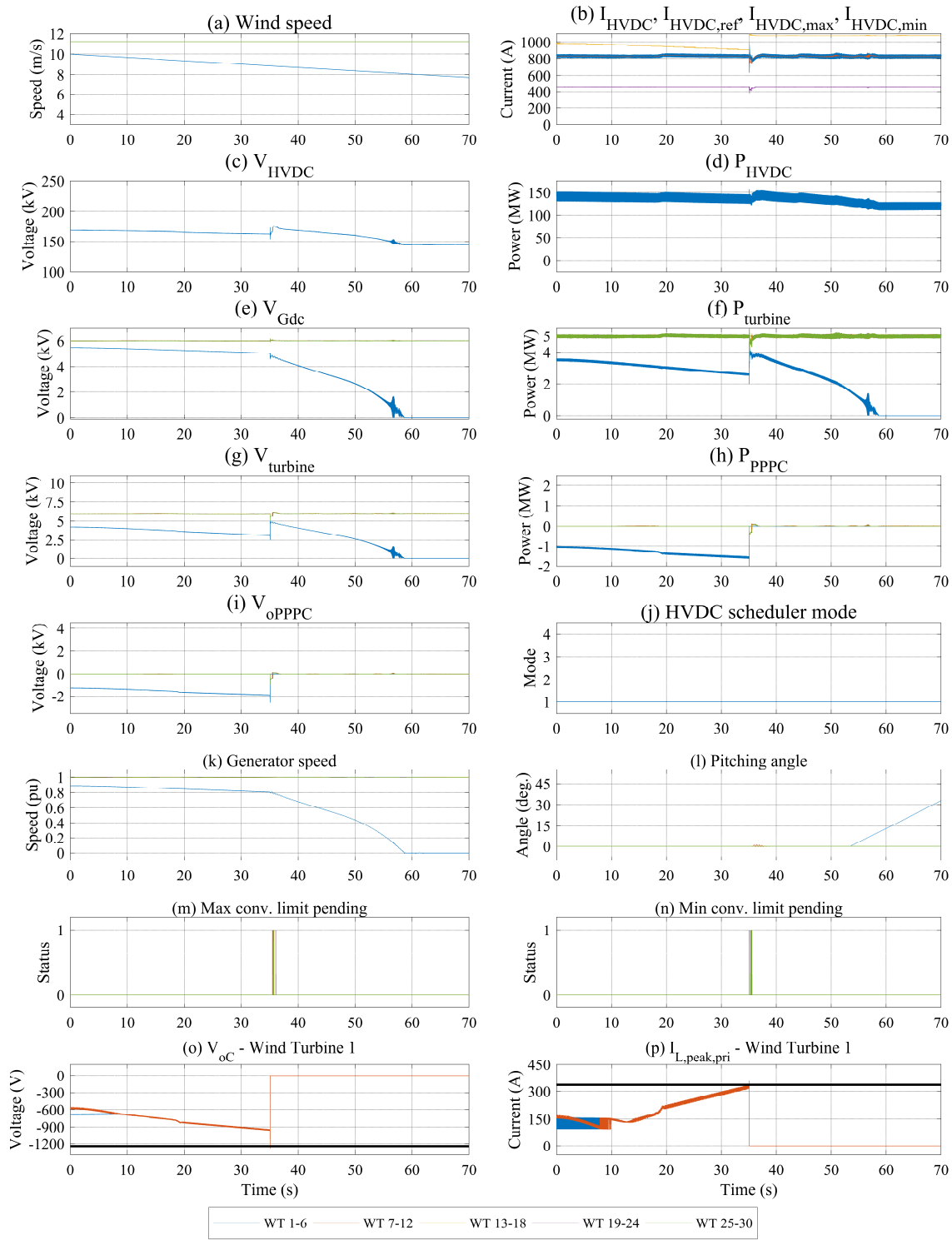
Figure 4.17 Simulation results of the first converter limits test case.

4. Increase I_{HVDC} when it is scheduled in such a way that V_{HVDC} is expected to exceed its rated value.

5. HVDC brake activated due to LVRT event, or to limit high HVDC link current

It can be seen that the HVDC scheduler remains in mode 1 for the entire operation. This means that it operates to minimize the total PPPC power processed by scheduling the HVDC link current at 1pu to match the rectified DBR current in wind turbines 7-30. As a result, those wind turbines are able to operate with their PPPCs deactivated (or only active at times for small controller action), as indicated in Figure 4.17 (i) and (h). Wind turbines 1-6 operate with less output power (Figure 4.17 (f)). As a result, their PPPCs are required to operate with negative output power and voltage. The more their wind speed falls, the more negative output power and voltage become to maintain optimal tip speed ratio. Figure 4.17 (o) displays the DAB output voltages for wind turbine 1: blue indicates V_{oC} for the first DAB, red for the second. As can be seen, initially the first DAB is scheduled to operate with fixed output voltage of 0.12pu, corresponding to M_{DAB} equal to one. The second DAB operates with an increasingly negative output voltage to realize the overall required PPPC output voltage. When both DABs reach M_{DAB} equal to one, they both operate with the same output voltage, as defined in the control laws of section 4.3. The negative output voltage rating is indicated in this graph with a bold black line near -1200V.

Similarly, Figure 4.17 (p) shows the DAB primary-side transformer peak currents for wind turbine 1. The current rating is indicated with a bold black line at 310A.

Whenever a PPPC controller limits PPPC operation due to proximity to maximum or minimum converter ratings, a value of one is shown in Figure 4.17 (m) and Figure 4.17 (n), respectively.

As wind turbines 1-6 produce less power due to a falling wind speed, the maximum possible HVDC link current $I_{HVDC,max}$ continues to fall, as well. This is a result from the changes in wind turbine output power, and DC voltage V_{Gdc} for wind turbines 1-6. Similarly, it can be seen in Figure 4.17 (o) and (p) that DAB voltages and currents approach their rated values. At t=35 s, the DAB current (Figure 4.17 (p)) reaches its rated values. The controllers adjust the SPS phase shift in such a way to maintain operation at rated current and prevent exceeding it. However, due to negative power operation of the DAB, this results in a negative runaway of the DAB output voltages as indicated in Figure 4.17 (o) at t=35 s. Since there is insufficient DAB converter capacity available to stabilize operation at a new steady-state, the DABs are deactivated entirely

when their output voltage reaches rated values (compare to Figure 4.17 (o) at t=35 s). Resulting from the necessary deactivation of DABs in wind turbines 1-6, the wind turbine output power increases. With PPPCs operating with negative power, I_{Gdc} could be held at a value lower than I_{HVDC}, since I_{PPPCin} is negative. With PPPCs deactivated, I_{Gdc} increases to I_{HVDC} and the wind turbine output power becomes equal to $V_{Gdc} \times I_{HVDC}$. Since this power is above the maximum power available from the wind, the wind turbine starts to decelerate quickly until it comes to a halt, as shown in Figure 4.17 (k). As the wind turbine reaches a very low generator speed, the shutdown sequence became activated near t=55s activating the mechanical disc brake and pitching rotors out of the wind. Exact operating schedules in situations like these can be further adjusted, should there be further requirements from the aeromechanical system, such as earlier activation of braking and pitching systems.

At the time when DABs of wind turbines 1-6 become deactivated, these turbines are taken out of consideration for the HVDC-link current scheduling algorithm. This algorithm is only applied to fully operating wind turbines. As a result, the maximum possible HVDC-link current $I_{HVDC,max}$ increases to the value when all wind turbines are operating at rated wind speed following the events at t=35s.

This simulation demonstrates that operation near or at converter limits is possible and that violations of converter limits operating with negative PPPC power can be handled successfully. Necessitated by the DAB output voltage runaway possible at negative converter limits, it usually is required to deactivate a DAB in such conditions and curtailed operation below maximum power cannot be maintained. If such operation was desired, it would be necessary to alter the HVDC-link current scheduling algorithm to prevent a violation of negative PPPC converter limits in the first place. However, this would result in other wind turbines in the wind farm reaching their *maximum* PPPC limits instead, leading to power curtailment. Future work could investigate prediction schemes to decide which scenario is more preferable in different operating conditions.

In the second test case, all wind turbines start operating at a wind speed of 4m/s, as shown in Figure 4.18 (a). Wind speed for wind turbines 1-6 is then ramped up to rated wind speed within 200s. A margin of 0.1pu current has been chosen for HVDC-link current scheduling modes 2 and 3: scheduled HVDC-link current will be kept higher or lower than the absolute extreme value, respectively.
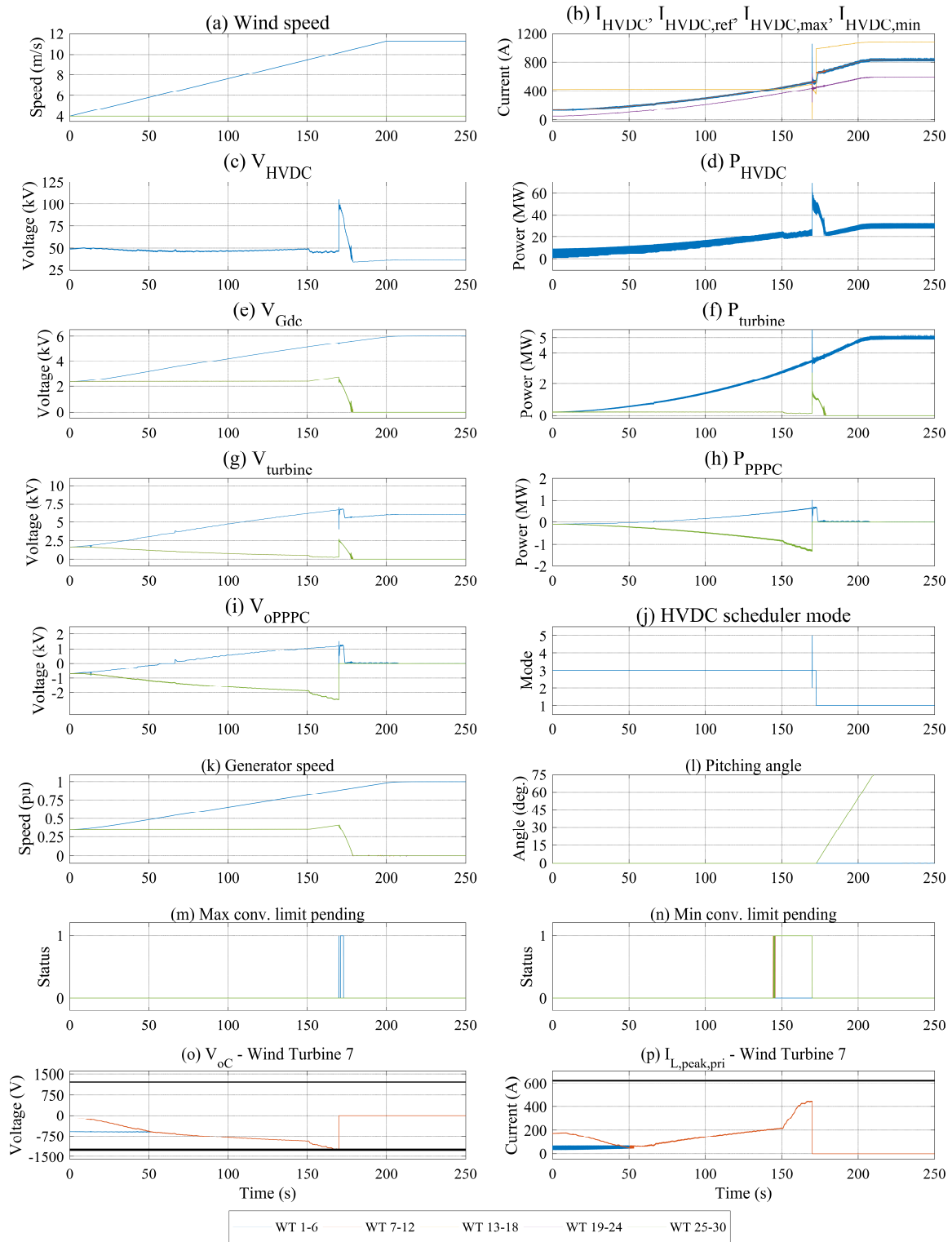
Figure 4.18 Simulation results of second converter limits test case.

For this reason, at t=0s, the HVDC-link current scheduler already operates in mode 3. HVDC-link current for mode 1 would be approx. 0.07pu above minimum HVDC-link current, thus violating the margin selected. As a result, all wind turbine start operating with a slight negative PPPC output power and voltage, as seen in Figure 4.18 (h) and (i). As wind speed for wind turbines 1-6 increases, their output power and generator speed increases according to MPPT (Figure 4.18 (f) and (k)). Likewise, PPPC output voltage and power increase gradually (Figure 4.18 (i) and (h)). Near t=145s, the converters for wind turbines 7-30 reach their maximum negative PPPC power limit (phase shift equal to 90°). As a result, the PPPCs cannot maintain the desired PPPC output voltages anymore and they start to decrease at a faster rate (as seen in Figure 4.18 (i) near t=150s). When the DAB output voltages reach their negative rated value (Figure 4.18 (o)), the DABs are deactivated at t=170s. At that time, the sudden deactivation of 24 PPPCs creates a fast transient on the HVDC link as apparent in Figure 4.18 (c). As a result, the onshore station's current control loop experiences a temporary large transient in HVDC-link current, but is able to maintain stable control (Figure 4.18 (b)). To aid limiting the HVDC-link current excursion during this transient, the HVDC brake chopper is briefly activated, as indicated by the HVDC scheduler mode switching to mode 5 (Figure 4.18 (j)). After this transient has settled, wind turbines 7-30 are outside their normal operating region and proceed a shutdown similar to the previous test case. As a result, only wind turbines 1-6 are included in the HVDC link scheduling from t=170s onward. Consequently, the HVDC-link current is scheduled in such a way that PPPCs of wind turbines 1-6 can operate at or near zero output voltage and power, minimizing the total amount of power processed by PPPCs.

This test case demonstrates that the presented scenario can be handled successfully without violating any converter limits.

4.7.3   Low-Voltage Ride-Through

In this scenario, the wind farm is operating at rated wind speeds and power. At time t=20s, the AC grid voltage amplitude is reduced to 0pu due to a severe grid fault near the wind farm grid connection point. The grid voltage recovers after 4 seconds. As seen in Figure 4.19, the wind farm can maintain stable operation during the fault and resume normal power delivery after the fault. Upon detection of the fault, the braking chopper is activated to take over control of the HVDC-link current. During this time, generated power is dissipated in the chopper resistors, therefore P_{HVDC}, I_{HVDC} and V_{HVDC} remain virtually unchanged. As a result, offshore wind turbine operation can continue nearly

undisturbed and a fast LVRT action is provided. As seen in Figure 4.19 (b), (e) and (f), each wind turbine continues to be exposed to the same HVDC-link current level and maintains the same output voltage and power. Upon fault recovery, the Thyristor converter can resume power delivery, at which point the braking chopper is deactivated and the Thyristor converter resumes full control of the HVDC-link current. As depicted in Figure 4.19 (b) and (c), the transitions between Thyristor converter operation and braking chopper cause transients in the HVDC-link voltage and current. However, these values remain within the range of rated values in addition to commonly chosen safety margins.
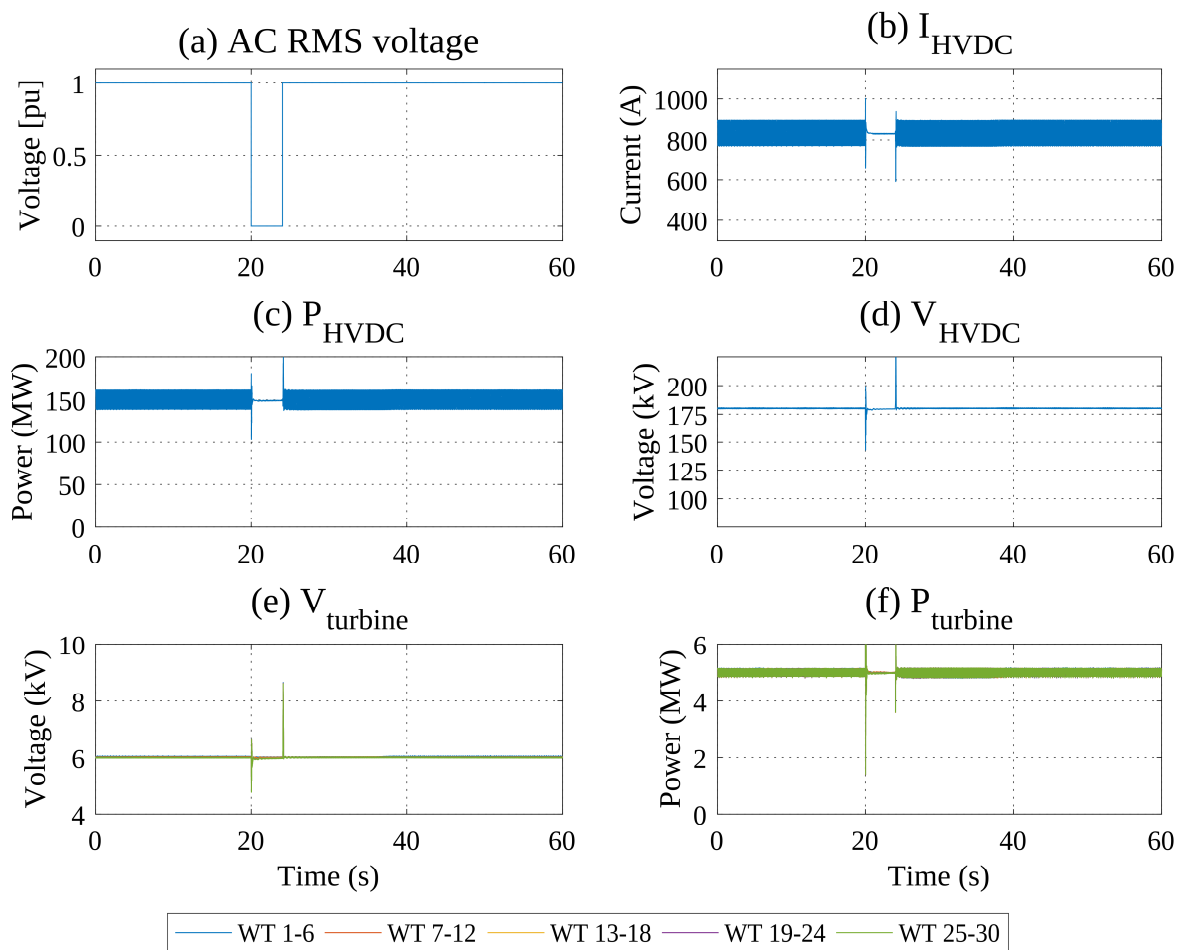
Figure 4.19 Simulation results for LVRT scenario. "WT" = Wind turbine.

4.7.4 Active Power Control / Power Curtailment

In the following scenario, active power curtailment is demonstrated. Here, all wind turbines are operated at a wind speed of 7.5m/s and an MPP farm output power of 45MW. At t=40s, an output power reference of 22.5MW is set for the wind farm. At t=130s, this curtailment request is lifted. The simulation results in Figure 4.20 show that the wind farm can seamlessly transition to curtailment operation and resume regular operation afterwards. In Figure 4.20 (a), the reference and actual wind farm power is shown. As a rate limiter is implemented in the wind turbine control loop (see Figure 4.1), actual wind farm power ramps down until the power reference is reached. As seen in Figure 4.20 (c) and (e), pitch control engages to limit the wind turbine rotational speed during curtailment.
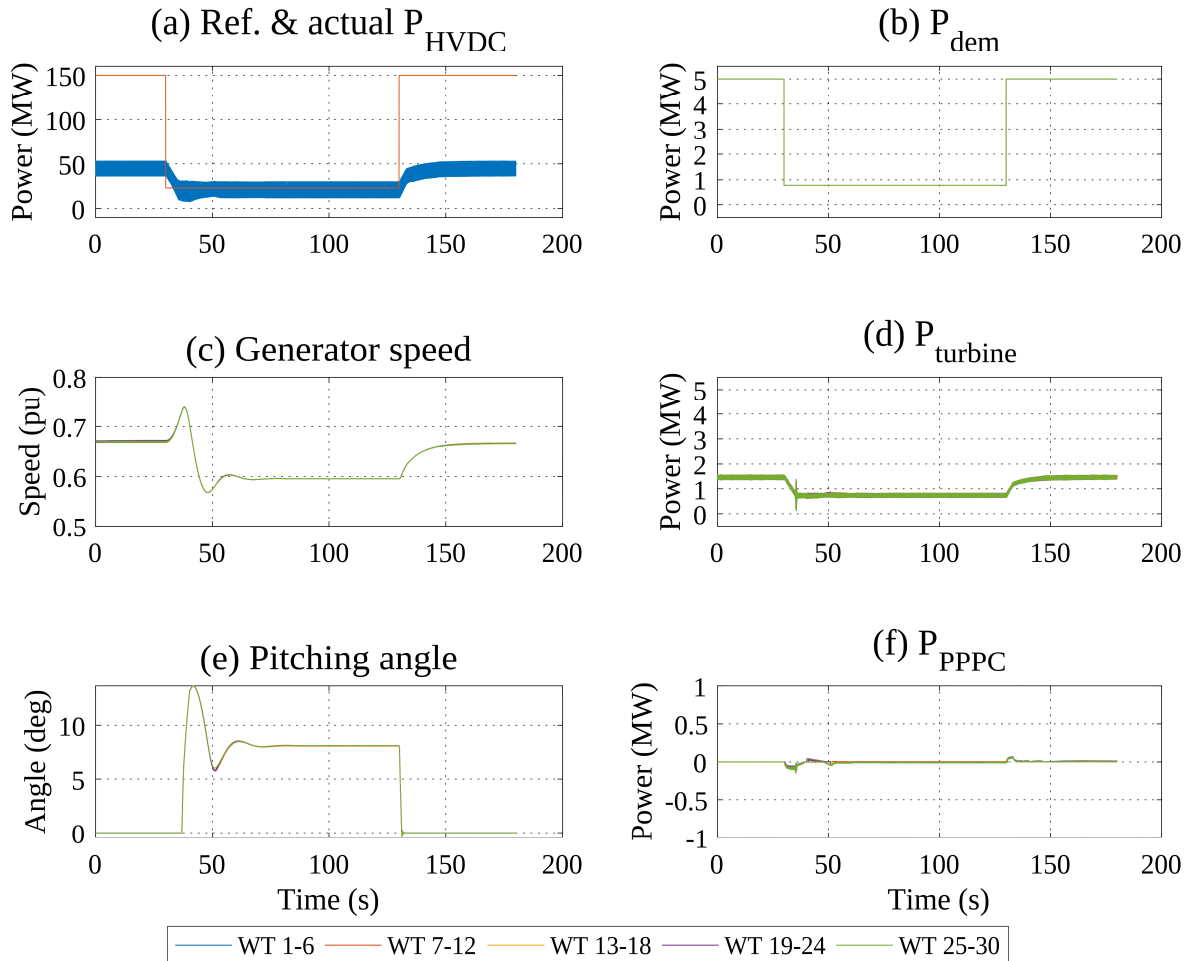
Figure 4.20 Simulation results for active power control. "WT" = Wind turbine.

4.7.5 Inertial Response

During a wind farm operation at rated wind speed and power, a grid frequency event is simulated to test the wind farm inertia response. The frequency excursion is shown in Figure 4.21 alongside simulation results of the wind farm's response. As it can be seen in Figure 4.21 (e), the wind farm increases output power temporarily according to the derived inertia power reference shown in Figure 4.21 (c). This reference is derived in the onshore station controller following the scheme in Figure 4.12 based on local grid frequency measurements. A short transient can be observed in the wind turbine output power for wind turbines 25-30 near t=23s due to an unfolder polarity change and subsequent DAB control loop reactivation.
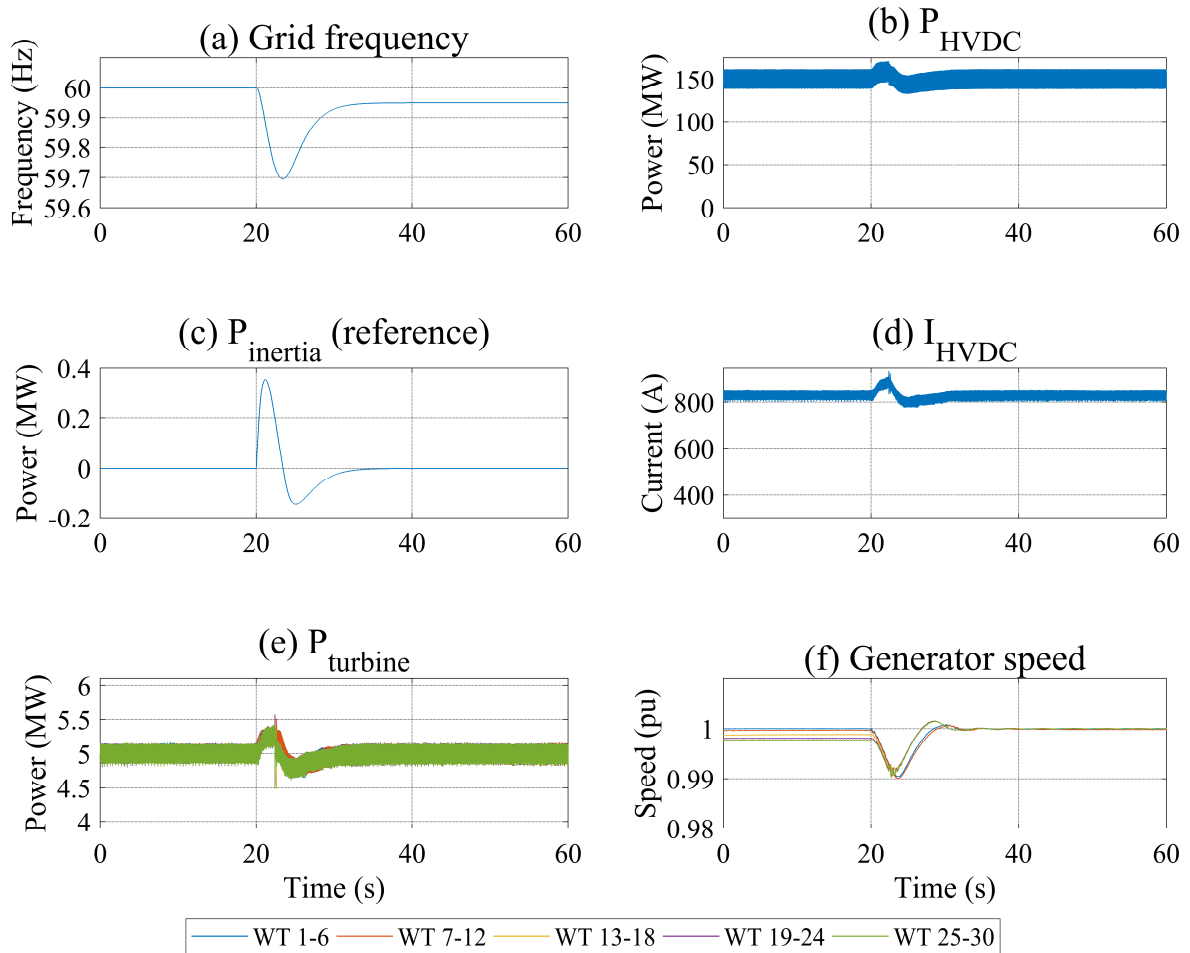
Figure 4.21 Simulation results for inertia response. "WT" = Wind turbine.

4.7.6 Operation during communication system outage

This scenario explores wind farm operation during a temporary communication system outage. For this purpose, the WEICan wind profile was simulated with a loss of communication being detected at t=20s. It is assumed that the communication system resumes regular operation at t=450s. Figure 4.22 shows that wind farm is able to maintain stable operation, very similar to the simulation results obtained with communication system in place (Figure 4.15). A slight change in HVDC-link current (Figure 4.22 (b)) can be observed during the transitions (t=20s and t=450s) which stems from the change in scheduling algorithm. As a result, the minimization of total PPPC cannot be maintained anymore. Consequently, the total amount of PPPC power processed is larger by up to 92% near t=135s, as seen in Figure 4.23. As differences are smaller for the majority of time in this test case, the HVDC-link current scheduling strategy presented in section 4.4 maintains only minor drawbacks over the communication-based default method during regular system operation.
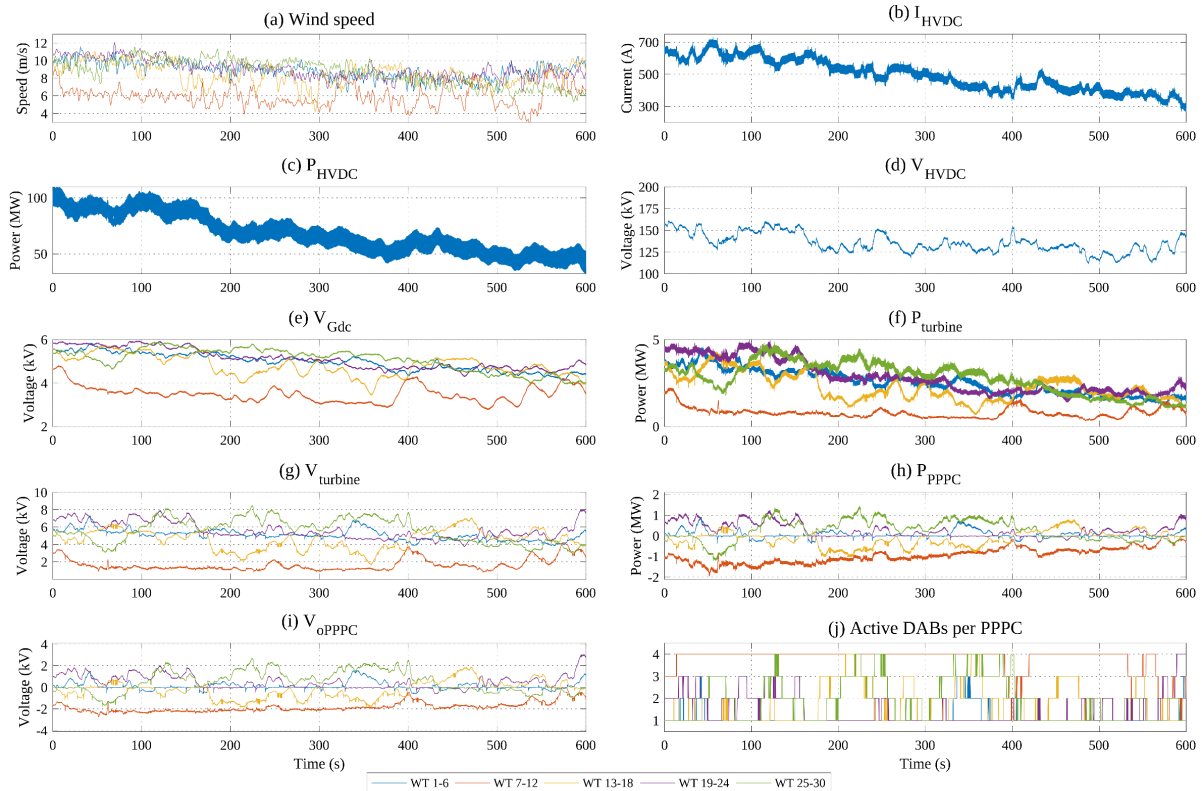
Figure 4.22 Simulation results for the WEICan wind profile during a communication system outage. "WT" = Wind turbine.
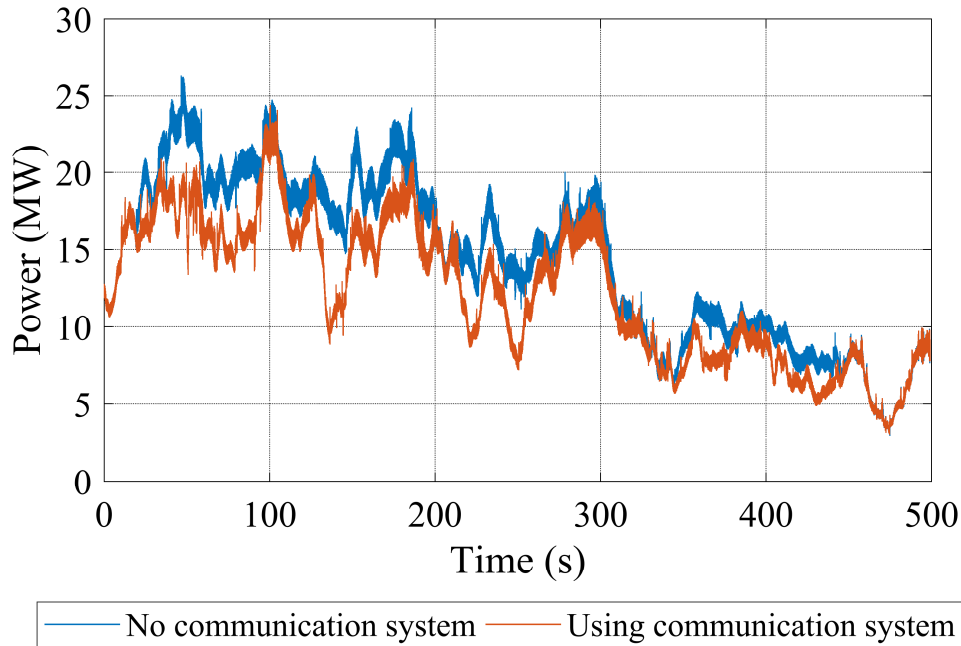
Figure 4.23 Total PPPC power processed for WEICan wind profile during communication system outage.

4.7.7 Summary

This chapter discussed the control-related concepts and issues for the proposed wind farm configuration. Control loops were designed or adapted to operate wind turbines following established variable-speed schemes. Control systems for the electrical systems ensure the stable trasfer of generated power while optimizing system operating points for low losses and respecting wind turbine converter ratings. It has been shown that ancillary services, such as LVRT, active power control and inertial response can be provided. While the presented wind farm configuration commonly requires a communication link for optimal operation, a communication-less operation scheme has also been derived and demonstrated to enable regular system operation with only few drawbacks. Dynamic simulations confirm the viability, stability and functionality of the proposed wind farm configuration and its control loops.

Chapter 5

A Sizing Framework for Wind Turbine Converters

In this chapter, a generic wind turbine converter sizing framework applicable to single-string, series-connected DC wind farms is introduced. As will be shown, unique operating characteristics of the electrical systems in series-connected DC wind farms render traditional approaches of determining converter ratings insufficient. In this chapter, the proposed sizing framework is applied to the wind farm configuration presented in Chapter 3, as well as two other configurations for comparison purposes. Results from this chapter are incorporated in the comparative economic assessment in Chapter 7.

5.1   Overview and Previous Work

In single-string, series-connected DC wind farms (Figure 5.1), the HVDC voltage and current typically are both a function of the operating states of all wind turbines [33][16], unlike with conventional wind farms where the HVDC voltage is fixed [53]. As a result, the operating conditions of each wind turbine converter are influenced by its operating points, as well as those of all other wind turbines in the farm. Consequently, the choice of component ratings for a wind turbine converter is dependent on the expected operating points of its wind turbine and simultaneous operating points of all other wind turbines in the farm. Several works have explored the valid operating regions for particular wind farm configurations based on sample sets of wind turbine operation

[72][16][35]. For conventional wind turbines with AC voltage output, collection system buses operate at fixed voltage and the operating points of one wind turbine converter do not affect those of other wind turbine converters. Hence, converter ratings are chosen based on the operating conditions at full-power operation. Most previous studies on series-connected DC wind farms have been based on a pre-determined set of converter ratings. The authors of [92]–[96] discuss various control approaches utilizing the modification of wind farm operating points and/or wind power curtailment to limit extreme operating points and overvoltage conditions in series-connected wind farms based on fixed component ratings. In [72], aerodynamic wake modeling is applied to a series-parallel wind farm based on VSCs to demonstrate the adequacy of chosen component ratings and maximize energy production. A similar wake model is used in [96]. In [46] and [97], the application of energy storage in wind turbines is considered to avoid undervoltage and overvoltage conditions. [46] recognizes the probabilistic nature of energy storage capacity requirements; yet associated likelihoods are not derived systematically.
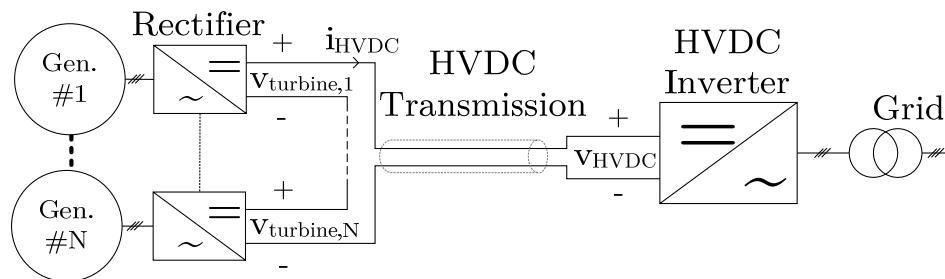
Figure 5.1 General structure of a single-string, series-connected DC Wind Farm. ("Gen." = Generator)

In contrast with the previous works that are largely focused on optimizing wind farm operation based on a fixed and chosen set of wind farm component ratings, or rely on assumed likelihoods for extreme operating conditions, component ratings are considered variable in this chapter. A methodology to aid determining desirable component ratings is proposed. In particular, this thesis contributes a methodology for sizing the voltage and current ratings of wind turbine converters' components in single-string, series-connected wind farms. This methodology allows capturing the influence of wind turbine converter topology, wind conditions at the chosen site, and wind farm layout on wind turbine converter ratings. The methodology determines the amount of annual energy curtailment due to converter rating limitations in order to allow for optimizing the trade-off between converter ratings and related annual energy curtailment.

5.2 Converter Sizing Challenges in Series-Connected DC Wind Farms

In conventional wind turbines featuring a full-scale back-to-back VSC for fixed AC voltage output (as shown in Figure 5.2) the determination of component voltage and current ratings (sizing) tends to be governed by the system operation at full power. For example, IGBT voltage ratings of a 2-level VSC are based on the nominal voltage of the internal DC bus, as well as a certain safety margin. IGBT current ratings are largely based on the expected currents at full-power operation. Overall, the sizing of wind turbine converters is independent of expected of actual operating states of neighboring wind turbines.
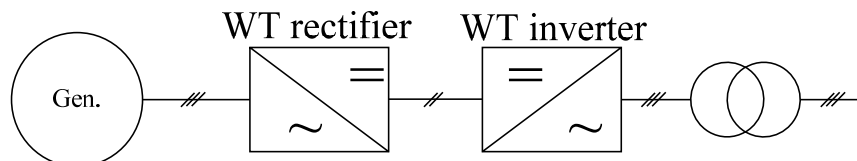
Figure 5.2 Conventional wind turbine electric power conversion system.

In contrast, the sizing of wind turbine converters for series-connected DC wind farms is dependent on operating states of neighboring wind turbines, and not necessarily entirely based on full-power operating conditions. Figure 5.1 shows the general structure of a single-string, series-connected DC Wind Farm, consisting of N wind turbines and incorporating an HVDC link. To illustrate the difference, this section discusses two sample operating conditions of a single-string series-connected wind farm using a VSC as rectifier in each wind turbine. This wind farm features two 5MW wind turbines and 3.3kV generators. Furthermore, it is considered that the minimum VSC DC output voltage, $V_{turbine,n}$, is equal to $\frac{2\sqrt{2}}{\sqrt{3}}$ times the generator line-to-line terminal voltage to ensure PWM operation in the linear region is maintained and over-modulation is avoided [98], ignoring effects of the stator impedance, as well as reactive power flows.

In the first operating condition, both wind turbines operate at rated power. To satisfy the minimum VSC DC output voltage requirement, both VSCs have to operate with an output voltage of at least 5.4kV as shown in Figure 5.3. This results from both generators operating at rated speed and AC voltage. In Figure 5.3, the green area indicates the range of HVDC-link current that can be chosen, such that the VSC output voltage is higher than 5.4kV at the given operating condition. The pink area indicates a range of

HVDC-link currents that would require a VSC output voltage below its minimum output voltage, in order to operate with rated output power. As a result, the string current I_{HVDC} must (be controlled to) be equal to or less than 928A. Hence, the VSCs' IGBTs must be rated to withstand a voltage of at least 5.4kV plus a safety margin.
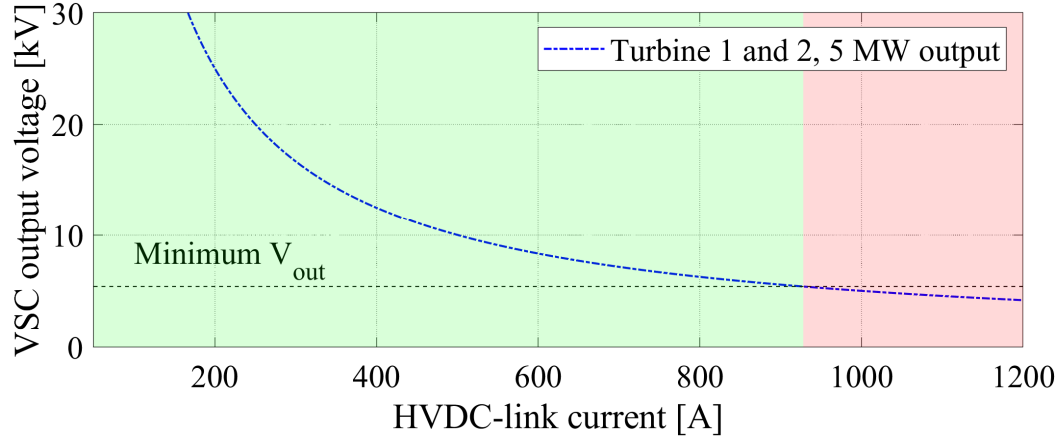
Figure 5.3 Illustration of required DC output voltages and valid HVDC-link currents of a wind farm with two wind turbines featuring VSCs as rectifiers operating at rated output powers. Green area: valid rectifier operating points; pink area: minimum VSC output voltage criterions violated.

Now considering a second operating condition at lower total power output, it will be shown that a higher IGBT voltage rating is required. Here, wind turbine 1 operates at rated power (5MW), while wind turbine 2 operates at 30% rated power (1.5MW). As shown in Figure 5.4, the minimum VSC output voltage for wind turbine 2 drops, as the generator speed and AC voltage is lower at wind conditions resulting in 1.5 MW output power for a variable-speed wind turbine operating at optimal tip-speed ratio. The maximum string current I_{HVDC} corresponds to the point where a VSC's output voltage reaches its minimum value first as string current is increased. In this case, the lower minimum output voltage of wind turbine 2 requires the string current I_{HVDC} to be at most 232A to satisfy the minimum DC output voltage requirement of the VSC of wind turbine 2, as seen in Figure 5.4. This significantly lowers the string current and forces the VSC of wind turbine 1 to operate at a significantly elevated output voltage level of at least 21.5kV. Accordingly, the VSCs' IGBTs would have to be rated to at least 21.5kV to allow this operating condition to exist without power curtailment. In typical wind farm designs, each wind turbine would be installed with the same converter ratings, including the higher voltage rating for its VSCs.
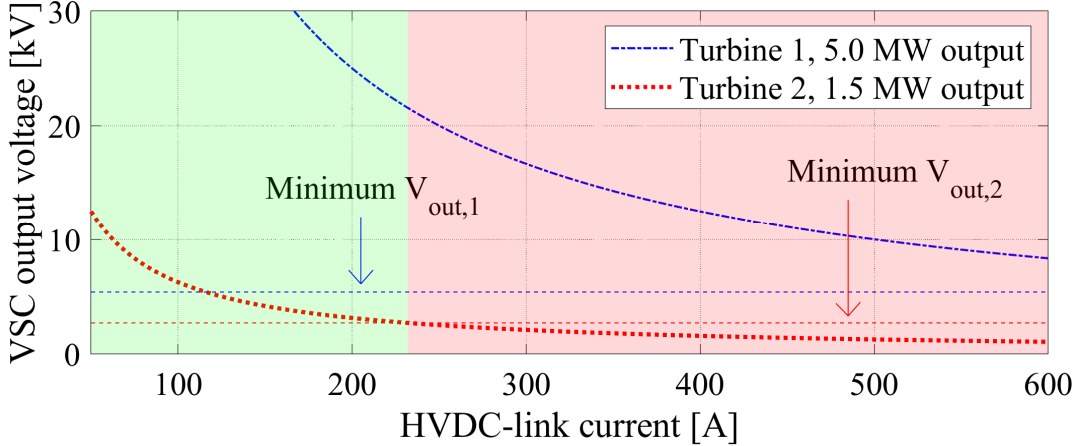
Figure 5.4 Illustration of required DC output voltages and valid HVDC-link currents of a wind farm with two wind turbines featuring VSCs as rectifiers operating at differing output powers. Green area: valid rectifier operating points; pink area: minimum VSC output voltage of rectifier 2 violated.

This example demonstrates that in series-connected DC wind turbines, the sizing of wind turbine converters introduces an interdependency among wind turbines and is not entirely based on operation at full power.

5.3 A Generic Converter Sizing Framework for Wind Turbine Converters in Single-String, Series-Connected Wind Farms

In this section, a generic wind turbine converter sizing framework for single-string, series-connected DC wind farms is developed that addresses the interdependencies outlined in section 5.2.

5.3.1 System description

This section considers the general structure of a single-string, series-connected DC Wind Farm shown in Figure 5.1. The output power of wind turbine n, P_n, is generated according to internal control laws at a particular generator line-to-line voltage $V_{gen,n}$ and electrical frequency $f_{gen,n}$. A rectifier is used in each wind turbine to convert the AC to DC output power, such that the output voltage of wind turbine n, $V_{turbine,n}$, adheres to

$$V_{turbine,n} = \frac{P_n}{I_{HVDC}} \tag{5.1}$$

where I_{HVDC} is the HVDC-link current. In the rest of this study, the states of wind turbine n in a string of N turbines are represented in vector $\boldsymbol{S_n}$:

$$\boldsymbol{S_n} = [\boldsymbol{S_{T,n}} \quad \boldsymbol{S_{I,n}}]^T \tag{5.2}$$

This vector consists of the converter terminal state vector $\boldsymbol{S_{T,n}}$ and converter internal state vector $\boldsymbol{S_{I,n}}$. While $\boldsymbol{S_{I,n}}$ is specific to the chosen converter topology, $\boldsymbol{S_{T,n}}$ is generally defined as:

$$\boldsymbol{S_{T,n}} = [P_n \quad V_{gen,n} \quad f_{gen,n} \quad I_{HVDC}]^T \tag{5.3}$$

For each wind turbine rectifier type, a steady-state, topology-specific relationship between converter terminal and internal states, and rectifier output voltage $V_{turbine,n}$ can be established:

$$V_{turbine,n} = f(\boldsymbol{S_n}) \tag{5.4}$$

For a particular converter topology, (5.4) would model the complete steady-state internal relationships of such converter, unlike in (5.1) which expresses $V_{turbine,n}$ based on converter terminal quantities. Equation (5.4) will be used to consider converter component limitations for the purpose of sizing the converter. In this study, it is being assumed that the converters in all wind turbines of a farm have the same components ratings.

In a single-string series-connected DC Wind Farm, I_{HVDC} is actively controlled by the HVDC inverter station [33]. As a result, the HVDC-link voltage V_{HVDC} becomes

$$V_{HVDC} = \frac{1}{I_{HVDC}} \sum_{n=1}^{N} P_n \tag{5.5}$$

The HVDC-link current reference is derived from an HVDC-link current scheduling law specific to the topology and design of wind farm and power converter. Various objectives can be implemented with such law, such as eliminating an offshore-onshore communication link [33], maintaining a constant HVDC-link voltage [33], minimizing processed power [99], maximizing energy yield (compare to [72]), or minimizing required converter ratings. Once an HVDC-link current scheduling law has been selected, all basic electrical system states are known as per (5.1)-(5.3) and (5.5), other than P_n, $V_{gen,n}$ and $f_{gen,n}$ that depend on the incoming wind conditions. Unlike with conventional offshore

wind farms featuring an AC voltage collection system, wind turbine and HVDC link voltages, $V_{turbine,n}$ and V_{HVDC} are not held constant. Instead, they all are functions of wind turbine output power P_n and the HVDC-link current I_{HVDC}.

5.3.2 Generic sizing problem formulation

The choice of wind turbine rectifier topology, converter ratings, and HVDC-link voltage rating introduce constraints on the range of feasible HVDC-link currents. This directly affects wind turbine output voltages, particularly in the presence of wind speed and output power differences within the series string, as illustrated in section 5.2.

The rectifying converter can introduce minimum and/or maximum constraints on wind turbine output power $P_n(\boldsymbol{S_n})$ or wind turbine output voltage $V_{turbine,n}(\boldsymbol{S_n})$. Some of these constraints can depend on the wind turbine's current state $\boldsymbol{S_n}$. The limitations result from the component ratings within the converter, and from the choice of converter topology.

In addition, the HVDC-link insulation rating introduces a maximum possible HVDC-link voltage constraint $\overline{V_{HVDC,R}}$ and I_{HVDC} should not exceed values that cause an excessive HVDC-link voltage. Similarly, there is a maximum rated HVDC-link current $\overline{I_{HVDC,R}}$. Furthermore, wind turbine startup and shutdown can introduce additional constraints on converter sizing or HVDC link operation [100], as well as wind farm configuration-specific fault handling schemes and certain fault-ride through schemes. For example, certain wind turbine output converter voltage or current ratings can be required to facilitate wind turbine startup [100], or withstand faults in the DC collection system [101].

5.3.3 Full operational range sizing

To ensure that all wind turbines can realize all possible electric operating points within the series string, wind turbine converter ratings can follow a full operational range sizing approach. In this approach, one can consider a wind farm consisting of two series-connected wind turbines (as shown in Figure 5.1, assuming $N = 2$). Wind turbine 1 operates at an operating point that puts the wind turbine converter at the maximum of its operational range. Typically, this could refer to the wind turbine converter operating at maximum output voltage while the wind turbine outputs rated power. Wind turbine 2 operates at an operating point that puts the wind turbine converter at the minimum of its operational range. Typically, this could refer to the wind turbine converter operating at minimum output voltage while the wind turbine operates at cut-in wind

speed. Converter ratings are then chosen to enable this operating condition. Furthermore, additional constraints related to wind turbine startup or fault handling may need to be observed. Sample realizations of this approach are provided in sections 0 and 5.6.

5.3.4   Partial operational range sizing

In certain wind farm configurations, it may happen that the likelihood of operation at or near the full operational range component ratings is very low, or the required component ratings to realize full operational range sizing are considered excessive. In such cases, it can be meaningful to examine the benefits of intentionally reducing converter ratings to only cover a fraction of the full operational range within the wind farm and implement a curtailment scheme for those operational points that are beyond the implemented converter ratings. In addition, full operational range sizing may not prevent violations of the HVDC-link voltage constraint $\overline{V_{HVDC,R}}$. For these cases, a partial operational range sizing approach is discussed next.

As shown in section 5.2, for all wind turbine operating conditions, there is a range of feasible HVDC-link currents that can be selected. To express the interaction between scheduled HVDC-link current and converter limits, it is meaningful to derive each limit of a particular converter as a function of minimum or maximum possible HVDC-link current. This allows the prediction of violations of converter limits as a function of I_{HVDC} for given wind turbine powers P_n, and informs the choice of HVDC-link current during operation, as well as the prediction of required converter ratings to make an expected operating condition feasible for a particular HVDC-link current.

Within the topology-specific, steady-state relationship of (5.4), there can be numerous limitations on (internal) state variables or relationships based on (internal) state variables. These limitations can be of static nature, mostly related to component ratings. However, dynamic, $\boldsymbol{S_n}$-dependent limitations can also exist in some converter topologies.

For many of these limitations, the topology-specific relationships of (5.4) can be solved for I_{HVDC} analytically or numerically, where the limited variable is represented by its rated boundary value or relationship. For instance, for a wind turbine converter with a rated maximum output voltage $\overline{V_{turbine,R,n}}$, (5.1) can be reformulated to yield the minimum HVDC-link current, $\underline{I_{HVDC,\overline{V_{turbine,R,n}}}}$, to avoid exceeding $\overline{V_{turbine,R}}$:

$$I_{HVDC,\overline{V_{turbine,R,n}}} = \frac{P_n}{V_{turbine,R}} \tag{5.6}$$

Limits that are not a function of I_{HVDC} indicate that the series-connection of wind turbines has no influence on the determination of that component rating and a traditional sizing approach could be taken. For example, power electronic switches facing the generator might often be chosen to withstand the maximum current that occurs at full-power operation. For this reason, limits that are independent of I_{HVDC} are not discussed further in this study.

5.3.5   Limits on HVDC-link current

To summarize I_{HVDC}-dependent limits, equations for all converter limits can be formulated from the topology-specific relationship of (5.4). The $N \times M$ matrix $\boldsymbol{L_{I_{HVDC}}}$ holds minimum HVDC-link current values for all N turbines and all M limits derived previously that result in a lower HVDC-link current limit. Equivalently, the $N \times G$ matrix $\overline{\boldsymbol{L_{I_{HVDC}}}}$ holds all maximum HVDC-link current values for all N turbines and G limits that result in an upper HVDC-link current limit.

To ensure that the maximum rated HVDC-link voltage $\overline{V_{HVDC,R}}$ is not exceeded under any operating condition, another minimum limit on the HVDC-link current, $I_{HVDC,\overline{V_{HVDC}}}$, must be considered:

$$I_{HVDC,\overline{V_{HVDC}}} = \frac{\sum_{n=1}^{N} P_n}{V_{HVDC,R}} \tag{5.7}$$

The overall maximum and minimum allowable HVDC-link currents $\overline{I_{HVDC}}$ and $\underline{I_{HVDC}}$ can then be expressed as:

$$\overline{I_{HVDC}} = \min\left(\overline{\boldsymbol{L_{I_{HVDC}}}}\right) \tag{5.8}$$

$$\underline{I_{HVDC}} = \max\left(\begin{bmatrix} \max\left(\underline{\boldsymbol{L_{I_{HVDC}}}}\right) \\ I_{HVDC,\overline{V_{HVDC}}} \end{bmatrix}\right) \tag{5.9}$$

For as long as $\overline{I_{HVDC}} \geq \underline{I_{HVDC}}$, I_{HVDC} should be chosen, such that

$$\underline{I_{HVDC}} \leq I_{HVDC} \leq \overline{I_{HVDC}} \tag{5.10}$$

This ensures that no converter in the wind farm operates at or beyond its limits and no full or partial wind power curtailment is necessary to avoid exceeding converter limits. For such case, HVDC-link current scheduling laws can be used to optimize for objectives not related to converter ratings.

If $\underline{I_{HVDC}} > \overline{I_{HVDC}}$, there is no HVDC-link current that can be chosen to maintain all converters operating within their limits. In such case, output power curtailment becomes necessary in one or more wind turbines, to ensure that converter limits are not violated.

5.3.6 Sizing wind turbine converters and incoming wind conditions

In the previous section, the converter's state dependence on I_{HVDC} was discussed. However, the converters' states also depend on wind turbine states, such as P_n, $V_{gen,n}$ and f_{gen}, related to the incoming wind conditions, wind turbine control laws and dynamic response of the aero-mechanic system.

To eliminate unknowns relating to the incoming wind conditions that will appear in (5.7) and (5.9) - such as P_n, $V_{gen,n}$ and f_{gen} - sizing wind turbine converters in series-connected DC wind farms requires a formulation of such wind conditions expected to be present during the operation of such a wind farm for its operational life (e.g., compare to [72]).

Provided that a formulation of the expected wind turbine operating conditions and their likelihoods for the life of the wind farm is available, it then becomes possible to predict the likelihood of operating points of wind turbine converters over the life of the wind farm. As a result, it is possible to estimate the likelihood of converters to be operating within their limits and avoiding power curtailment due to converter limits, using relationships (5.7), (5.9) and (5.10). This allows making informed design decisions on the converter ratings and converter topological choices for a series-connected DC offshore wind farm. The proposed key metric during this design process is the expected annual wind energy curtailment due to exceeding converter limits. A flowchart of the proposed sizing framework is provided in Figure 5.5. Subsection 5.7.1 expands on the approach taken to estimate wind turbine operational states for a particular wind farm site.
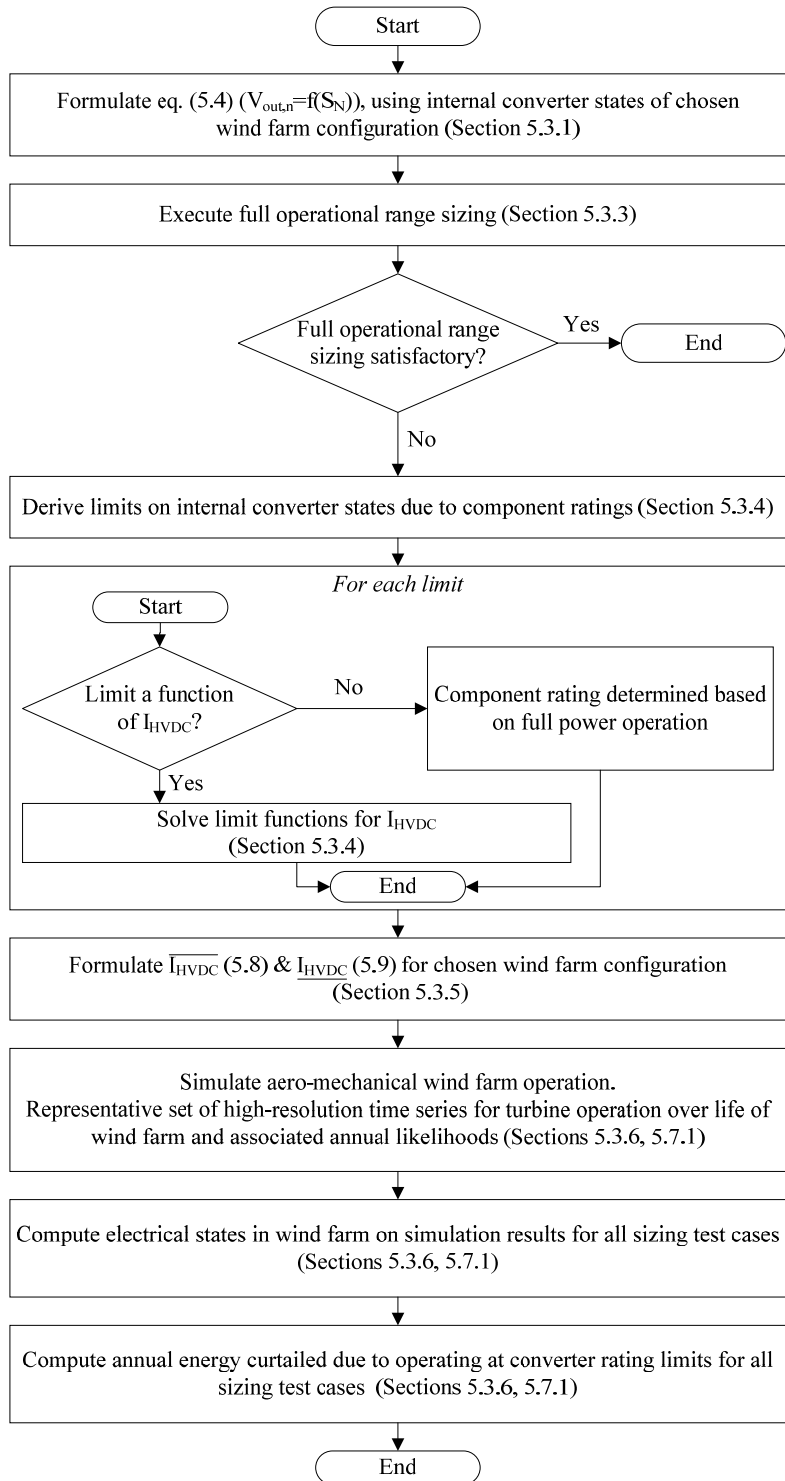
Figure 5.5 Flowchart of partial operational range sizing framework for wind turbine converters in single-string, series-connect DC wind farms.

5.4 Sizing Methodology for Dual-Active Bridge Converters as PPPCs

This section discusses the implementation of the partial operating range sizing methodology presented in section 5.2 on the wind farm configuration featuring differential power processing (DPP) as discussed in Chapter 3 (page 28), denominated as "DCS-PPPC" in this chapter. A full operational range sizing is derived in section 5.7 for reference purposes. This section is based on the system model discussed in sections 3.3 and 3.5. However, for simplicity of presentation, a multi-converter design is not considered.

The topology-specific, steady-state relationship of (5.4) for this wind farm configuration consists of the numerical relationship $V_{Gdc,n} = f(P_n, V_{gen,n}, f_{gen,n})$ of Figure 3.6, and (3.4)-(3.5),(3.7)-(3.8) to obtain a relationship for $V_{turbine,n}$ involving internal DBR and PPPC states:

$$V_{turbine,n} = \frac{V_{Gdc,n} V_{oDAB,n} N_{ps}}{2\pi f_s L_t I_{HVDC}} \phi_n \left(1 - \frac{|\phi_n|}{\pi}\right) + V_{Gdc,n} \tag{5.11}$$

5.4.1 I_{HVDC}-dependent converter limits

As discussed in section 5.3.3, converter limits that are not a function of I_{HVDC} would lead to a conventional sizing approach and are neglected in this analysis. In particular, this relates to the DBR diodes' voltage and current ratings, as well as the voltage rating of the primary DAB switches S1-S4.

Component ratings depending on I_{HVDC} that are derived from converter limits in this wind farm configuration are:

- Current rating of all DAB switches
- Voltage rating of switches S5-S8 and S1u-S4u
- DAB leakage inductance L_t and switching frequency f_s, related to maximum PPPC power capability

The converter limits that need to be considered in relation to these component ratings are on the:

1. DAB output voltage $V_{oPPPC,n}$: $\overline{V_{oPPPC,n}}$ and $\underline{V_{oPPPC,n}}$
2. Peak current of DAB transformer current $i_{L,n}$: $\overline{|i_{L,pk,n}|}$

3. Maximum and minimum DAB power (related to maximum and minimum DAB phase shift ϕ): $\overline{P_{PPPC,n}}$ and $\underline{P_{PPPC,n}}$

5.4.2   PPPC output voltage limits

As discussed in section 4.2.3, to not violate the maximum and minimum PPPC output voltage limits, the minimum and maximum HVDC-link current values are defined as:

$$\frac{P_n}{\overline{V_{oPPPC,n}} + V_{Gdc,n}} < I_{HVDC} < \frac{P_n}{\underline{V_{oPPPC,n}} + V_{Gdc,n}} \tag{5.12}$$

5.4.3   Internal DAB current limit

To determine the DAB switch current ratings, as well as DAB switching frequency and leakage inductance, it is necessary to determine the DAB transformer peak current. This has already been discussed in section 4.2. Using (4.2)-(4.4) and (4.7), it then becomes possible to numerically determine the peak currents in the DABs primary and secondary switches S1-S8 as a function of P_n, $V_{Gdc,n}$ and I_{HVDC}, as well as converter parameters:

$$i_{L,pk,n} = g(P_n, V_{Gdc,n}, I_{HVDC}) \tag{5.13}$$

Conversely, (5.13) can also be solved numerically for I_{HVDC} as a function of $i_{L,pk,n}$, P_n and $V_{Gdc,n}$. To ensure that the resulting function has unique solutions, it is done for $P_{PPPC.n} \geq 0$ and $P_{PPPC,n} < 0$ separately. For $P_{PPPC,n} \geq 0$:

$$I_{HVDC} = k^+(P_n, V_{Gdc,n}, i_{L,pk,n}) \tag{5.14}$$

Similarly, for $P_{PPPC,n} < 0$:

$$I_{HVDC} = k^-(P_n, V_{Gdc,n}, i_{L,pk,n}) \tag{5.15}$$

This separation is necessary since $i_{L,pk,n}$ is monotonically increasing as $\left|P_{PPPC,n}\right|$ increases, yielding two solutions for I_{HVDC} for many operating points without such separation.

5.4.4   DAB power limit

The DAB phase shift ϕ_n is bound within the range of $-\pi/2$ to $\pi/2$. At the two extremes, the DAB processes the minimum and maximum possible amounts of power, respectively [79]. Using (3.4) and (3.8), (3.7) can be rewritten to:

$$I_{HVDC} = \frac{V_{Gdc,n}N_{ps}}{UF_n \times 2\pi f_s L_t}\phi_n\left(1 - \frac{|\phi_n|}{\pi}\right) \tag{5.16}$$

Since the unfolder polarity UF_n is defined as $sign(P_{PPPC,n}) = sign(\phi_n)$, (5.16) resolves to the same solution for $\phi_n = \pi/2$ and $\phi_n = -\pi/2$. An upper limit to the HVDC-link current results to maintain stable DAB operation within its power limits:

$$I_{HVDC} < V_{Gdc,n}N_{ps}/8f_s L_t \tag{5.17}$$

5.4.5 Wind turbine startup and shutdown

The scheme presented in Chapter 6 demonstrates a wind turbine startup and shutdown procedure that does not significantly affect converter sizing. For this reason, wind turbine startup and shutdown is not considered further in this analysis.

5.4.6 Fault ride-through

As shown in [99], low-voltage ride-through (LVRT) is handled using an onshore braking chopper that maintains the operating conditions of the offshore wind farm during an LVRT event. Therefore, LVRT does not influence converter sizing for this wind farm configuration.

5.4.7 Fault handling

It is assumed that wind turbine internal faults in a single-string, series-connected wind farm can be handled by de-energizing and bypassing a wind turbine in the string. Faults in the collection system could be handled by adopting fault handling schemes, such as those discussed in [101], which show that faults can be handled without affecting the PPPC input current or output voltage ratings, and allow clearing a ground fault with an HVDC-link current peak of approximately 2.5pu. For this reason, a minimum peak output current rating constraint of 2.5pu is considered here.

5.4.8 Internal wind turbine states $S_{I,n}$

Using the steady-state relationship between $V_{Gdc,n}$ and P_n provided in Figure 3.6, the steady-state average model of sections 3.3 can be computed. Additionally, for the purpose of evaluating component limits, it is necessary to determine the DAB peak current $i_{L,pk,n}$ following section 4.2.2 and equation (5.13). As a result, the internal state vector $S_{I,n}$ is defined as:

$$S_{I,n} = [V_{Gdc,n} \quad i_{L,pk,n}]^T \tag{5.18}$$

5.4.9 Allowable HVDC-link currents

In summary, the maximum and minimum allowable HVDC-link currents $\underline{I_{HVDC}}$ and $\overline{I_{HVDC}}$ are derived and written in matrix form as discussed in section 5.3.3:

$$\underline{L_{I_{HVDC}}} = \begin{bmatrix} P_n/(V_{Gdc,n} + \overline{V_{oPPPC}}) \\ k^+(P_n, V_{Gdc,n}, i_{L,pk,n} = \overline{I_{S1-S4}}) \\ k^+\left(P_n, V_{Gdc,n}, i_{L,pk,n} = \dfrac{\overline{I_{S5-S8}}}{N_{ps}}\right) \end{bmatrix} \tag{5.19}$$

$$\overline{L_{I_{HVDC}}} = \begin{bmatrix} P_n/\left(V_{Gdc,n} + \underline{V_{oPPPC}}\right) \\ k^-(P_n, V_{Gdc,n}, i_{L,pk,n} = \overline{I_{S1-S4}}) \\ k^-\left(P_n, V_{Gdc,n}, i_{L,pk,n} = \dfrac{\overline{I_{S5-S8}}}{N_{ps}}\right) \\ V_{Gdc,n} N_{ps}/8f_s L_t \end{bmatrix} \tag{5.20}$$

where in $\underline{L_{I_{HVDC}}}$ and $\overline{L_{I_{HVDC}}}$ the rows represent the PPPC output voltage limit, primary bridge DAB peak current limit, and secondary bridge DAB peak current limit, respectively. The last row of $\overline{L_{I_{HVDC}}}$ represents the maximum DAB power limit.

The minimum and maximum allowable HVDC link currents for this wind farm configuration can then be determined following (5.7)-(5.9).

5.5 Sizing of a Voltage-Source Converter-Based Wind Farm
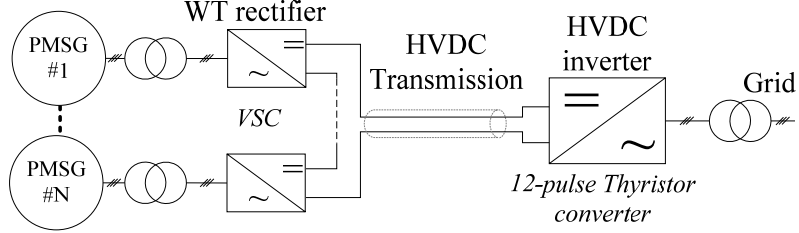
Figure 5.6 Structure of the DCS-VSC configuration.

This section implements the sizing methodology for a VSC-based wind farm, as discussed in [102], adapted to a single-string configuration from [16] and denominated as "DCS-VSC". In this wind farm configuration, VSCs are used as wind turbine converters as shown in Figure 5.6. All other wind farm components are identical to those of the DCS-PPPC configuration. The wind turbine output voltage is given by [73] as:

$$V_{out,n} = \frac{2\sqrt{2}}{\sqrt{3}} \frac{V_{gen,n}}{m_a} \tag{5.21}$$

where $V_{gen,n}$ is the generator line-to-line RMS voltage and m_a the modulation index. To maintain linear PWM modulation, the modulation index is assumed to be equal or less than one. As a result it is required that

$$V_{out,n} \geq \frac{2\sqrt{2}}{\sqrt{3}} V_{gen,n} \tag{5.22}$$

The HVDC-link current is determined such that each wind turbine operates with a feasible output voltage in addition to a margin k (e.g., 110%) for control action:

$$I_{HVDC} = \frac{P_n}{\max\limits_{1 \leq n \leq N} k \frac{2\sqrt{2}}{\sqrt{3}} V_{gen,n}} \tag{5.23}$$

The VSC's switch current ratings are determined from rated AC currents which are not a function of I_{HVDC}.

5.5.1 Full operational range sizing

Considering the wind turbine converter output voltages of a two-turbine series string operating at extreme operating points, one can write:

$$V_{out,1} = \frac{P_{rated}}{I_{HVDC}} \tag{5.24}$$

$$V_{out,2} = \frac{P_{min}}{I_{HVDC}} \tag{5.25}$$

where $V_{out,1}$ and $V_{out,2}$ are the converter output voltages of wind turbine 1 and 2, respectively, and P_{rated} and P_{min} are the wind turbine powers at rated and cut-in wind speeds. Using (5.22), (5.24) and (5.25) can be rewritten as (5.26) and (5.27) to yield conditions for feasible values for I_{HVDC}:

$$I_{HVDC} \leq \frac{P_{rated}}{k\frac{2\sqrt{2}}{\sqrt{3}}V_{gen,rated}} \tag{5.26}$$

$$I_{HVDC} \leq \frac{P_{min}}{k\frac{2\sqrt{2}}{\sqrt{3}}V_{gen,min}} \tag{5.27}$$

where $V_{gen,rated}$ and $V_{gen,min}$ are the generator voltages at rated and cut-in operating conditions, respectively.

Numerical analysis of (5.26) and (5.27) for a wind turbine design presented in section 3.6 reveals that condition (5.27) is tighter for the entire output power range. Using (5.27), solving (5.1) for I_{HVDC} and considering rated converter output voltage $V_{out,rated}$ leads to:

$$V_{out,rated} \geq \frac{2\sqrt{2}k}{\sqrt{3}}V_{gen,min}\frac{P_{rated}}{P_{min}} \tag{5.28}$$

For the presented wind turbine parameters, the rated output voltage would need to be at least 61.2kV for a 3300V generator, assuming k equal to 1.1, $\frac{P_{rated}}{P_{min}}$ equal to 33.21 and $V_{gen,min}$ equal to 1129V.

5.5.2   Partial operational range sizing

Given the very high required output voltage rating for full operational range sizing, partial operational range sizing appears worth exploring. Given the converter output voltage constraint of (5.22), the maximum HVDC-link current constraint due to this output voltage constraint, $\overline{I_{HVDC,\underline{V_{out,R,n}}}}$, can be written as:

$$\overline{I_{HVDC,\underline{V_{out,R,n}}}} = \frac{P_n}{\frac{2\sqrt{2}}{\sqrt{3}}V_{gen,n}} \tag{5.29}$$

As a result, the maximum and minimum allowable HVDC-link currents $\underline{I_{HVDC}}$ and $\overline{I_{HVDC}}$ are derived and written in matrix form as discussed in subsection 5.3.3:

$$\underline{\boldsymbol{L_{I_{HVDC}}}} = [0] \tag{5.30}$$

$$\overline{\boldsymbol{L_{I_{HVDC}}}} = \left[\frac{P_n}{\frac{2\sqrt{2}}{\sqrt{3}}V_{gen,n}} \right] \tag{5.31}$$

The overall minimum and maximum allowable HVDC link currents for this wind farm configuration can then be determined following (5.7)-(5.9).

a.   Wind turbine startup and shutdown

Wind turbine startup of this wind farm configuration may face challenges similar to those reported in [100]. For the purpose of this study, it is assumed that additional hardware and/or control algorithms are used to facilitate wind turbine startup that do not result in further sizing constraints on the VSC.

b.   Fault-ride-through and fault handling

Fault ride-through can be handled in the same way as discussed in section 5.4.6. Similarly, it is assumed that fault handling is realized in a way similar to that discussed in subsection 5.4.7. However, VSC switch current ratings may not already be sufficient and may require an increased rating to withstand a 2.5pu current peak during ground faults, as discussed in [101].

5.6 Sizing of a Farm based on Diode-Bridge Rectifier and Buck Converter
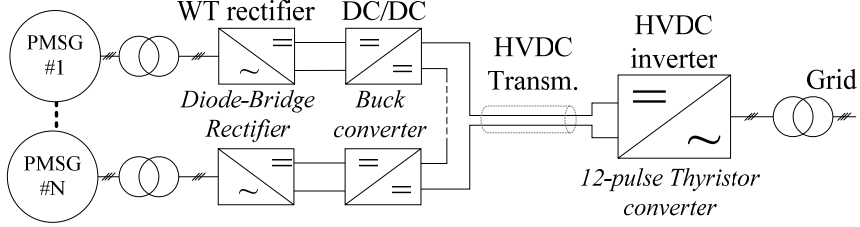
Figure 5.7 Structure of the DCS-Buck configuration.
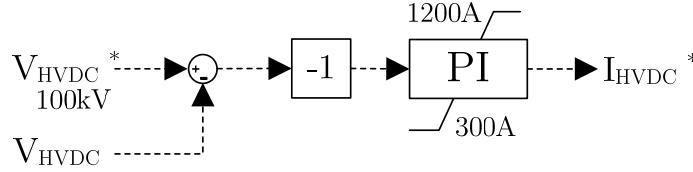
Figure 5.8 HVDC-link current scheduling scheme of [33].

Finally, the sizing of a wind farm configuration featuring diode-bridge rectifiers and buck converters [33] is discussed in this section. This configuration is labelled as "DCS-Buck" and shown in Figure 5.7. All components are identical to those of DCS-PPPC, aside from the wind turbine converter. The HVDC-link current scheduling scheme of [33] is shown in Figure 5.8. Due to the buck converter, the wind turbine output voltage must be less than or equal to the diode-bridge rectifier's DC-side voltage $V_{Gdc,n}$:

$$V_{out,n} \leq V_{Gdc,n} \tag{5.32}$$

$V_{Gdc,n}$ as a function of P_n has been derived in section 3.3 and is shown in Figure 3.6.

5.6.1 Full operational range sizing

Considering the wind turbine converter output voltages of a two-turbine series string operating at extreme operating points, one can write:

$$V_{out,1} = \frac{P_{rated}}{I_{HVDC}} \tag{5.33}$$

$$V_{out,2} = \frac{P_{min}}{I_{HVDC}} \tag{5.34}$$

where $V_{out,1}$ and $V_{out,2}$ are the converter output voltages of wind turbines 1 and 2, respectively, and P_{rated} and P_{min} are the wind turbine powers at rated and cut-in wind speed. Using (5.32), (5.33) and (5.34) can be rewritten as (5.35) and (5.36) to yield conditions for feasible values for I_{HVDC}:

$$I_{HVDC} \geq \frac{P_{rated}}{V_{Gdc,n}(P_{rated})} \tag{5.35}$$

$$I_{HVDC} \geq \frac{P_{min}}{V_{Gdc,n}(P_{min})} \tag{5.36}$$

Numerical analysis of (5.35) and (5.36) for a wind turbine design presented in section 3.6 reveals that condition (5.35) is tighter for the entire output power range. Using (5.35), solving (5.1) for I_{HVDC} and considering rated converter output voltage $V_{out,rated}$ leads to:

$$V_{out,rated} \geq V_{Gdc,n}(P_{rated}) \tag{5.37}$$

For the presented wind turbine parameters, the rated output voltage would need to be at least 5.8kV for a 5000V generator, and the required output current rating would be 862A, neglecting fault handling related issues. The authors of [33] chose an output voltage and current rating of 4166V and 1200A. In this design, the buck converter semiconductors still require a voltage rating of 5.8kV to withstand the maximum V_{Gdc} value, but require a higher current rating for an average output current of 1200A.

In this thesis, an alternate operational mode is considered as second test case. In this test case, the HVDC-link current scheduling scheme is replaced by one that minimizes HVDC-link current while adhering to the operational limits of all active converters (including a 5% safety margin). Allowing buck converters to operate at 100% duty cycle during rated conditions also allows to limit the converter output and transmission system current rating to 862A, instead of 1200A. In addition, it is likely to result in a better overall conversion efficiency. This is examined further in section 7.3.

Since operation at rated output values represents the only feasible operating point in this configuration to process rated power, the consideration of partial operational range sizing is not meaningful with the DCS-Buck configuration to reduce component sizes.

5.6.2 Wind turbine startup and shutdown

Due to the buck converter's ability to operate with zero output voltage and power, wind turbine startup of this wind farm configuration is expected to be similar to those of conventional schemes and without further implications on converter ratings.

5.6.3 Fault-ride-through and fault handling

Fault ride-through can be handled in the same way as discussed in section 5.4.6. Fault handling for this wind farm configuration has been studied in [35] and it is indicated that a peak current rating for short durations of 2pu may be required to contain DC link faults.

5.7 Converter Sizing Case Studies for a 450MW Offshore Wind Farm

To demonstrate the efficacy of the sizing methodology, three case studies for the 450MW Offshore Wind Farm of section 3.6 are discussed here. Additional parameters relating to DAB sizing and operation for the purpose of this study are given in Table 5.1. The first case study considers sizing such a wind farm with the DCS-PPPC configuration. A second study considers the DCS-VSC, followed by a last study on the DCS-Buck configuration.

Table 5.1 Additional DAB Parameters

DAB CONVERTER (ALL TEST CASES)	RATED / BASE VALUES
Turns ratio N_{ps}	2
Switching frequency	7500Hz
Capacitor C_o	540μF
Input voltage rating	6500V *
Output current rating	2864A
Rated HVDC voltage	± 113kV

* This includes the required safety margin for the IGBTs.

5.7.1 Determination of wind turbine operational states and energy curtailment

To predict expected wind turbine and wind farm states, 7 years of 10 minute-resolution wind measurements of the FINO3 met mast (average rotor equivalent wind speed, wind direction and turbulence intensity) were binned into 7508 unique wind conditions and the likelihood of occurrence for each bin was recorded. The bin sizes are 1m/s, 10 degrees, and 1% for wind speed, direction and turbulence intensity, respectively. For each of these 7508 wind conditions, the entire wind farm was simulated using the SimWindFarm toolbox available for MATLAB/Simulink [84]. This toolbox realizes time-transient, dynamic simulations of aerodynamic-mechanical systems of wind turbines in a wind farm, taking into account upwind wind speed, wind direction, turbulence intensity and wake effects. For each of the 7508 simulation runs, the wind turbine output power, rotational speed and rotor-equivalent wind speeds were recorded with a 1-second time resolution for a duration of a wind field passing the wind farm twice at any given average wind speed. These simulations were executed on heterogeneous computational clusters (Compute Canada: Cedar, Graham; local computational nodes of the power electronics lab) due to large computational and memory requirements of such a simulation.

It was assumed that electrical transients are significantly faster than the 1-second time step, such that near steady-state operation can be assumed for all electrical systems with respect to the chosen time step. The time series of wind turbine power, rotational speed and wind speed simulation were then used to compute the operational states of the electric wind farm components using their steady-state models as discussed in the following paragraphs specific to each wind farm configuration.

Finally, the average amount of energy curtailed per second due to converter limits was computed for each of the 7508 simulations. This average energy curtailment per case was then weighed by the likelihood of occurrence of each of the 7508 cases, as recorded by the FINO3 met mast. The final amount of energy curtailment is then obtained as:

$$E_{curt,year} = \sum_{n=1}^{7508} P_{curt}[n] \times \phi[n] \times (60 \times 60 \times 24 \times 365)\frac{s}{a} \qquad (5.38)$$

where $E_{curt,year}$ is the expected amount of energy curtailed per year due to converter limits, the index number n denoting each of the 7508 cases observed by the FINO3 met mast, $P_{curt}[n]$ the average energy curtailed per second for case n, and $\phi[n]$ he associated likelihood of occurrence of case n. This workflow is depicted in Figure 5.9.
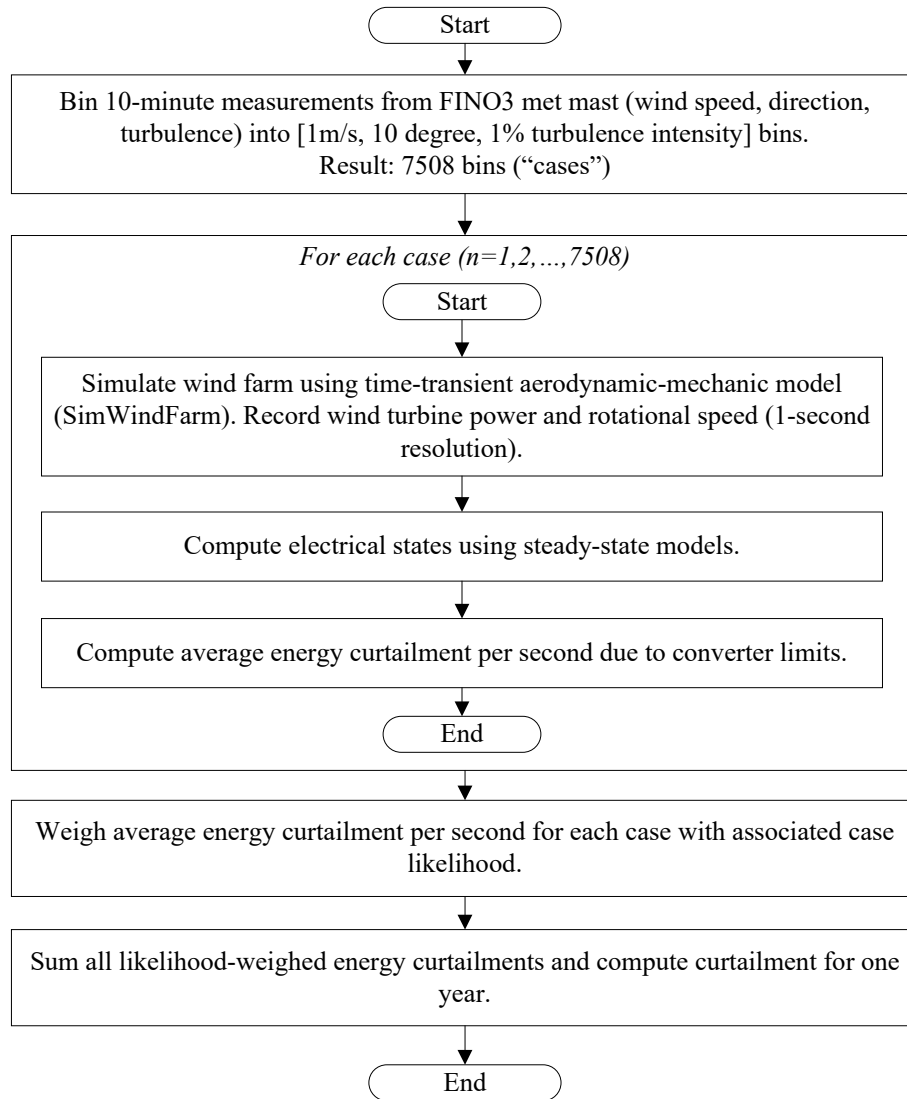
Figure 5.9 Determination of wind turbine operational states and energy curtailment for 450MW wind farm sizing case studies.

For the DCS-PPPC configuration, electrical converter states were calculated based on relations in section 5.4 and Chapter 3. To study different converter sizing options, eight candidate converter ratings have been applied to the calculation of converter operating conditions as shown in Table 5.2 and visualized in Figure 5.10. Test cases 1-7 represent a partial operating range sizing, as there is no valid HVDC-link current to realize unconstrained converter operation at cut-in and rated output power simultaneously. Test case 8 represents a full operational range sizing, as an HVDC-link current of

approximately 0.5pu allows an unconstrained operation of converters at full and cut-in wind turbine power, as shown in Figure 5.10.

Table 5.2 DAB Converter Test Cases

TEST CASE	LEAKAGE INDUCTANCE L_t	OUTPUT VOLTAGE RATING	INPUT CURRENT RATING
1	740μH	1247V = 0.22pu	336A = 0.39pu
2	592μH	1558V = 0.27pu	419A = 0.49pu
3	493μH	1870V = 0.32pu	503A = 0.58pu
4	423μH	2181V = 0.38pu	587A = 0.68pu
5	370μH	2493V = 0.43pu	671A = 0.77pu
6	247μH	3739V = 0.65pu	1007A = 1.17pu
7	185μH	4986V = 0.86pu	1342A = 1.56pu
8	118μH	5800V = 1.00pu	2097A = 2.43pu
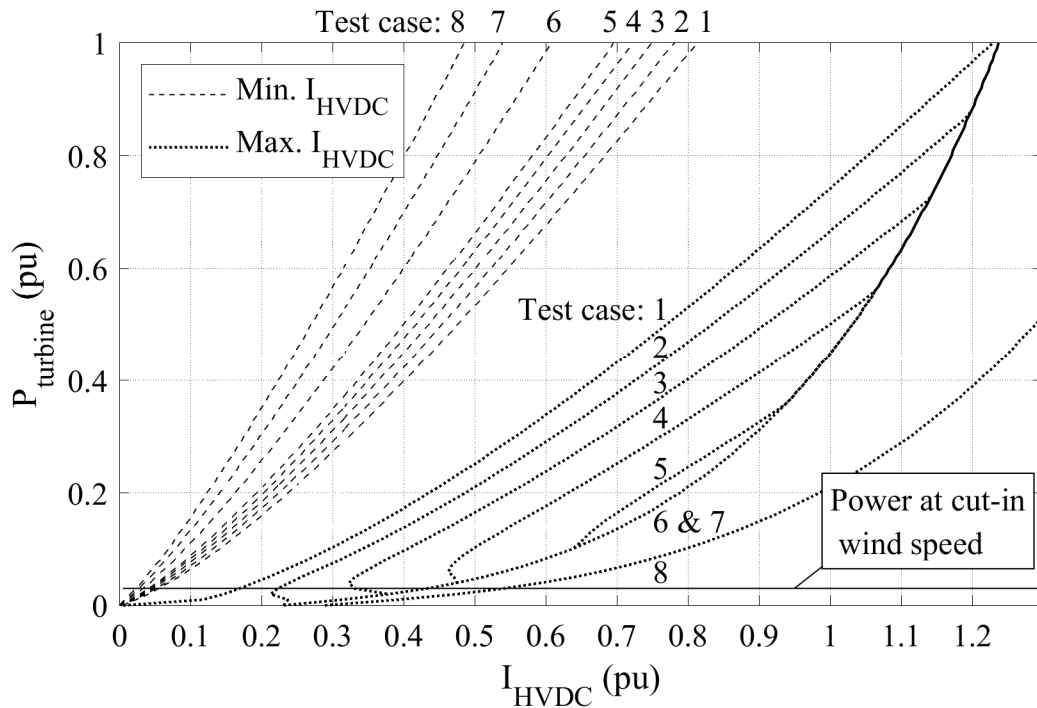
Figure 5.10 Possible wind turbine operating points without PPPC sizing-related power curtailment for different HVDC-link currents and all 8 DCS-PPPC test cases.

Converter operating conditions for the DCS-VSC configuration have been calculated based on relations given in section 5.5 and [72]. Seven test cases have been considered

for this configuration to assess potential benefits from a partial operational range sizing, compared to a full operational range sizing that is represented by an eighth test case. VSC output voltage ratings are set to multiples of 9kV, up to 63kV. It is worth noting that a VSC with a 63kV output voltage rating can be challenging to implement given limited IGBT output voltage ratings available. Such high output voltage rating is analyzed mainly to outline the trends on energy curtailment with sizing up to full operational range sizing.

For the DCS-Buck configuration, diode-bridge rectifier states were derived using the relations depicted in Figure 3.6. Remaining states were calculated using relations discussed in section 5.6 and [35]. As partial operational range sizing has been found infeasible for this configuration, two test cases based on full operational range sizing are evaluated to confirm that no energy curtailment is to be expected from these sizing choices. The first test case is based on the converter output ratings originally discussed in [35] (4166V and 1200A), whereas the second test case examines the converter output ratings suggested in section 5.6 (5800V and 862A).

To preserve the general trends of this analysis, component ratings have not been matched with commonly available device ratings. In a final design iteration, these and desired safety margins should be considered.

It has been assumed that wind turbine operation at or beyond converter limits results in a partial or full wind power curtailment: a wind turbine converter operating at maximum limits curtails the wind turbine power to the maximum that can be processed with the converter at its current limit, while pitch control ensures proper speed control of the turbine; a converter operating beyond minimum limits results in the wind turbine coming to a stand-still, as the converter cannot reduce the (inherent) DBR's natural power draw at a given HVDC-link current sufficiently to restore a balance of power between incoming wind power and electric power absorption. It is worth noting that the minimum limit does not apply to the DCS-Buck configuration, as the buck converter is capable of operating down to and at zero output voltage and power at any operating condition. The HVDC-link current was scheduled in such a way to minimize the occurrence of curtailment action as discussed in section 4.4.2.

Based on this analysis, the amount of annual energy curtailment due to the converters operating at their limits can be predicted. This is used to inform the sizing of such converters.

5.7.2 Results – DCS-PPPC
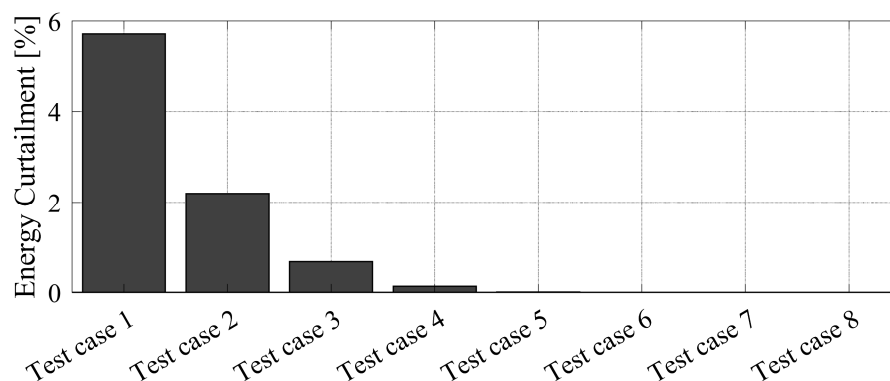
Figure 5.11 Estimated annual energy curtailment of DCS-PPPC configuration as percentage of annual energy production due to PPPC component rating limitations.

The annual energy curtailment due to exceeding converter limitations has been estimated using the simulations outlined in the previous section. As can be seen in Figure 5.11, there is a significant difference in annual energy curtailment due to wind turbine converter sizing decisions. If the PPPCs are rated for 0.22pu output voltage rating (test case 1), more than 5% of potential annual energy production is lost due to curtailment. As PPPC ratings increase, less energy curtailment is necessary. For a PPPC output voltage rating of 0.38pu and input current rating of 0.68pu, only 0.13% of annual energy production potential is curtailed (test case 4). A further increase of PPPC ratings decreases the need for curtailment only marginally. Numerical results indicate the presence of a negligible amount of energy curtailment for test cases 5, 6 and 7 ($<0.01\%$). The full operational range sizing case (test case 8) results confirms that the wind farm could operate without energy curtailment due to converter limits. However, it is expected that the increase in switch ratings will contribute negatively to converter losses and capital cost of wind turbines, compared to partial operational range sizing test cases (such as test cases 4 and 5, for example). In particular, it requires 2.6 times the PPPC output voltage and 3.6 times the PPPC input current rating compared to test case 4.

This demonstrates how the presented PPPC sizing methodology can be applied to inform decisions about component ratings for power converters for wind farms with single-string series-connected DC collection systems.

Based on these results, it appears reasonable to consider converter ratings similar to those of test case 4 or 5 as there is only a negligible decrease in annual energy production to be expected. Based on local electricity market conditions, an economic assessment

between converter cost and value of curtailed energy due to converter rating limitations can further solidify the choice of converter ratings.

5.7.3   Results – DCS-VSC
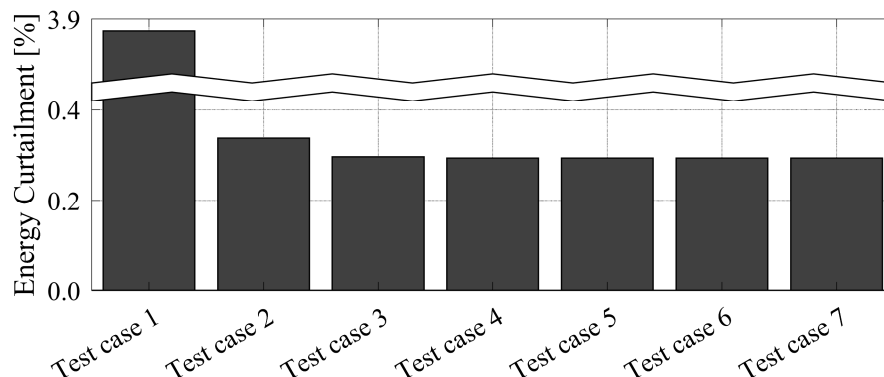
Figure 5.12 Estimated annual energy curtailment of DCS-VSC configuration as percentage of annual energy production due to converter component rating limitations.

The expected annual energy curtailment due to converter limits has also been estimated for the DCS-VSC configuration. The results are shown in Figure 5.12. As can be seen, a VSC with output voltage rating of 9kV (test case 1) results in approximately 3.9% of available energy to be curtailed due to converter limits. However, VSC output voltage ratings of 18kV and higher only result in approximately 0.3% of annual energy production to be curtailed. For test cases 3 to 7, most energy curtailment stems from preventing excessive HVDC-link voltages. There are several design aspects in series-connected DC wind farms to be considered, such as maximum possible insulation to ground (i.e., maximum HVDC-link voltage) and system design for high conversion efficiencies [102]. It may be possible to optimize the system to reduce or eliminate the HVDC-link voltage rating-related curtailment. Ultimately, an economic assessment might be useful to find the lowest-cost design trade-off between rated HVDC-link voltages, wind turbine voltage levels, number of wind turbines per string and conversion losses – all of which are factors that can relate to the amount of energy curtailment due to excessive HVDC-link voltages or stem from measures addressing these.

5.7.4   Results – DCS-Buck

Following the methodology discussed in section 5.6, annual energy curtailment has been estimated for the DCS-Buck configuration. Since both test cases followed the full operational range sizing approach, no energy curtailment due to converter limits was

expected. The simulation of both test cases confirmed that there is no energy curtailment due to converter limits to be expected. The second test case examining converter output ratings suggested in section 5.6 (5800V and 862A) resulted in overall higher HVDC-link voltages and lower HVDC-link currents. This indicates that there is a potential for efficiency improvements in the collection and transmission systems through current reduction on an annual average compared to the sizing initially suggested in [35].

5.8 Summary

In this chapter, a methodology for determining the component ratings of wind turbine converters in single-string, series-connected DC wind farms has been developed. As demonstrated in this work, the series connection of wind turbines with DC output results in a strong interdependence of operating points among the wind turbines in a wind farm. Consequently, traditional methods of sizing wind turbine converters are not useful for determining all component voltage and current ratings in these kinds of wind farms. First, this chapter presents a generic sizing framework, applicable to all single-string, series-connected DC wind farms. A distinction between full and partial operational range sizing approaches is made. It then applies the analytical framework to a wind farm configurations featuring differential power processing, voltage-source converters, and diode-bridge rectifiers and buck converters. The main design consideration in this sizing methodology is the reduction of energy curtailment resulting from finite component ratings while minimizing component ratings to partial operational range sizing. Finally, a case study for a 450MW wind farm demonstrates the implementation of the proposed sizing methodology and shows that converter output voltage rating of about 0.38pu and input current ratings of 0.68pu are sufficient for a proper wind farm operation for the wind farm configuration featuring differential power processing, with negligible energy curtailment despite finite converter ratings, and avoiding extra installation costs due to oversizing. Similarly, a voltage-source converter-based wind farm configuration may operate with low energy curtailment using converters rated at 18kV or higher. The wind farm configuration featuring diode-bridge rectifiers and buck converters requires full-size converters but operates without energy curtailment.

Chapter 6

Wind Turbine Startup and Shutdown

In conventional wind turbines with AC voltage output, wind turbine startup usually is facilitated using a special control region defined for the speed and pitch controllers [103]. For example, power set point values from the speed controller of the NREL 5MW reference wind turbine [81] are shown in Figure 6.1, recomputed from torque reference data in [81][84]. For low generator speeds, the power reference is held at zero, such that all wind energy is used to accelerate the rotor during startup. Additionally, the pitch control system is adjusted to facilitate a certain rate of rotor acceleration [103][104][105]. Conventional wind turbine converters possess the ability to regulate the power absorption from the generator from zero to rated power independently of other wind turbines within a wind farm. This makes wind turbine startup and shutdown relatively straightforward procedures with regards to the electrical subsystems of a conventional wind turbine. However, this simplicity relies on the availability of full-scale converters operating independently of one another in a wind farm. Such a configuration is not available in the wind farm configuration proposed in this thesis, which features a differential power processing approach. Intentionally limited converter power capacity and state dependence on the operating points of other wind turbines in a series string create challenges in starting a wind turbine without introducing additional or oversized hardware requirements. Wind turbine startup and shutdown procedures for this wind farm configuration are therefore discussed in this chapter.
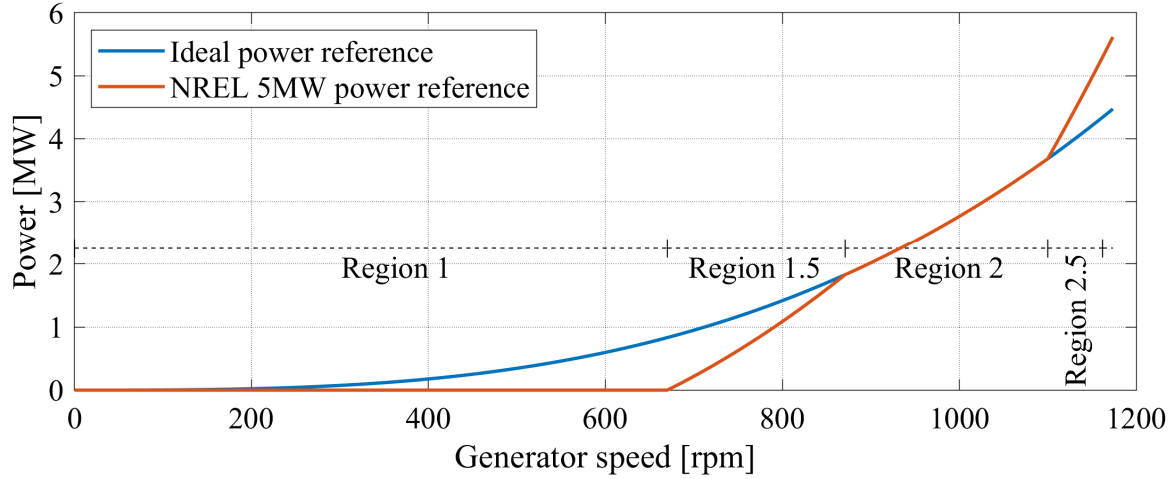
Figure 6.1 NREL 5MW speed controller power references (orange) and ideal power reference for MPPT operation (blue).

The presented wind turbine startup procedure enables wind turbines to successfully start under any operating condition, while avoiding increased requirements on the component ratings of the converters of each wind turbine. Successful wind turbine startup and shutdown for all important wind conditions are demonstrated through simulation.

For the purpose of studying wind turbine startup and shutdown, PPPC device ratings listed in Table 6.1 were considered. This was done to simplify the analysis compared to previously discussed multi-converter configurations. Conclusions for those more complex configurations and ratings are provided in section 6.2.3.

Table 6.1 PPPC device ratings for startup and shutdown study

PARAMETER	SYMBOL	DEFAULT VALUE
Number of Multi Converters	N_{MC}	1
DAB Output Voltage Rating	0.86pu	
DAB output capacitor	C_o	540µF
DAB transformer turns ratio	N_{ps}	2
DAB transformer leackage inductance (referred to primary side)	L_t	185µH

118
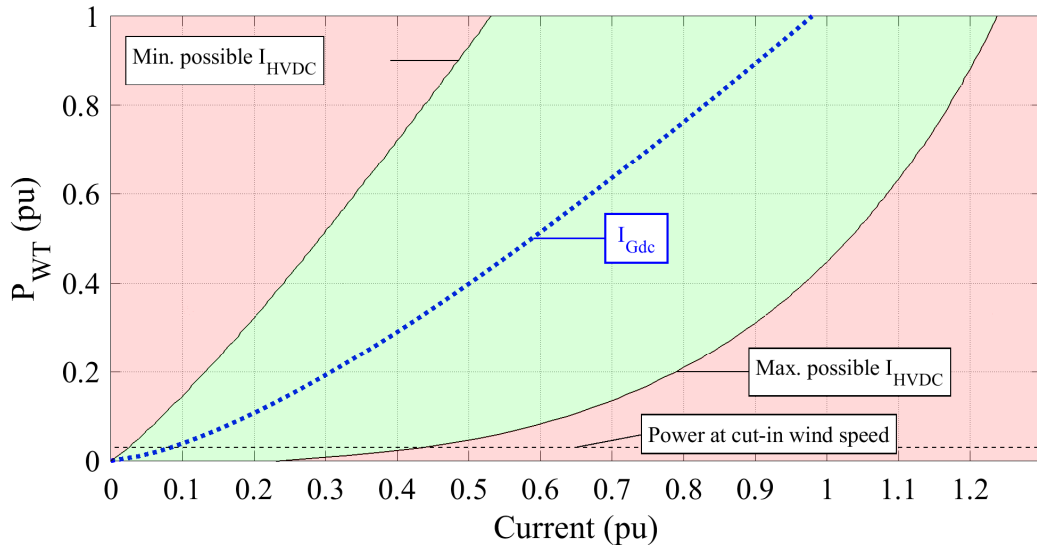
Figure 6.2 Viable HVDC-link currents for different wind turbine powers P_{WT}, PPPC and wind turbine ratings listed in Table 6.1.

In section 4.2, relations were derived to predict the wind turbine operating conditions for which a wind turbine converter operates within or outsite its component ratings. Calculated for the component ratings discussed in 3.6 and Table 6.1, the green area in Figure 6.2 represents the range of HVDC-link current and wind turbine output power in which the chosen DAB device ratings will not be exceeded for one wind turbine, unlike in the pink area. It becomes apparent, that the choice of HVDC-link current directly influences the PPPC's ability to follow a certain wind turbine power reference P_{ref}. For example, while P_{WT} is equal to 1.0pu, an HVDC-link current in the range of 0.53 to 1.24pu is possible for the given converter ratings. As all wind turbines in a series string experience the same HVDC-link current, there are restrictions to the maximum wind turbine output power differences that can be handled in this string. For example, if I_{HVDC} was chosen 1.0pu, a low-power wind turbine would lose its ability for MPP operation at powers below 0.45pu.

6.1 Challenges in Wind Turbine Startup

The control loops presented Chapter 4 do not directly address wind turbine startup. This section highlights the challenges of wind turbine startup when applying those controls. In particular, two potential approaches are examined: (1) starting the wind turbine with its Diode-Bridge Rectifier (DBR) electrically connected, but with the PPPC

bypassed, and (2) starting the wind turbine with the PPPC activated and operating according to controls presented in Chapter 4.

6.1.1 Rotor acceleration with DBR connected from stand-still (PPPC deactivated)
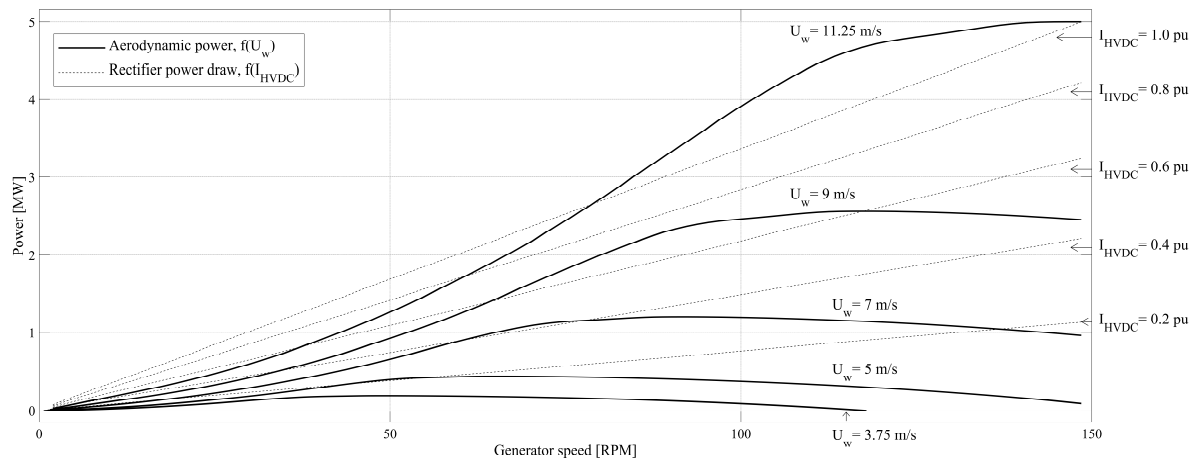
Figure 6.3 Wind turbine maximum aerodynamic power available at wind turbine generator and natural Diode-Bridge Rectifier power draw (no PPPC operation) versus generator speed.

If the wind turbine was to be started with the DBR connected from a standstill, it is difficult to guarantee that the aerodynamic torque τ_{rot} consistently supersedes the electromechanical developed torque τ_{gen} referred to the rotor side of the gearbox. Figure 6.3 shows the maximum aerodynamic power available at the wind turbine generator for different wind speeds and rotational speeds for the 5MW NREL reference wind turbine when using the theoretically optimal pitch setting. It also shows the amount of power, the DBR would absorb at different rotational speeds for different HVDC-link currents using the matching wind turbine design listed in section 3.6. As it can be seen, for a significant proportion of operating conditions, aerodynamic power is less than what the DBR would absorb. For a wind turbine to start up successfully, aerodynamic power would need to be consistently larger than electric power draw, however.

Furthermore, simulation results shown in Figure 6.4 show a startup attempt from standstill for the 5MW wind turbine. This simulation demonstrates further challenges during the initial acceleration of the wind turbine rotor. In this simulation, a wind turbine is provided with a startup command at t=10s. Its PPPC is deactivated, unfolder polarity $UF = 1$, and an HVDC-link current, regulated to approx. 0.5pu, flows at the

DBR DC terminals. As it can be seen in Figure 6.4 (b), no meaningful rotor acceleration can be achieved. The difference between generator mechanical and electromagnetic counter torques never develops a significant offset to provide rotor acceleration. Initially at zero generator speed, the full HVDC-link current flows through all DBR diodes resulting in zero V_{Gdc}. A rise in V_{Gdc} is only possible, if generator currents exceed the I_{HVDC} value in order to change the DBR diode conduction pattern to that of an operating DBR. This can be observed in Figure 6.4: a rise in V_{Gdc}, shown in Figure 6.4 (e), only happens when the generator currents, depicted in Figure 6.4 (f), are equal or slightly exceed the HVDC link current which is regulated to 0.5pu, here. Following a rise in V_{Gdc} there is sufficient power drawn by the electrical system to bring the generator and rotor to a halt again, as can be seen in Figure 6.4 (b). This further demonstrates that a wind turbine startup without PPPC operation cannot be guaranteed under all operating conditions.
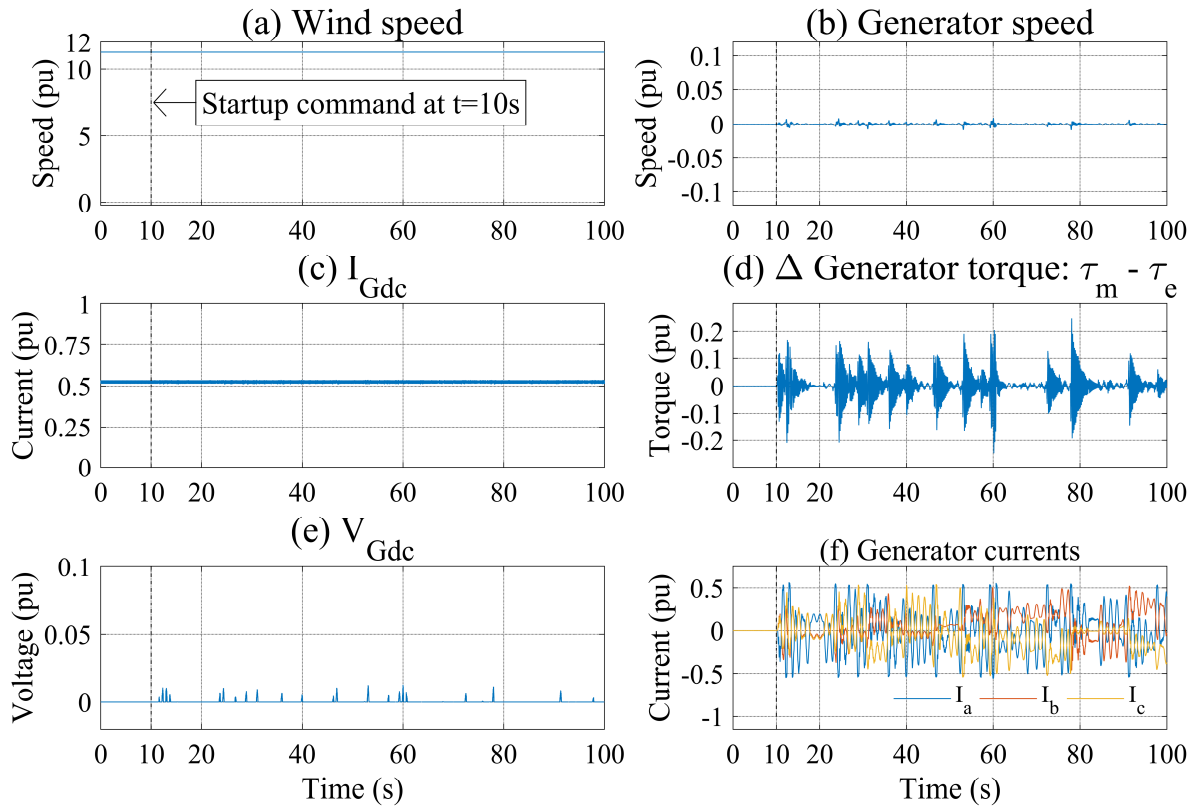
Figure 6.4 Wind turbine rotor acceleration failing when DBR is exposed to HVDC-link current from stand still. Wind turbine startup commanded at t=10s at rated wind speed.

6.1.2 Rotor acceleration with DBR connected from stand-still (PPPC activated)

To avoid the previously discussed challenges, it might be possible to activate the PPPC operation during startup. However, as indicated in Figure 6.2, the PPPC would be operating outside its ratings for most HVDC-link currents that could be prevailing during startup. As shown in Figure 6.2, the HVDC-link current should not exceed approximately 0.2pu for PPPCs in startup in order to not exceed PPPC component ratings. However, such HVDC-link current would be infeasible for any other wind turbines in the same series string operating above an output power of approximately 0.35pu. Therefore, a wind turbine startup with PPPCs and control of Chapter 4 is difficult to realize in certain wind conditions without affecting neighbouring wind turbines. To widen the range of valid operation points during a wind turbine startup,

an increase of DAB voltage and current ratings would be required. For this reason, this procedure is not meaningful and not investigated further.

6.2 Wind Turbine Startup Procedure

In this section, the procedures available for shutdown and startup of the proposed wind farm configuration are discussed.

6.2.1 Mechanisms for wind turbine deceleration

There are several mechanisms available for slowing a wind turbine down to a standstill. For the wind turbine configuration considered here, the most notable deceleration mechanisms are: (1) aerodynamic braking using the pitch system, (2) shaft-mounted disc brake, and (3) electrical braking using the DBR.

While methods (1) and (2) are available to all pitch-controlled large-scale wind turbines, method (3) is specific to the wind turbine design under consideration. It relies on the uncontrolled power draw through the DBR when a wind turbine is connected to the series-string and the PPPC is inactive. The power draw then becomes:

$$P_{WT} = V_{Gdc}I_{HVDC} \tag{6.1}$$

A rotor deceleration solely based on method (3) can only be achieved if the aerodynamic power is less than $V_{Gdc}I_{HVDC}$ (neglecting losses). Therefore, it typically requires the additional use of the aerodynamic brake. If the PPPC power was negative before PPPC deactivation, an additional braking effect could be achieved through this method with less reliance on aerodynamic braking, since under this condition I_{Gdc} would be operated at a value larger than I_{HVDC}.

The advantages of method (3) are the avoidance of fast transients in the voltages V_{Gdc} and V_{HVDC} in many cases that can result from a sudden disconnection of the DBR at high-power operation, and that more energy is delivered to the transmission system without additional hardware required.

6.2.2 Mechanism for wind turbine acceleration

In order to accelerate a wind turbine rotor from standstill under sufficient wind conditions, the rotor torque τ_{rot} must be larger than the generator electromagnetic counter referred to the rotor side of the gearbox (neglecting losses). Various approaches are available to either increase τ_{rot}, or keep τ_{gen} low. To maximize τ_{rot}, the pitch system

can be adjusted in order to operate the rotor with the maximum power coefficient available for the given tip speed ratio. The following approach is aimed at keeping τ_{gen} low by rejecting any DBR power draw during early rotor acceleration while operating without the PPPC's dual-active bridge converter.

To avoid PPPC-related disadvantages and restrictions discussed in section 6.1.2, an alternate scheme has been devised to reject any power draw through the DBR, avoiding the PPPC to be operating at or outside its ratings.

In this scheme, the PPPC output capacitor C_o in Figure 3.7 (page 37), wind turbine bypass diode D_{out} in Figure 3.3 (page 30) and the unfolder circuit are leveraged to divert the HVDC-link current from the DBR and PPPC switches through bypassing them. The related circuit configuration is shown in Figure 6.5.
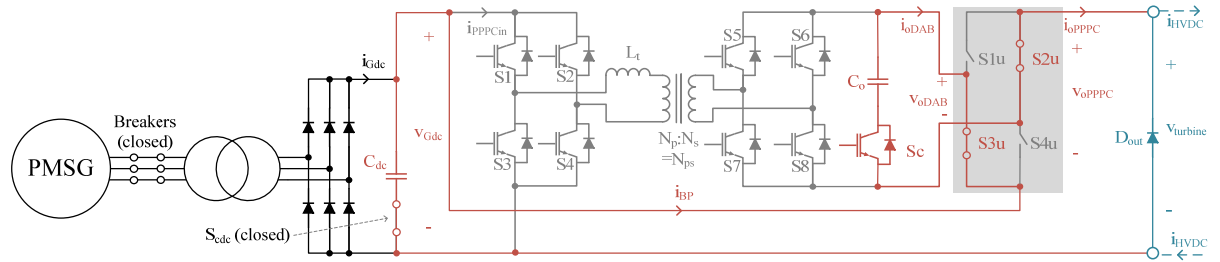
Figure 6.5 Wind turbine converters during startup in 'DBR power rejection' scheme. Inactive components in gray; bypass path I involving C_{dc} and C_o in red; bypass path II involving D_{out} in blue. Bypass path I is used to forward bias D_{out} of bypass path II.

In this configuration, the AC-side DBR breakers are closed, the unfolder polarity UF is set to -1, and PPPC switches S1-S8 are deactivated. This leads to the bypass current i_{BP} flowing into capacitor C_o, causing V_{oDAB} to rise to positive and V_{oPPPC} to fall to negative values. The rate of voltage decrease for V_{oPPPC} is:

$$\frac{dV_{oPPPC}}{dt} = -\frac{I_{BP}}{C_o} \tag{6.2}$$

The rectifier DC voltage V_{Gdc} is determined by the voltage induced in the generator because of its (increasing) rotational speed. As a result, the DC-link capacitor C_{dc} is charged slowly as the wind turbine accelerates.

To ensure zero wind turbine output power, the output voltage $V_{turbine}$ has to be zero, such that the output-side diode D_{out} is forward biased bypassing the HVDC-link current. This is achieved when

$$-V_{oPPPC} \geq V_{Gdc} \qquad (6.3)$$

To ensure that (6.3) holds under all expected operating conditions, C_o has to be sized properly, as discussed next. From (6.3) one can derive that the rate of fall of V_{oPPPC} must at least be equal to the rate of rise of V_{Gdc}:

$$-\frac{dV_{oPPPC}}{dt} \geq \frac{dV_{Gdc}}{dt} \qquad (6.4)$$

Furthermore, due to rectifier and output diodes:

$$I_{BP} \leq I_{HVDC} \qquad (6.5)$$

(6.2)-(6.5) lead to the inequality

$$\frac{I_{HVDC}}{C_o} \geq \frac{I_{BP}}{C_o} \geq \frac{dVG_{dc}}{dt} \qquad (6.6)$$

resulting in the sizing constraint for C_o:

$$C_o \leq \frac{I_{HVDC,min}}{\left(\frac{dV_{Gdc}}{dt}\right)_{max}} \qquad (6.7)$$

where $I_{HVDC,min}$ is the minimum HVDC-link current expected to be used in the wind farm and $(dV_{Gdc}/dt)_{max}$ is the maximum slope in V_{Gdc} expected during wind turbine startup. Both quantities are averaged over one fundamental period.

Once the rotor has gained sufficient speed, normal circuit configuration can be restored and normal system operation is resumed for that wind turbine. This transition point must be chosen such voltage values for V_{Gdc} and V_{oPPPC} do not exceed the PPPC's output voltage rating before the transition. Yet, it is desirable to delay the transition, in order to minimize the impact on remaining wind turbines in the series string due to limited PPPC ratings, as illustrated in Figure 6.2.

It is worth mentioning that this scheme is superior to a scheme in which rotor speed is increased by keeping AC breakers opened, due to the lack of inrush current that a sudden charging of C_{dc} would cause upon reclosing of AC breakers.

6.2.3   PPPC component voltage and current rating requirements for wind turbine startup

In order to enable a successful wind turbine startup, minimum voltage rating requirements on the DAB output stage components (S5-S8, S1u-S4u, S_c and C_o) have to

be met. While operating during a wind turbine startup (according to section 6.2.2), the DAB output components are exposed to voltages of magnitude V_{Gdc}. As generator speed increases, V_{Gdc} increases. The largest magnitude of V_{Gdc} during this procedure is experienced at the transition point towards normal operation. Here, this transition point has been chosen to be at the generator speed that represents steady-state operation at cut-in wind speed. At this operating point, V_{Gdc} is equal to 0.38pu. As a result, DAB output stage components must be rated to withstand an output voltage of at least the voltage at the transition point (here, 0.38pu).

In addition, the initiation of a wind turbine startup is only feasible if the wind turbine's steady-state operating point can be maintained in its series string given the prevailing wind conditions and component ratings. Online predictions about this can be made from the data shown in Figure 6.2.

When the PPPC is realized in a multi-converter configuration with N_{MC} larger one, all DABs need to be operated simultaneously as described in this chapter. The sum of output voltage ratings must adhere to the discussions in this chapter for a single-DAB PPPC.

As wind turbine shutdown does not necessarily involve an activated PPPC, and can solely be performed using the aerodynamic and mechanical brakes, and uncontrolled DBR operation, there are no additional requirements on electrical component ratings in order to ensure reliable wind turbine shutdowns.

6.3   Wind Turbine Shutdown Procedure

The wind turbine shutdown procedure is shown in Figure 6.6. The shutdown procedure is activated by the wind turbine/farm control system, when generator speed falls below minimum speed $\omega_{min,1}$ due to low-wind conditions, or when a high-wind cutout is deemed necessary. The majority of wind turbine deceleration can be achieved by using the aerodynamic brake in conjunction with the uncontrolled operation of the DBR, while the PPPC is deactivated (shutdown step 2 in Figure 6.6). Once the rotor speed has come very close to a stand-still at $\omega_{min,2}$, the electrical systems are disconnected and bypassed, and the mechanical disc brake is employed.

Wind turbine shutdown

(1) Normal operation
- Mechanical Brake: off
- Pitch: normal operation
- PPPC (switching & control loop): on
- Unfolder: normal operation
- DBR AC-side breakers: closed
- S_c: closed
- S_{cdc}: closed

$\omega < \omega_{min1}$ *OR*
$U_w > U_{w,cutout}$ *OR*
Manual Shutdown request

(2) Slow-down
- Mechanical Brake: off
- Pitch: *braking position*
- PPPC (switching & control loop): *off*
- Unfolder: *UF=0*
- DBR AC-side breakers: closed
- S_c: *opened*
- S_{cdc}: closed

$\omega < \omega_{min2}$

(4) Wind turbine off
- Mechanical Brake: *on*
- Pitch: *off position*
- PPPC (switching & control loop): *off*
- Unfolder: *UF=0*
- DBR AC-side breakers: *opened*
- S_c: *opened*
- S_{cdc}: *opened*

$\omega = 0$

(3) Shutdown to standstill
- Mechanical Brake: *on*
- Pitch: *braking position*
- PPPC (switching & control loop): *off*
- Unfolder: *UF=0*
- DBR AC-side breakers: *opened*
- S_c: *opened*
- S_{cdc}: *opened*

Figure 6.6 Wind turbine shutdown procedure.

6.4   Wind Turbine Startup Procedure

The wind turbine startup procedure is shown in Figure 6.7. If the wind turbine/farm control system demands a wind turbine startup, and sufficient wind energy is available (wind speed U_w at or above cut-in speed $U_{w,cutin}$), a startup is initiated. First, (if previously applied) the disc brake is deactivated and the pitch angle is adjusted to support rotor acceleration. As elaborated in section 6.1.1, the electrical system is configured as shown in Figure 6.5 in order to reject any electrical power draw while the DBR is connected to the generator. As a result, the wind turbine rotor can accelerate. At rotor speed $\omega_{start,thres}$, which usually is set to the rotor speed at operating conditions near cut-in wind speed, normal system operation is resumed, i.e., the PPPC switching and control loop operation is resumed. Further rotor acceleration to the new steady-state operating point is facilitated through normal operation following the wind turbine speed-torque controls discussed in section 4.1 (page 50).

Wind turbine startup

(1) Wind turbine off
Mechanical Brake: *on*
Pitch: *off position*
PPPC (switching & control loop): *off*
Unfolder: *UF=0*
DBR AC-side breakers: *opened*
S_c: *opened*
S_{cdc}: *opened*

$U_w > U_{w,cutin}$ AND/*OR*
Manual Startup request

(2) Spin-up, DBR power rejection
• Mechanical Brake: off
• Pitch: *startup position*
• PPPC (switching & control loop): *off*
• Unfolder: *UF=-1*
• DBR AC-side breakers: closed
• S_c: closed
• S_{cdc}: closed

$\omega > \omega_{start,thres}$

(3) Normal operation
Mechanical Brake: off
Pitch: normal operation
PPPC (switching & control loop): on
Unfolder: normal operation
DBR AC-side breakers: closed
S_c: closed
S_{cdc}: closed

Figure 6.7 Wind turbine startup procedure.

6.5   Case Study: Wind Turbine Startup/Shutdown in series-connected Wind Farm

To confirm the effectiveness of the discussed wind turbine shutdown and start procedures, a series string of five 5MW wind turbines has been simulated in MATLAB/Simulink using the Simscape Specialized Technology toolbox. Each test case starts with all wind turbines operating at steady state, followed by a shutdown and a startup procedure for wind turbine 1. The test cases are designed to consider all common conditions for startup and shutdown, i.e., (1) operation at low wind conditions, (2) operating at rated wind speeds, and (3) operation near cut-out wind conditions. In a fourth test case, all wind turbines are commanded a shutdown, followed by staggered startup commands. This demonstrates the wind farms capability to start from a full shutdown. In all cases, the PPPC component ratings are not exceeded.

6.5.1   Case 1: Operation at low wind speed

In this case, all five wind turbines operate at 5m/s, near cut-in wind speed. At t=10s, the wind speed for wind turbine 1 is set to 0m/s, in order to provoke a wind turbine shutdown. At t=105s, the wind speed for wind turbine is set back to 5m/s in order to initiate a startup operation. Simulation results of this case are shown in Figure 6.8.

As it can be seen in Figure 6.8 (c), rotor speed starts to drop as available wind energy drops at t=10s. As soon as rotor speed reaches its minimum value $\omega_{min,1}$, the wind turbine shutdown procedure is activated automatically. This entails the deactivation of the PPPC (as can be observed in Figure 6.8 (b) and Figure 6.8 (d)), and activation of aerodynamic brake, as seen in Figure 6.8 (e). As the speed of aerodynamic brake activation has been limited in this design, the majority of rotor deceleration is achieved through the DBRs power draw. Upon wind speed recovery, a wind turbine startup procedure is initiated. As shown in Figure 6.8 (d), during startup $V_{Gdc} = -V_{oPPPC}$ and PPPC power (Figure 6.8 (b)) remains zero. This demonstrates the turbine startup procedure with DBR power rejection, as described in section 6.2.2. As soon as rotor speed has reached the transition point $\omega_{start,thres}$, PPPC operation is resumed. Further rotor acceleration to the steady-state operating point is achieved using regular wind turbine controls.

Figure 6.8 Simulation results of test case 1: Operation at low wind speeds. Waveforms are shown for wind turbine 1. Operation in startup and shutdown procedures (steps (2) and (3) of Figure 6.6, and (2) of Figure 6.7) highlighted in gray.

6.5.2 Case 2: Operation at rated wind speed

In this scenario, all wind turbines operate at rated wind speed. At t=10s, a manual shutdown command is issued to wind turbine 1. At t=85s, a manual startup command is sent. The simulation results are shown in Figure 6.9. The shutdown and startup procedures are executed in a very similar way to that for case 1. However, after wind turbine startup, a short delay in PPPC operation is caused due to the large power differences in the series string and resulting power limitations within the PPPC. As soon

as the HVDC-link current reaches a low enough value, PPPC operation resumes and rotor speed is increased to its rated value through regular wind turbine controls.

Figure 6.10 is based on Figure 6.2 and shows the operating points of all wind turbines within the range of valid operating points given the chosen PPPC ratings. The transition point from startup with DBR power rejection to regular wind turbine operating with activated PPPC is highlighted. As it can be seen, the startup mode with DBR power rejection successfully transitions the wind turbine from an operating point outside of what the PPPC could handle to an operating point within the valid range of PPPC ratings. Afterwards, the PPPC is activated and remaining wind turbine power increase is achieved using default controls presented in Chapter 4.
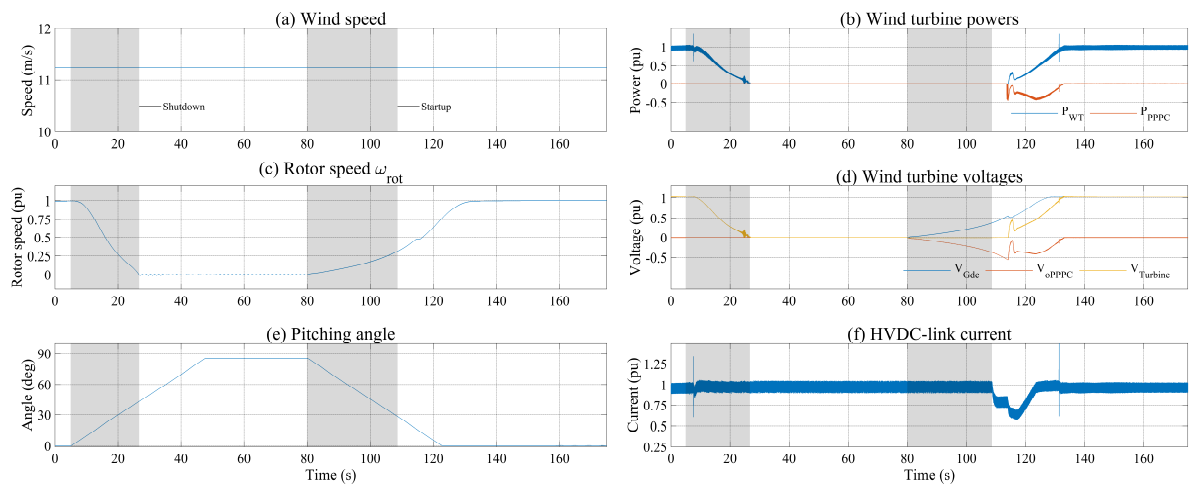
Figure 6.9 Simulation results of test case 2: Operation at rated wind speeds. Waveforms are shown for wind turbine 1. Operation in startup and shutdown procedures (steps (2) and (3) of Figure 6.6, and (2) of Figure 6.7) highlighted in gray.
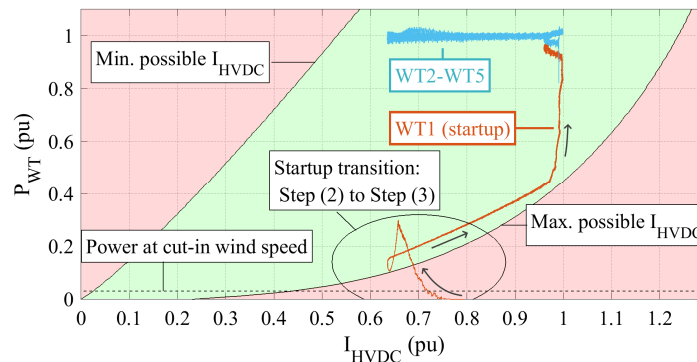
Figure 6.10 Simulation results of test case 2: Progression of wind turbine output powers in the range of valid PPPC output powers (highlighted in green) during wind turbine startup as a function of average HVDC-link current.

130

6.5.3   Case 3: Operation near cut-out wind speed

The third test case is designed to verify wind turbine shutdown and startup at high-wind conditions. Initially, all wind turbines are operated near cut-out wind speed. At t=10s, wind turbine 1 experiences a step change to 28m/s in wind speed, which triggers a shutdown procedure. At t=85s, wind speed is set back to 24m/s, such that this wind turbine will start up and resume operation at rated power. The simulation results for this case are depicted in Figure 6.11.

Both shutdown and startup are performed very similarly to those in case 2. However, with the rate of pitch angle reduction selected here, the higher rate of rotor acceleration is due to higher wind energy available. To reduce the acceleration rate, a slower reduction of pitch angle or a feedback control around rotor acceleration could simply be implemented. A small overshoot in rotor speed after wind turbine startup can be observed which is governed by the wind turbine pitch controller design. A slower deactivation of aerodynamic brake, or changes to the pitch controller could be used to reduce this overshoot, if desired.
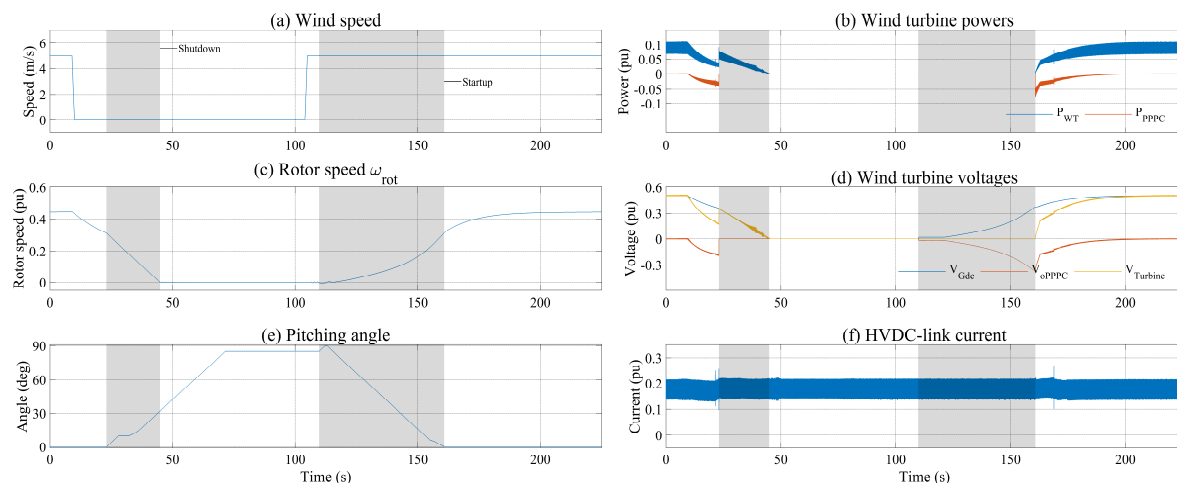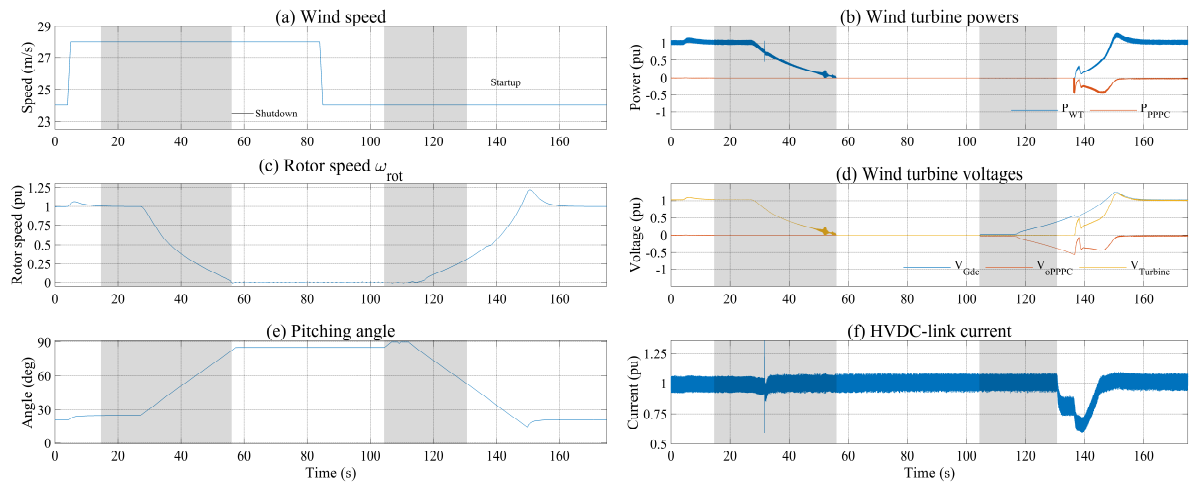

Figure 6.11 Simulation results of test case 3: Operation near cut-out wind speeds. Waveforms are shown for wind turbine 1. Operation in startup and shutdown procedures (steps (2) and (3) of Figure 6.6, and (2) of Figure 6.7) highlighted in gray.

6.5.4   Case 4: Wind farm start from full shutdown

In the last case, a full farm shutdown and restart is tested. With the wind farm operating at rated wind speed, a shutdown is commanded to all turbines at t=10s. Starting at t=85s, the wind turbines are commanded a startup sequence one after another. As apparent in Figure 6.12, all wind turbines can successfully transition from

rated power operation to stand still and return to rated power operation. While no turbine is in operation, the HVDC link has been deactivated. Prior to the first turbine's initiation of startup sequence, the HVDC link operation is resumed at its minimum current value, set to 0.1pu.
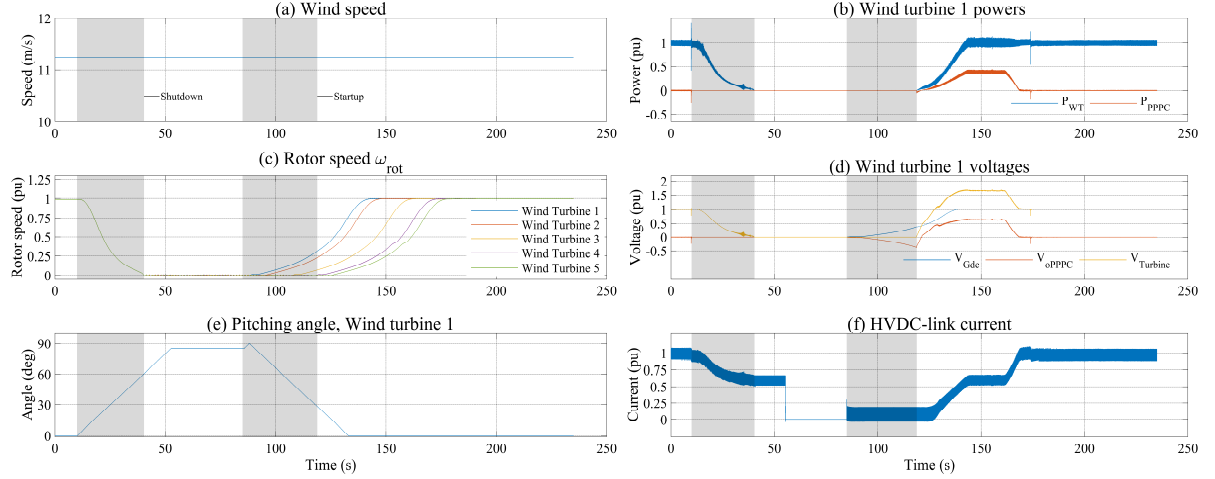
Figure 6.12 Simulation results of test case 4: Full wind farm shutdown at rated wind speeds. Waveforms are shown for wind turbine 1, except in (c). Operation in startup and shutdown procedures (steps (2) and (3) of Figure 6.6, and (2) of Figure 6.7) highlighted in gray.

6.5.5 PPPC output capacitor size constraints

(6.7) describes the condition on C_o for the aforementioned startup scheme to be stable and successful. For the three presented cases, the maximum allowable PPPC output capacitor sizes have been calculated, based on the assumption that the minimum possible HVDC-link current is 10% of its rated value. The simulation case with the fastest rotor acceleration causes the fastest rise in V_{Gdc}. This is the case for simulation case 3 where wind speeds are near cut-out levels. For this simulation case and PPPC ratings, the maximum allowable PPPC output capacitance C_o has been found to be 32mF. Conventional design of C_o resulted in the choice of 540μF. This value was found mainly based on considerations for output voltage ripples. It becomes apparent that in practice the additional constraint on C_o (here, 32mF) does not affect the choice of C_o value, as conventional design approaches result in a C_o value far lower than the maximum value possible for startup.

6.6 Summary

In this chapter, wind turbine startup and shutdown procedures have been introduced that leverages unique features available in the proposed wind farm configuration. Due to a limited differential power processing capability range available to the converters in a wind farm, conventional wind farm startup mechanisms are not applicable to this wind farm or would require excessive converter component ratings not utilized in normal operation. To mitigate this challenge, an alternative wind turbine startup procedure has been proposed that uses the converters' capacitors to reject any electric power draw from the turbine during initial rotor acceleration. As a result, restrictions on converter ratings are no longer dominated by the startup procedure. Dynamic simulations and component rating calculations of a series string of five wind turbines for all dominant startup and shutdown scenarios prove the effectiveness of the proposed approach.

Chapter 7

A Comparative Economic Assessment

In this chapter, an economic assessment of a selection of wind farm configurations is presented. In addition to the proposed wind farm configuration ("DCS-PPPC"), a conventional AC wind farm with dedicated HVDC link ("AC+HVDC"), as well as the additional series-connected DC wind farm configurations of Chapter 5 ("DCS-VSC" and "DCS-Buck") are considered. For all wind farm configurations, all systems are identical except for those electrical systems that are defining a particular wind farm configuration. The economic assessement considers capital expenses, maintenance cost, revenues and decommissioning costs for a project lifetime of 27 years. In addition, it considers the impact of conversion losses and converter ratings for all candidate wind farm configurations, as well as multiple converter rating test cases for each of the DC wind farm configurations. System reliability is considered based on data in [85], however differences in reliability for DC wind farms have been assumed to be negligible. A comprehensive study on system reliability and availability for the DC wind farm configurations of interest is an important item for future work.

In the following, the economic model is introduced and all wind farm configurations are revisited briefly. This is followed by a documentation of efficiency modeling performed for all wind farm configurations and a summary of the converter sizing results of Chapter 5. Finally, economic indicators and results are discussed to highlight the overall economic differences between the wind farm configurations discussed, and to

identify a candidate converter rating for the proposed wind farm configuration (DCS-PPPC).

Due to various cost information across the globe, this chapter is written as a comparative economic assessment to highlight structural differences between wind farm configurations, instead of aiming to predict very reliable absolute values for levelized cost of energy (LCOE). The base dataset for investment, maintenance and decomissioning costs originates from the United Kingdom where many offshore wind farms have already been commercially deployed. Hence, the economic assessment is performed in British Pounds (GBP).

7.1 Methodology

In this section, the economic model is discussed. Largely, it has been adopted from [85]. The economic base data for capital, financing, maintenance and decommissioning expenses, as well as project data have been taken from [106] and are being presented in summarized form in this section. Annual energy production (energy yield) for each wind turbine including wake and tubulence effects, as well as any necessary curtailment due to converter rating limits has been obtained through the computations performed in section 5.7.

Economic base data from [106] is shown in Table 7.1, Table 7.2 and Table 7.3. This cost data has been assembled from various companies and consultancies for a fictional 1GW wind farm located 60km from shore, using 10MW wind turbines at a 10m/s wind site and anicipated start of operation in 2022. The anticipated lifetime is 27years.

Table 7.3 lists a cost breakdown of planning, capital, operations and maintenance, installation, and decommissioning expenditures for the wind farm of Table 7.1. A more detailed breakdown is available in [106]. This wind farm is based on a high-voltage AC transmission system. Based on [107], it has been assumed that the installation cost of an offshore HVDC converter station is 5.5 times higher compared to an offshore HVAC substation. Furthermore, it has been assumed that the cost of a converter system in a wind turbine nacelle (£70,000/MW) accounts for two back-to-back voltage-source converters rated at the full wind turbine power rating. As a result, individual power electronic converters have been costed at £35,000 per installed megawatt. For the purpose of this study, the cost of a VSC has been assumed to be comparable to that of a DAB at £35,000 per installed megawatt. Furthermore, based on the analysis in [85],

a wind farm availability of 81.22% has been assumed. Also, the discount rates for capital and maintenance expenditures, r_c, and energy production, r_p, have been assumed to be 6% [85]. Transmission cable costs have been assumed to scale linearly with respect to length.

Table 7.1 Wind farm base parameters used in cost model of [106].

PARAMETER	VALUE
Wind farm rating (MW)	1000
Wind turbine rating (MW)	10
Water depth at site (m)	30
Annual mean wind speed at 100m height (m/s)	10
Distance to shore, grid, port (km)	60
Date of financial investment decision to proceed (FID)	2019
First operation date	2022

Table 7.2 High-level project parameters and results of [106].

PARAMETER	VALUE
Total capital expenditures (CAPEX)	£2,370,000/MW
Annual average operating expenditures (OPEX)	£76,000/MW
Lifetime	27 years

Table 7.3 Cost breakdown of wind farm components [106].

CATEGORY*			ROUNDED COST (£/MW)
Project development and management			**120,000**
Turbine			**1,000,000**
	Nacelle		400,000
		Converter system within nacelle	70,000
		Other (Drivetrain, Generator, Control system, etc.)	330,000
	Rotor		190,000
	Tower		70,000

	Other		340,000
Balance of plant (transmission system)			**600,000**
	Cables		170,000
		Export cable (AC, 60km)	130,000
		Array cable (AC)	35,000
		Cable protection	2,000
	Turbine foundation		280,000
	Offshore substation (HVAC transmission)		120,000
	Onshore substation (HVAC transmission)		30,000
	Operations base		3,000
Installation and commissioning			**650,000**
	Foundation installation		100,000
	Offshore substation installation		35,000
	Onshore substation construction		25,000
	Onshore export cable installation		5,000
	Offshore cable installation		220,000
	Turbine installation		50,000
	Offshore logistics		3,500
	Other		212,000
Operation, maintenance and service (per annum and MW)			**75,000/year/MW**
	Operations		25,000/year/MW
	Maintenance and service		50,000/year/MW
Decomissioning			**330,000**
	Turbine		45,000
	Foundation		75,000
	Cable		140,000
	Substation		65,000

* Individual cost categories are broken down to further sub-categories as indicated in formatting. The sum of cost for all sub-categories equals that of the overall category.

Given that with this information, CAPEX and OPEX can be calculated for all wind farm configurations (assuming a system design following section 3.6), the levelized cost of energy (LCOE) can be calculated as follows [108]:

$$LCOE = \frac{CAPEX + \sum_{t=1}^{n} \frac{OPEX}{(1+r_c)^t}}{\sum_{t=1}^{n} \frac{AEP \times availability}{(1+r_p)^t}} \tag{7.1}$$

Levelized cost of energy is defined "as the present value of all costs, divided by the present value of all energy produced over the energy project's lifetime" [108]. In (7.1), *CAPEX* represents the present value of all capital expenses, *OPEX* the annual operating expenses, *AEP* the annual energy production in kWh, n the project lifetime, and *availability* the wind farm availability (assumed to be 81.22% as discussed above and in [85]).

7.2   Candidate Wind Farm Designs

In this section, four wind farm configurations are summarized, such that a comparative economic assessment can be conducted on them. All wind farms follow the design presented in section 3.6 and only differences, or additional parameters required for efficiency modeling, are discussed below.

The conventional AC Wind Farm with HVDC-link ("AC+HVDC") consists of wind turbines featuring a 3.3kV generator, back-to-back three-level voltage-source converters, a step-up transformer for 33kV collection system voltage. The collection system consists of 9 strings of 10 parallel-connected wind turbines. The wind farm HVDC transmission system is assumed to be similar to the BorWin 1 system [109]. It connects to the offshore collection system through a 33kV/155kV transformer and operates at ±250kVdc. Both HVDC converter stations are based on half-bridge modular multi-level converters (HB-MMC). The offshore substation is located in the center of the wind farm. This configuration is shown in Figure 7.1.
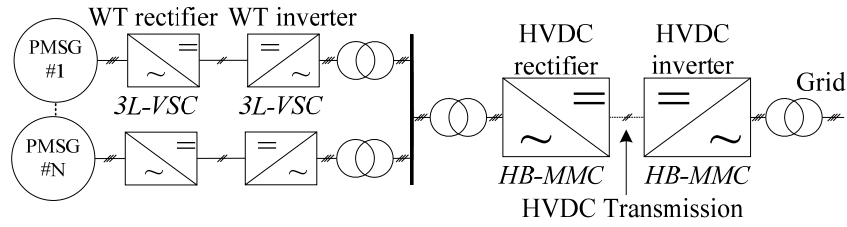
Figure 7.1 Single line diagram of the conventional AC+HVDC configuration.

All remaining (DC) wind farm configurations have been discussed in Chapter 5 and are recalled in Figure 7.2 to Figure 7.4.
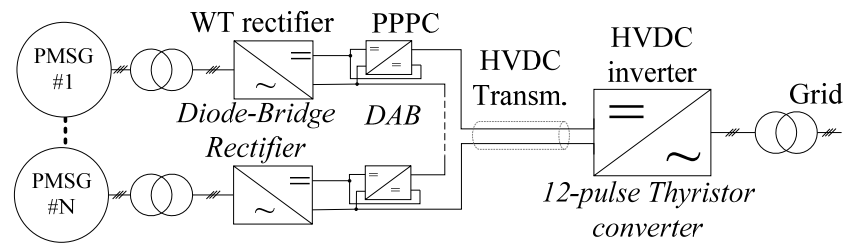
Figure 7.2 Single line diagram of the DCS-PPPC configuration.
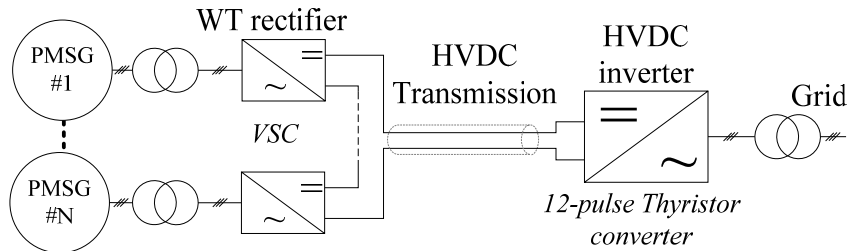
Figure 7.3 Single line diagram of the DCS-VSC configuration.
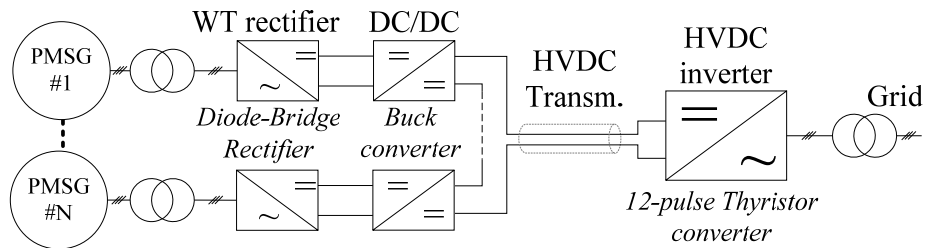
Figure 7.4 Single line diagram of the DCS-Buck configuration.

7.3   Loss Modelling

During the state estimation performed in section 5.7, converter states and losses for all candidate wind farm configurations have been computed for all available data. Generator copper losses were computed based on the stator resistance. Losses in generator-side rectifiers, wind turbine converters, and HVDC MMCs have been calculated from datasheet information, based on the voltages and currents experienced in all devices that were obtained from time-domain simulations in MATLAB/ Simulink. All switch and diode losses (switching, conduction, and reverse recovery) were derived from datasheet information, and calculated for the simulated waveforms at the respective operating points.

PPPC losses have been calculated based on the conventional analysis presented in [110] and [111]. PPPC medium-frequency (MF) transformer losses were calculated based on a transformer model approximating the transformer design of [15] and [112]. High-voltage, line-frequency (HV, LF) transformer losses were modeled based on efficiency curves shown in [9], and medium-voltage, line-frequency (MV, LF) transformer losses were approximated from [113]. Core losses of the wind turbine isolation transformers at variable generator voltage and frequency have been derived from core losses at rated conditions under the assumption that all losses are due to hysteresis losses (worst-case scenario). All transformer efficiency curves are shown in Figure 7.5. Losses in the thyristor-based onshore station were modeled after recommendations made in [114] (filter, transformer, and auxiliary losses), and thyristor valve losses were calculated from datasheet information on power losses versus DC current. Collection and transmission cable losses were calculated based on datasheet information on the AC or DC resistances. Losses due to any potential reactive power flow in the AC wind farm collection system have been neglected.
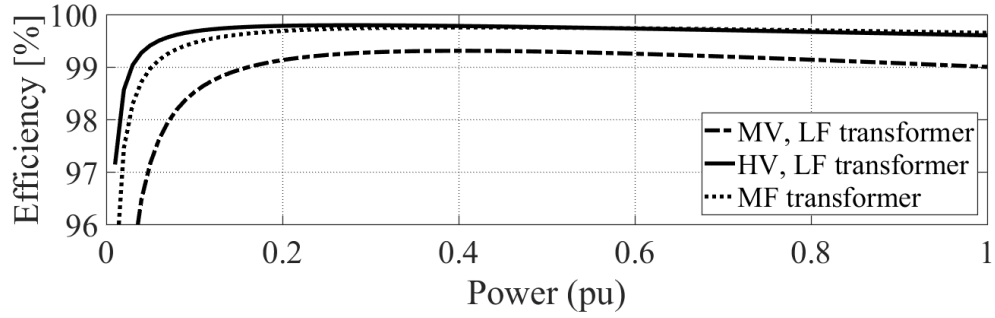
Figure 7.5 Transformer efficiency curves for operation at rated voltage.

For the AC+HVDC and DCS-VSC configurations, a 3.3kV generator was assumed. In the DCS-PPPC and DCS-Buck configurations, a 5kV generator voltage is supportive of achieving a high HVDC-link voltage, reducing overall losses, whereas for the AC wind farm, a higher generator voltage does not provide as much of a benefit to counterbalance the disadvantage of higher converter voltage ratings and insulation requirements. Annual energy production and losses have been calculated analogous to the computation of annual energy curtailment following equation (5.38). Parameters and device selections for the purpose of efficiency modeling are given in Table 7.4.

Table 7.4 Wind farm parameters for efficiency modeling.

Component	DCS-PPPC	DCS-Buck [33]	DCS-VSC	AC+HVDC
WT Generator	5MW, PMSG, 5kV (DCS-VSC & AC+HVDC: 3.3kV), L_d=L_q=0.4337pu. R_s=0.012pu.			
WT rectifier	3-ϕ diode-bridge rectifier. Diodes: I90D. 5MW insulation transformer.			3-level VSC (NPC). IGBTs: H45. Diodes: H45D; n_p: 2. f_s=720.3Hz. AC+HVDC: n_s: 2, V_{DC}=7kV. DCS-VSC: n_s: 6, V_{DC}: see section 5.5.
DC wind farms: DC/DC converter; *AC wind farm*: WT inverter	$N_{MC} = 1 \ldots 4$: (test cases as per chapter 5; test cases 1-4: $N_{MC} = 1$, incrementing after) Primary bridge H65. Secondary bridge H17. Unfolder devices: H17D MFT turns ratio: 1:8. f_s=7.5kHz. Leakage inductance as: Table 5.2.	IGBT: H45, n_s: 2, n_p: 2. Diode:H65D, n_s: 2,n_p: 2.f_s= 1kHz. L=1mH, R_L=0.02Ω.	*N/A.*	3-level VSC (NPC). IGBTs: H45. Diodes: H45D, n_s: 2, n_p: 2. f_s=1260Hz. V_{DC}=7kV, V_{AC}=3.3kV (60Hz). Filter inductor: 5mH. Step-up LFT: 5MW, 3.3/33kV.
Collection system cables	Rectifier at WT ground level, tower: 100m. Cable: 2x (DCS-VSC: 1x) Nexans A4305055, 132kV$_{AC}$, 898A, 800mm²			WT: NX V333x09516, 352A, 95mm². String: NX V333x15025, 446A, 150mm². Substation: NX V333x63035, 904A, 630mm²
Offshore station	*Not applicable.*			See "HVDC onshore station", but: HV LFT: 33/155kV.
HVDC cables	2x (DCS-VSC: 1x) Nexans A4305055, 132kV$_{AC}$, 898A, 800mm²,			ABB 330kV, 800mm², 100km.
HVDC onshore station	12-pulse thyristor converter. Devices: M12K. n_s: 2 × 8, n_p: 1. LFT: 2x250MW 103kV/230kV.			HB-MMC, 144 submodules per arm (864 submodules total). Devices: A45, A45D, n_s: 1 & n_p: 3 per submodule. f_s=300Hz. V_{DC}=$\pm$250kV, V_{AC}= 155kV. Arm filter inductors L_a=31.6mH, R_{La}=0.238mΩ. HV LFT: 2x315MW, 155/230kV.

Abbreviations: "WT": Wind Turbine. "n_s" / "n_p": number of series / parallel connected devices per converter switch element; "NPC": Neutral Point Clamped; "LFT": Low/Line frequency transformer; "MFT": Medium frequency transformer; "MV": Medium voltage; "HV": High voltage. "f_s": switching frequency. "RD": Rotor diameter. IGBTs: "H65"= Hitachi MBN750H65E2, "H45"= Hitachi MBN800H45E2-H, "H17" = Hitachi MBN3600H17F"., "A65"= ABB 5SN0750G650300. Diodes: "H45D"= Hitachi MDM800H45E2-H, "H17D" = Hitachi MBDM600H17F"., "I90D"= Infineon D2601NH, "A65D"= ABB 5SDD10F6000Thyristors: "M12K"= Mitsubishi FT1500AU-240. "NX" = Nexans.

7.3.1 Results

Results of modeling efficiency for all candidate wind farm configurations are shown in Figure 7.6. The considered test cases are identical to those in section 5.7. The DCS-Buck case replicating the design of [33] is labeled "DCS-Buck Original", whereas the test case featuring altered HVDC-link current control (to minimize HVDC-link current and thus maximize HVDC-link voltage) and converter sizing as proposed in section 5.6 is labeled "DCS-Buck Update". In addition, the AC wind farm featuring an MMC-HVDC system is labeled as "AC+HVDC".

Efficiency results have been obtained for the operation of candidate wind farms for one year. The annual conversion efficiency shown in Figure 7.6 demonstrates that series-connected DC wind farms have a significant potential to improve the overall electric conversion efficiency of wind farms from wind turbine to onshore connection. Consistent with other models, such as [53], the AC+HVDC conversion efficiency is 90-91%. The DCS-Buck original conversion efficiency is similar. While there are no losses associated with an offshore converter station with series-connected DC wind farms, the HVDC-link current control law of [33] leads to relatively high HVDC-link currents and associated transmission system losses. Simly by changing the HVDC-link current control law, annual conversion efficiency of the DCS-Buck system can be increased by about 2.5 percent points, as demonstrated by the "DCS-Buck Update" case. Annual conversion efficiency is above 94% for all DCS-PPPC cases with only minor variations among the test cases. For the DCS-VSC configuration, conversion efficiency starts very high for test case 1 (output voltage rating of 9kV), but drops sharply as VSC output voltage ratings increase in 9kV increments. This is due to the fact that the same (or similar) VSC voltages and currents are processed by converters with more and more switching devices, as the VSCs are rated for higher and higher voltages. This severely reduces wind turbine converter efficiency. Analysis of energy curtailment due to converter ratings in section 5.7.3 (and repeated below) shows that approximately 4% of available energy is curtailed for the DCS-VSC test case 1, negating any efficiency benefits that this test case may have.
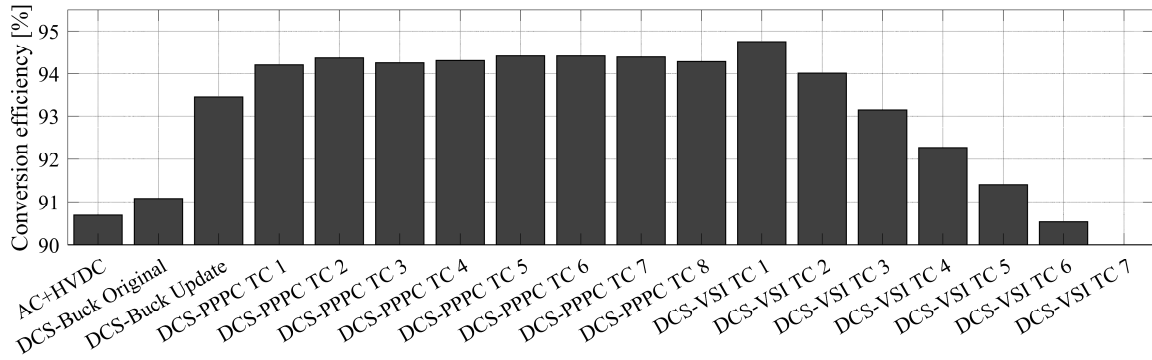
Figure 7.6 Annual conversion efficiency for all wind farm test cases. "TC" = test case.

7.4 Sizing

Converter sizing and related necessary annual energy curtailment has been discussed in Chapter 5. Section 5.7 presents results for all series-connected DC wind farm configurations that were considered. For reference purposes, these results are shown again in Figure 7.7. As discussed in section 5.7, the DCS-PPPC and DCS-VSC configurations operate with some energy curtailment due to converter ratings because of partial operational range sizing. The AC+HVDC and DCS-Buck test cases employ conventional or full operational range sizing resulting in no sizing-related curtailment.

For the DCS-PPPC test cases, energy curtailment diminishes to low levels for test cases 4 and above. The full operational range sizing test case (test case 8) results in no sizing-related curtailment.

For the DCS-VSC configuration, test case 1 (9kV output voltage rating) results in approximately 4% of available energy to be curtailed due to the limited converter output voltage rating. For all other test cases, approximately 0.4% of available annual energy production is curtailed due to limitations of the HVDC-link voltage ratings, even for full operational range sizing. This indicates that from a sizing perspective, a VSC output voltage rating of 18kV (test case 2) or higher might be preferential for the examined wind farm system and location.
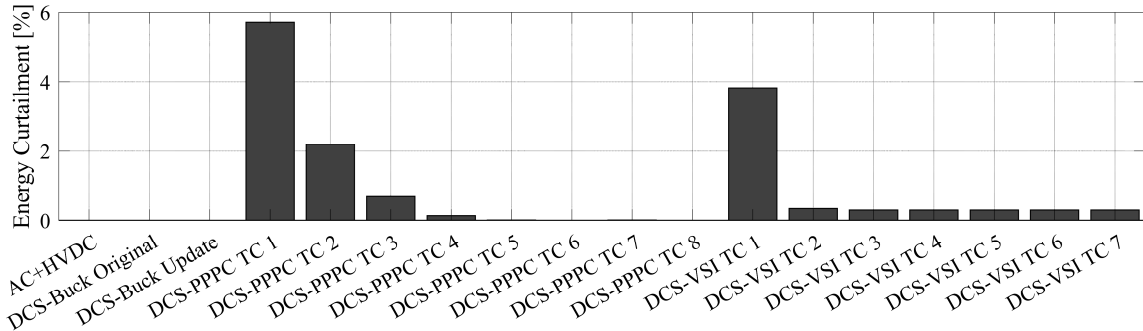
Figure 7.7 Annual energy curtailment due to converter limits for all wind farm test cases. "TC" = test case.

7.5 Economic indicators

In this section, basic economic indicators are discussed for all test cases, in order to compute levelized cost of energy (LCOE) for all wind farm configurations and test cases, following the methodology of section Figure 7.1. First, it is important to determine the annual energy production (AEP). This is obtained from the simulations performed in section 5.7. Conversion losses and sizing-related curtailment are subtracted. The resulting AEP is shown in Figure 7.8. In this figure, it can be seen that AEP is lower for the AC+HVDC and DCS-Buck (Original) test cases despite the lack of sizing-related curtailment, which relates to lower conversion efficiency. The wind farms' capacity factors are in the range of 48% to 50% for the different test cases. The improvement of conversion efficiency for the DCS-Buck (Update) test case directly improves AEP. For the DCS-PPPC configuration, conversion efficiency was comparatively similar among all test cases. As a result AEP is mostly sensitive to sizing-related annual energy curtailment. For the DCS-VSC configuration, the highest AEP is achieved for test case 2. In test case 1, the high amount of curtailment overcompensates the efficiency gains available. As VSC ratings increase (test cases 3 and above), AEP decreases due to declining annual conversion efficiency.

Capital expenditures (CAPEX) are significantly lower for all series-connected DC wind farm configurations, mainly due to the lack of an offshore converter station, as shown in Figure 7.9. CAPEX variations within the series-connected DC wind farm configurations stem from differences in wind turbine converter ratings. Most notably, test cases with higher voltage ratings for the DCS-VSC configurations have a noticeable higher CAPEX, while all other configurations are relatively comparable.
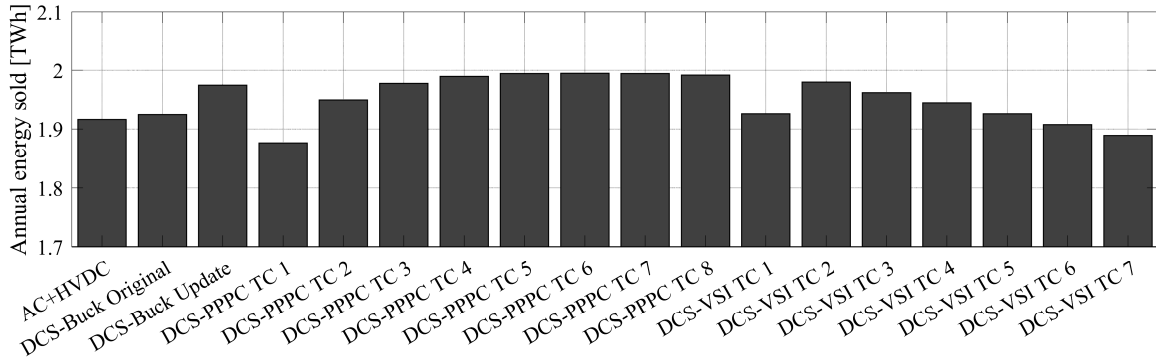
Figure 7.8 Annual energy sold for all wind farm test cases. "TC" = test case.
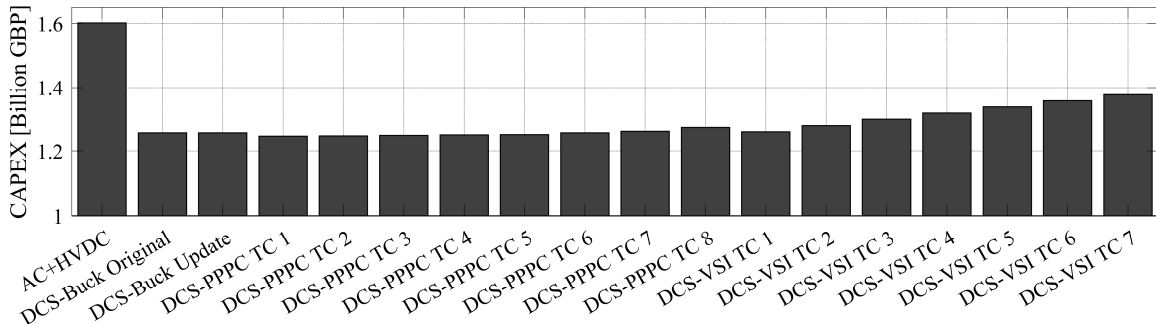
Figure 7.9 Capital expenditures (CAPEX) for all wind farm test cases. "TC" = test case.

Operating expenditures (OPEX) are shown in Figure 7.10. While the presented model considers absolute expenditure per year and MW comparable among configurations, this cost is distributed among a variable AEP. As a result, OPEX is higher for test cases 1 of DCS-PPPC and DCS-VSC. It is lowest for test cases 5-7 of DCS-PPPC and similar for test case 2 of DCS-VSC and the DCS-Buck (Update) case.

With these indicators, it is possible to compute the LCOE for each wind farm configuration and test case. The results are shown in Figure 7.11 and tabulated in Table 7.5. Here, it can be seen that the lowest LCOE is achieved in test case 5 of the DCS-PPPC configuration. Compared to the AC+HVDC configuration, this represents a 20.9% reduction. Similar reductions can also be achieved with the DCS-Buck configuration, if employing the updated HVDC-link current control law and converter sizing, as proposed in section 5.6 (19.9% reduction). Test case 2 of the DCS-VSC configuration is calculated to result in a reduction of 19.0%.
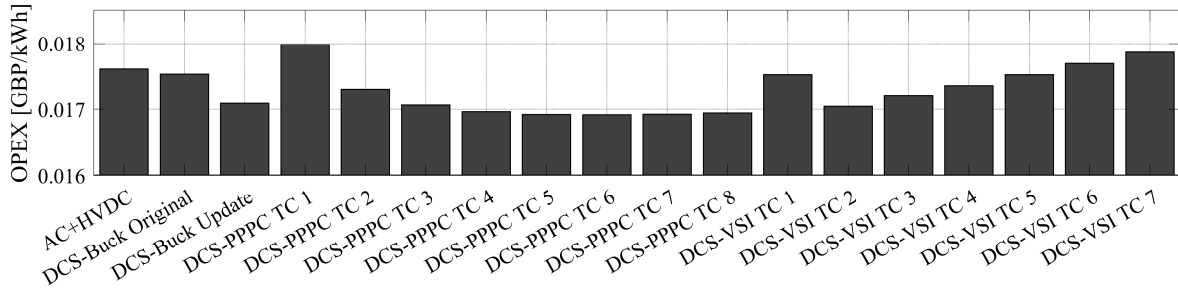
Figure 7.10 Operating expenditures (OPEX) for all wind farm test cases. "TC" =
test case.
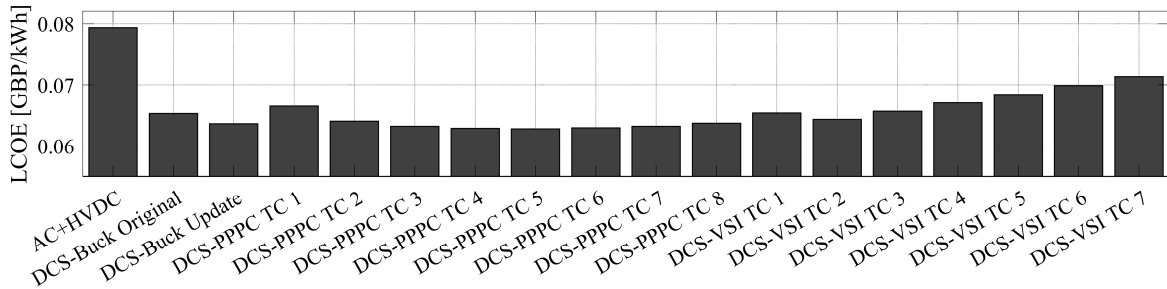
Figure 7.11 Levelized cost of energy (LCOE) for all wind farm test cases. "TC" =
test case.

Table 7.5 Levelized cost of energy (LCOE) and reductions with respect to
AC+HVDC configuration for all wind farm test cases.

WIND FARM CONFIGURATION AND TEST CASE	LCOE (GBP/KWH)	% REDUCTION, COMPARED TO AC+HVDC
AC+HVDC	0.07936	-
DCS-Buck Original	0.06527	17.8%
DCS-Buck Update	0.06360	19.9%
DCS-PPPC Test Case 1	0.06649	16.2%
DCS-PPPC Test Case 2	0.06405	19.3%
DCS-PPPC Test Case 3	0.06320	20.4%
DCS-PPPC Test Case 4	0.06287	20.8%
<u>DCS-PPPC Test Case 5</u>	<u>0.06277</u>	<u>20.9%</u>
DCS-PPPC Test Case 6	0.06296	20.7%
DCS-PPPC Test Case 7	0.06319	20.4%
DCS-PPPC Test Case 8	0.06372	19.7%
DCS-VSC Test Case 1	0.06537	17.6%

147

DCS-VSC Test Case 2	0.06431	19.0%
DCS-VSC Test Case 3	0.06566	17.3%
DCS-VSC Test Case 4	0.06704	15.5%
DCS-VSC Test Case 5	0.06845	13.8%
DCS-VSC Test Case 6	0.06988	12.0%
DCS-VSC Test Case 7	0.07134	10.1%

As mentioned beforehand, LCOE is influenced by a multitude of factors, such as conversion efficiency, curtailment and converter ratings, CAPEX, and OPEX. Furthermore, it can also be influenced by reliability, wind farm site, wind farm layout, regulatory requirements, availability of skilled labour and companies, currency conversion effects and others. To avoid issues with currency conversion effects, this study has been conducted using British Pounds. This is owed to the fact that the original data set for cost information is given in British Pounds and focused on the offshore market in the European North Sea. To minimize effects of wind farm site, layout or other local effects, this economic assessment was conducted as a comparative assessment, in which only parameters characterizing the unique differences of a particular wind farm configuration are changed while others are held constant. As a result, the value in this comparative economic assessment should rather be seen in the relative differences between test cases, rather than in its absolute cost information, as absolute cost information can vary widely among different markets.

7.6 Summary

This chapter presented a comparative economic assessment four wind farm configurations:

- Wind farm with AC collection system and dedicated MMC-based HVDC-link ("AC+HVDC")
- Wind farm with series-connected DC collection system, and diode-bridge rectifiers and buck converters as wind turbine converters ("DCS-Buck", 2 test cases)

- Wind farm with series-connected DC collection system, and diode-bridge rectifiers and partial power processing converters as wind turbine converters ("DCS-PPPC", 8 test cases)

- Wind farm with series-connected DC collection system, and voltage-source converters as wind turbine converters ("DCS-VSC", 7 test cases)

This chapter also contains an efficiency modeling for all considered configurations and test cases for a (fictional) 450 MW wind farm operating at the site of the FINO3 meteorolocial mast in the European North Sea, based on estimated annual performance.

Due to the lack of an offshore converter station for DC configurations, a significant advantage in terms of conversion efficiency and capital expenditures is shared among most of the considered DC wind farm test cases. Furthermore, conversion efficiency has been found highest and least sensitive to varying converter ratings with the DCS-PPPC configuration. An updated DCS-Buck configuration offers similar, albeit inferior conversion efficiency, while the DCS-VSC configuration is challenged with reductions in efficiency from the need for high output voltage ratings. Taking into account converter ratings, CAPEX and OPEX, the most preferential wind farm configuration appears to be DCS-PPPC, test case 5. This test case offers a 20.9% reduction in LCOE, compared to the AC+HVDC case. However, other configurations, such as DCS-Buck (Update), or DCS-VSC test case 2 offer economic advantages of similar amounts (19.9% and 19.0%, respectively). The comparative economic assessment takes into account differences in losses, converter equipment, losses, annual energy production, and operating and maintenance expenses. It reduces the impact of external factors, such as wind farm site and layout through its comparative nature. As such, this comparative economic assessment allows to directly compare a range of series-connected wind farm configurations to the conventional AC wind farm design.

Chapter 8

Conclusion

This Chapter summarises the presented research work, highlights the contributions made and gives directions for possible future work.

8.1 Summary

Chapter 1 introduced the motivations behind the work reported in this thesis. Based on the motivations, a literature survey was conducted and dominant characteristics, technical challenges and gaps in the research literature on series-connected DC wind farms were identified. Accordingly, thesis objectives have been derived and split into distinct working packages.

Chapter 2 presented a background review of fundamental concepts required in the analysis of offshore wind farms. This review covered energy conversion by horizontal-axis upwind wind turbines, the electromechanical energy conversion, characteristics of offshore wind farms, high-voltage DC transmission systems, and partial and differential power processing.

In Chapter 3, the wind farm configuration of this thesis was introduced. This wind farm configuration consists of wind turbine converters featuring diode-bridge rectifiers and partial-scale, partial power processing converters. This arrangement was used to exploit the observation from real-world data of the Horns Rev 1 wind farm, that output powers of wind turbines in offshore wind farms are very likely to be close to one another. In this chapter, the steady-state model of all electrical components, and operating principles of the PPPC were developed. Major design considerations on the wind turbine

converters and HVDC system, such as the choice of PPPC configurtion and HVDC voltage selection/insulation, were discussed. It has been shown that the PPPC of a wind turbine can be realized in a multi-converter input-parallel, output-series arrangement that further allows for reduction of conversion losses and increases available redundancy during converter outages. To enable in-depth studies on this and comparable wind farm configurations, a 450MW reference wind farm was developed based on 5MW wind turbines derived from the 5MW NREL reference wind turbine.

The work presented in Chapter 4 included wind farm control and dynamic simulation results. First, a slightly adapted wind turbine speed and pitch control loop was presented that was derived from conventional control laws. Secondly, generic relations were derived to allow the prediction of violation of DAB converter ratings under all possible operating conditions. This was used to limit converter operation within the converter control loops at real time, and to properly size wind turbine converters, as discussed later in Chapter 5. Wind turbine control loops and logic have been presented that enable MPP operation with PPPCs. Furthermore, matching HVDC-link current scheduling algorithms have been derived that minimize the total amount of power processed by PPPCs while maximizing operational range for available converter ratings. A backup control law for communication system outage periods has also been developed. Ancillary services can be provided by this wind turbine configuration. Thus, implementations for low-voltage ride-through, power curtailment/active power control and inertial response have been presented. Finally, dynamic simulations have been performed for a range of operating conditions to verify the feasibility of the presented wind farm configuration. In particular, regular operation was examined using two artificial step change wind profiles and one based on real-world wind speed measurements. Regular operation near converter limits has been examined using two wind speed profiles in which one wind turbine experiences a wind speed ramp such that the wind farm is pushed towards operation at converter limits. Ancillary services have been confirmed to be available through respective simulations, and it has been shown that a backup HVDC-link current scheduling law can operate without a communication link, although the total amount of power processed by PPPCs is not optimal in such scenario.

Chapter 5 presented a generic sizing framework for single-string series-connected DC wind farms. From a generic formulation of electric operating points and converter limits, specific applications of this framework were derived for the presented, as well as two other series-connected DC wind farm configurations. Based on large-scale, high-fidelity wind farm and wind flow simulations that are based on long-term met mast measurement

data (FINO3 campaign), the likelyhoods of energy curtailment necessary due to finite wind turbine converter ratings was computed on an annual basis for all three wind farm configurations. It was shown that a 'full operational range sizing' could guarantee no curtailment in two out of three wind farm configurations, while 'partial operational range sizing' could offer varying degrees of required curtailment. The results of this work have been incorporated in Chapter 7, in which a comparative economic assessment has been conducted.

In Chapter 6, it was shown that for a subset of series-connected DC wind farms, wind turbine startup was not straight forward and could not be facilitated using conventional control sequences. This also applies to the presented wind farm configuration. As a result, an alternative startup scheme has been developed that allows the successful startup of a wind turbine at any time, provided that the steady-state operating point is feasible according to overall converter limits (as per Chapter 5). In addition, options and control schemes for wind turbine shutdown have been explored, since additional (electric) deceleration mechanism are available in this wind farm configuration.

Chapter 7 presented a comparative economic assessment that seeked to develop the LCOE differences between conventional AC wind farms with HVDC link and those DC wind farms that were examined in Chapter 5. Based on the differences in capital expenses, conversion losses, sizing-related energy curtailment and O&M expenses, it has been shown that series-connected DC wind farms have a significant potential to offer a noticeably lower LCOE than AC wind farms with HVDC link. While most economic benefit is derived from the lack of an offshore HVDC converter station, the specific operating principles of the series-connected DC wind farm either allow to maximize benefits, or additional losses amount to a declining LCOE advantage. In particular, a PPPC output voltage rating of 0.43pu has been identified as the most preferable solution in terms of LCOE among all studied wind farm configurations. This thesis also proposed a small change to a wind farm configuration featuring diode-bridge rectifiers and buck converters than enables LCOE advantages comparable to those identified most preferable.

8.2   Contributions

During this research two conference papers and three journal papers have been published with IEEE. The list of publications is provided in **Error! Reference source not found.**.

The main contributions of this thesis can be summarized as follows:

- Quantifying the likelihood of wind turbine output power differences within a wind farm, based on high-fidelity measurements of the Horns Rev 1 wind farm.

- Developing a series-connected DC wind farm configuration that exploits those limited output power differences by means of differential power processing to derive economic benefits in terms of amount of conversion equipment required, overall conversion efficiency, and levelized cost of energy. Benefits are maximized through an optimization of wind turbine and HVDC-link operating points, system sizing, and application of a multi-converter configuration for PPPCs.

- Deriving a generic converter sizing framework for series-connected DC wind farms, that recognizes unique challenges in such wind farms regarding the determination of converter ratings. As in some cases, it can be technically or economically infeasible to rate wind turbine converters to cover all possible operating points, this framework uses annual energy curtailment due to potential converter rating violations as the measure that can be used by the designer to evaluate related design tradeoffs and ecnomic impacts.

- Identification of challenges for wind turbine startup for wind farm configurations such as the one presented in this thesis. An alternate startup scheme was developed that does not require any additional hardware. Furthermore, the wind turbine shutdown procedure for the presented wind farm configuration was developed.

- A comparative economic assessment has been conducted to quantify the ecnonomic impacts of design choices for a fictional 450MW wind farm located in the European North Sea. This comparative economic assessment demonstrated that the presented wind farm configuration is preferable over all other candidates in terms of LCOE. A modification proposed in this thesis to another wind farm configuration improves its operating points and results in a comparable economic case. All series-connected DC wind farms have been

found to be economically preferable over the benchmark AC wind farm with dedicated HVDC link.

8.3 Future Work

The presented work could be advanced in the following ways:

- Exploration of the differential power processing approach in series-parallel DC wind farms.

- Exploration of the use of one HVDC system shared among multiple nearby offshore wind farms, leveraging further differential power processing designs; investigation of integration of this wind farm configuration into offshore wind hubs, or application in offshore wind parks with many co-located farms of similar or differing wind farm configurations.

- Comprehensive study of system protection, reliability and availability of the proposed and other series-connected DC wind farms. Development of availability enhancements during PPPC outages.

- Optimization of string assignment of wind turbines within the 3x150MW wind farm.

- Experimental verification of the proposed wind farm.

- Exploration of MMCs as onshore converter station (as discussed in [86] for similar configurations) and inclusion of black start functionality.

- Exploration of the benefit of using separate HVDC-link current scheduling for the positive and negative conductor of a bipolar HVDC link scheme.

- In-depth study of offshore HVDC-link current stiffness and stability, as well as a comprehensive scheme to determine controller gains and the sizing of the offshore filter inductance.

- Analysis of this wind farm for onshore applications where there is a long distance to the grid connection point.

Bibliography

[1] J. F. Manwell, J. G. McGowan, and A. L. Rogers, *Wind energy explained: theory, design and application*, 2nd ed. Chichester, U.K: Wiley, 2009.

[2] "Offshore wind in Europe – key trends and statistics 2020," *WindEurope*. https://windeurope.org/data-and-analysis/product/offshore-wind-in-europe-key-trends-and-statistics-2020 (accessed Sep. 04, 2021).

[3] X. Lu, M. B. McElroy, and J. Kiviluoma, "Global potential for wind-generated electricity," *Proceedings of the National Academy of Sciences*, vol. 106, no. 27, pp. 10933–10938, 2009.

[4] V. Yaramasu, B. Wu, P. C. Sen, S. Kouro, and M. Narimani, "High-power wind energy conversion systems: State-of-the-art and emerging technologies," *Proceedings of the IEEE*, vol. 103, no. 5, pp. 740–788, May 2015, doi: 10.1109/JPROC.2014.2378692.

[5] T. Ackermann, Ed., *Wind power in power systems*. Chichester, West Sussex, England ; Hoboken, NJ: John Wiley, 2005.

[6] S. Lundberg, *Wind farm configuration and energy efficiency studies: series DC versus AC layouts*. Göteborg: Chalmers Univ. of Technology, 2006.

[7] C. Meyer, M. Hoing, A. Peterson, and R. W. D. Doncker, "Control and Design of DC Grids for Offshore Wind Farms," *IEEE Transactions on Industry Applications*, vol. 43, no. 6, pp. 1475–1482, Nov. 2007, doi: 10.1109/TIA.2007.908182.

[8] S. M. Muyeen, R. Takahashi, and J. Tamura, "Operation and Control of HVDC-Connected Offshore Wind Farm," *IEEE Transactions on Sustainable Energy*, vol. 1, no. 1, pp. 30–37, Apr. 2010, doi: 10.1109/TSTE.2010.2041561.

[9] J. Robinson, D. Jovcic, and G. Joos, "Analysis and Design of an Offshore Wind Farm Using a MV DC Grid," *IEEE Transactions on Power Delivery*, vol. 25, no. 4, pp. 2164–2173, Oct. 2010, doi: 10.1109/TPWRD.2010.2053390.

[10] S. Lundberg, "Evaluation of Wind Farm Layouts," *EPE Journal*, vol. 16, no. 1, pp. 14–21, Feb. 2006, doi: 10.1080/09398368.2006.11463608.

[11] L. Max and S. Lundberg, "System efficiency of a DC/DC converter-based wind farm," *Wind Energ.*, vol. 11, no. 1, pp. 109–120, Jan. 2008, doi: 10.1002/we.259.

[12] O. Beik and N. Schofield, "An Offshore Wind Generation Scheme With a High-Voltage Hybrid Generator, HVDC Interconnections, and Transmission," *IEEE Transactions on Power Delivery*, vol. 31, no. 2, pp. 867–877, Apr. 2016, doi: 10.1109/TPWRD.2015.2492472.

[13] O. Beik and N. Schofield, "Hybrid generator for wind generation systems," in *2014 IEEE Energy Conversion Congress and Exposition (ECCE)*, Sep. 2014, pp. 3886–3893. doi: 10.1109/ECCE.2014.6953929.

[14] J. L. Rodriguez-Amenedo, S. Arnalte, and J. C. Burgos, "Automatic generation control of a wind farm with variable speed wind turbines," *IEEE Transactions on Energy Conversion*, vol. 17, no. 2, pp. 279–284, Jun. 2002, doi: 10.1109/TEC.2002.1009481.

[15] G. Ortiz, J. Biela, D. Bortis, and J. W. Kolar, "1 Megawatt, 20 kHz, isolated, bidirectional 12kV to 1.2 kV DC-DC converter for renewable energy applications," in *Power Electronics Conference (IPEC), 2010 International*, 2010, pp. 3212–3219. Accessed: Jan. 29, 2016. [Online]. Available: http://ieeexplore.ieee.org/xpls/abs_all.jsp?arnumber=5542018

[16] M. H. Johnson, D. C. Aliprantis, and H. Chen, "Offshore wind farm with DC collection system," in *2013 IEEE Power and Energy Conference at Illinois (PECI)*, Feb. 2013, pp. 53–59. doi: 10.1109/PECI.2013.6506034.

[17] D. Jovcic, "Offshore wind farm with a series multiterminal CSI HVDC," *Electric Power Systems Research*, vol. 78, no. 4, pp. 747–755, Apr. 2008, doi: 10.1016/j.epsr.2007.05.023.

[18] H. J. Lee and S. K. Sul, "Wind power collection and transmission with series connected current source converters," in *Power Electronics and Applications (EPE 2011), Proceedings of the 2011-14th European Conference on*, Aug. 2011, pp. 1–10.

[19] M. Popat, Bin Wu, Fangrui Liu, and N. Zargari, "Coordinated Control of Cascaded Current-Source Converter Based Offshore Wind Farm," *IEEE Transactions on Sustainable Energy*, vol. 3, no. 3, pp. 557–565, Jul. 2012, doi: 10.1109/TSTE.2012.2191986.

[20] M. Popat, B. Wu, and N. R. Zargari, "DC link current control of cascaded current source converter based offshore wind farms," in *2011 IEEE International Electric Machines Drives Conference (IEMDC)*, May 2011, pp. 807–812. doi: 10.1109/IEMDC.2011.5994917.

[21] M. Popat, B. Wu, and N. R. Zargari, "Fault Ride-Through Capability of Cascaded Current-Source Converter-Based Offshore Wind Farm," *IEEE Transactions on Sustainable Energy*, vol. 4, no. 2, pp. 314–323, Apr. 2013, doi: 10.1109/TSTE.2012.2223246.

[22] M. Popat, B. Wu, and N. R. Zargari, "A novel decoupled interconnecting method for current source converter based offshore wind farms," in *2011 IEEE International*

Electric Machines Drives Conference (IEMDC), May 2011, pp. 711–716. doi: 10.1109/IEMDC.2011.5994898.

[23] Qiang Wei, Bin Wu, Dewei Xu, and N. R. Zargari, "Medium frequency transformer based configuration for voltage source converter based offshore wind farm," in *2016 IEEE 8th International Power Electronics and Motion Control Conference (IPEMC-ECCE Asia)*, May 2016, pp. 3521–3525. doi: 10.1109/IPEMC.2016.7512860.

[24] Q. Wei, B. Wu, D. Xu, and N. R. Zargari, "Bipolar Operation Investigation of Current Source Converter Based Wind Energy Conversion Systems," *IEEE Transactions on Power Electronics*, vol. 33, no. 2, pp. 1294–1302, Feb. 2018, doi: 10.1109/TPEL.2017.2683262.

[25] Q. Wei, B. Wu, D. Xu, and N. R. Zargari, "Further Study on a PWM Current-Source-Converter-Based Wind Energy Conversion System Considering the DC-Link Voltage," *IEEE Transactions on Power Electronics*, vol. 34, no. 6, pp. 5378–5387, Jun. 2019, doi: 10.1109/TPEL.2018.2866045.

[26] A. Garces and M. Molinas, "A control strategy for series connected offshore wind turbines," in *2011 IEEE Ninth International Conference on Power Electronics and Drive Systems*, Dec. 2011, pp. 1106–1111. doi: 10.1109/PEDS.2011.6147398.

[27] A. B. Mogstad, M. Molinas, P. K. Olsen, and R. Nilsen, "A power conversion system for offshore wind parks," in *2008 34th Annual Conference of IEEE Industrial Electronics*, Nov. 2008, pp. 2106–2112. doi: 10.1109/IECON.2008.4758282.

[28] N. Holtsmark, H. J. Bahirat, M. Molinas, B. A. Mork, and H. K. Hoidalen, "An All-DC Offshore Wind Farm With Series-Connected Turbines: An Alternative to the Classical Parallel AC Model?," *IEEE Transactions on Industrial Electronics*, vol. 60, no. 6, pp. 2420–2428, Jun. 2013, doi: 10.1109/TIE.2012.2232255.

[29] N. Holtsmark, E. Agheb, M. Molinas, and H. K. Høidalen, "High frequency wind energy conversion system for offshore DC collection grid — Part II: Efficiency improvements," *Sustainable Energy, Grids and Networks*, vol. 5, pp. 177–185, Mar. 2016, doi: 10.1016/j.segan.2015.10.008.

[30] E. Agheb, N. Holtsmark, H. K. Høidalen, and M. Molinas, "High frequency wind energy conversion system for offshore DC collection grid—Part I: Comparative loss evaluation," *Sustainable Energy, Grids and Networks*, vol. 5, pp. 167–176, Mar. 2016, doi: 10.1016/j.segan.2015.07.002.

[31] A. Garcés and M. Molinas, "Reduced matrix converter operated as current source for off-shore wind farms," in *Proceedings of 14th International Power Electronics*

and Motion Control Conference EPE-PEMC 2010, Sep. 2010, pp. T12-149-T12-154. doi: 10.1109/EPEPEMC.2010.5606549.

[32] A. Garcés and M. Molinas, "A Study of Efficiency in a Reduced Matrix Converter for Offshore Wind Farms," *IEEE Transactions on Industrial Electronics*, vol. 59, no. 1, pp. 184–193, Jan. 2012, doi: 10.1109/TIE.2011.2130502.

[33] E. Veilleux and P. W. Lehn, "Interconnection of Direct-Drive Wind Turbines Using a Series-Connected DC Grid," *IEEE Transactions on Sustainable Energy*, vol. 5, no. 1, pp. 139–147, Jan. 2014, doi: 10.1109/TSTE.2013.2276616.

[34] E. Veilleux and P. W. Lehn, "Interconnection of direct-drive wind turbines using a distributed HVDC converter station," in *2009 35th Annual Conference of IEEE Industrial Electronics*, Nov. 2009, pp. 584–589. doi: 10.1109/IECON.2009.5414986.

[35] Etienne Veilleux, "Interconnection of Direct-Drive Wind Turbines Using a Series Connected DC Grid," Master Thesis, University of Toronto, Toronto, 2009. Accessed: Jun. 14, 2016. [Online]. Available: https://tspace.library.utoronto.ca/bitstream/1807/18950/6/Veilleux_Etienne_200911_MASc_thesis.pdf

[36] S. Nishikata and F. Tatsuta, "A New Interconnecting Method for Wind Turbine/Generators in a Wind Farm and Basic Performances of the Integrated System," *IEEE Transactions on Industrial Electronics*, vol. 57, no. 2, pp. 468–475, Feb. 2010, doi: 10.1109/TIE.2009.2026765.

[37] S. Nishikata and F. Tatsuta, "A New Interconnecting Method for Wind Turbine/Generators in a Wind Farm," in *Wind Energy Conversion Systems*, S. M. Muyeen, Ed. Springer London, 2012, pp. 111–130. Accessed: Nov. 01, 2013. [Online]. Available: http://link.springer.com/chapter/10.1007/978-1-4471-2201-2_5

[38] A. Takemura, F. Tatsuta, H. Yokoyama, and S. Nishikata, "Studies on field current control method for constant tip speed ratios of series connected wind turbine generators in a wind farm," in *2012 15th International Conference on Electrical Machines and Systems (ICEMS)*, Oct. 2012, pp. 1–5.

[39] F. Tatsuta and S. Nishikata, "A Study on Steady-state Characteristics of Series-connected Wind Farm Using an Experimental Set of Laboratory Size," in *2018 International Power Electronics Conference (IPEC-Niigata 2018 -ECCE Asia)*, May 2018, pp. 4227–4232. doi: 10.23919/IPEC.2018.8507437.

[40] F. Tatsuta and S. Nishikata, "Dynamic performance analysis of a wind turbine generating system with series connected wind generators and bypass diodes using a current source thyristor inverter," in *The 2010 International Power Electronics*

Conference - ECCE ASIA -, Jun. 2010, pp. 1830–1836. doi: 10.1109/IPEC.2010.5543526.

[41] F. Tatsuta and S. Nishikata, "Dynamic performance analysis of a hybrid wind turbine generating system with series connected wind generators using a current source thyristor inverter," in *Automation and Motion International Symposium on Power Electronics Power Electronics, Electrical Drives*, Jun. 2012, pp. 1073–1078. doi: 10.1109/SPEEDAM.2012.6264534.

[42] F. Rong, G. Wu, X. Li, S. Huang, and B. Zhou, "ALL-DC Offshore Wind Farm With Series-Connected Wind Turbines to Overcome Unequal Wind Speeds," *IEEE Transactions on Power Electronics*, vol. 34, no. 2, pp. 1370–1381, Feb. 2019, doi: 10.1109/TPEL.2018.2834965.

[43] H. J. Bergveld *et al.*, "Module-Level DC/DC Conversion for Photovoltaic Systems: The Delta-Conversion Concept," *IEEE Transactions on Power Electronics*, vol. 28, no. 4, pp. 2005–2013, Apr. 2013, doi: 10.1109/TPEL.2012.2195331.

[44] G. Guo *et al.*, "Series-Connected-Based Offshore Wind Farms With Full-Bridge Modular Multilevel Converter as Grid- and Generator-side Converters," *IEEE Transactions on Industrial Electronics*, vol. 67, no. 4, pp. 2798–2809, Apr. 2020, doi: 10.1109/TIE.2019.2912777.

[45] N. Kawabata, N. kimura, T. Morizane, and H. omori, "New Modulation Control of Converter System Applied for Offshore Wind Farms," in *2018 International Power Electronics Conference (IPEC-Niigata 2018 -ECCE Asia)*, May 2018, pp. 2887–2894. doi: 10.23919/IPEC.2018.8507543.

[46] H. J. Bahirat and B. A. Mork, "Operation of DC Series–Parallel Connected Offshore Wind Farm," *IEEE Transactions on Sustainable Energy*, vol. 10, no. 2, pp. 596–603, Apr. 2019, doi: 10.1109/TSTE.2018.2839712.

[47] G. H. Kim, M. H. Kang, J. H. Ahn, E.-H. Kim, and S. H. Chae, "Operation of DC series connected offshore wind farm by using tap changing transformer with MMC-HVDC," in *2018 5th International Conference on Renewable Energy: Generation and Applications (ICREGA)*, Feb. 2018, pp. 291–295. doi: 10.1109/ICREGA.2018.8337616.

[48] C. Sun, G. Shi, J. Zhang, and X. Cai, "PWM plus phase-shift controlled DC-DC converter for use in series-connected DC wind farm," in *12th IET International Conference on AC and DC Power Transmission (ACDC 2016)*, May 2016, pp. 1–6. doi: 10.1049/cp.2016.0454.

[49] M. S. U. Khan, A. I. Maswood, K. Satpathi, M. T. Iqbal, and A. Tripathi, "Analysis of Brushless Wound Rotor Synchronous Generator with Unity Power Factor

Rectifier for Series Offshore DC Wind Power Collection," in *IECON 2018 - 44th Annual Conference of the IEEE Industrial Electronics Society*, Oct. 2018, pp. 1693–1698. doi: 10.1109/IECON.2018.8592721.

[50] P. Bresesti, W. L. Kling, R. L. Hendriks, and R. Vailati, "HVDC Connection of Offshore Wind Farms to the Transmission System," *IEEE Transactions on Energy Conversion*, vol. 22, no. 1, pp. 37–43, Mar. 2007, doi: 10.1109/TEC.2006.889624.

[51] Lena Max, "Energy Evaluation for DC/DC Converters in DC-Based Wind Farms," Chalmers University of Technology, Göteborg, Sweden, 2007. Accessed: Aug. 17, 2016. [Online]. Available: http://www.elforsk.se/Global/Vindforsk/Rapporter%20fran%20Vindforsk%20II/ V-204_LicLenaMax_webb.pdf

[52] H. J. Bahirat, B. A. Mork, and H. K. Høidalen, "Comparison of wind farm topologies for offshore applications," in *2012 IEEE Power and Energy Society General Meeting*, Jul. 2012, pp. 1–8. doi: 10.1109/PESGM.2012.6344689.

[53] P. Lakshmanan, J. Liang, and N. Jenkins, "Assessment of collection systems for HVDC connected offshore wind farms," *Electric Power Systems Research*, vol. 129, pp. 75–82, Dec. 2015, doi: 10.1016/j.epsr.2015.07.015.

[54] United States Tennesseealley Authority, "Wind Turbine Diagram." https://commons.wikimedia.org/wiki/File:Wind_turbine_diagram.svg

[55] E. Hau, *Wind turbines: fundamentals, technologies, application, economics*, 2nd [English] ed. Berlin ; New York: Springer, 2006.

[56] E. H. Camm *et al.*, "Characteristics of wind turbine generators for wind power plants," in *IEEE Power Energy Society General Meeting, 2009. PES '09*, Jul. 2009, pp. 1–5. doi: 10.1109/PES.2009.5275330.

[57] B. Fox and Engineering and Physical Sciences Research Council, *Wind power integration connection and system operational aspects*. London: Institution of Engineering and Technology, 2007. Accessed: Feb. 15, 2016. [Online]. Available: http://www.books24x7.com/marc.asp?bookid=10849

[58] Z. Zhang, A. Matveev, S. Ovrebo, R. Nilssen, and A. Nysveen, "State of the art in generator technology for offshore wind energy conversion systems," in *Electric Machines Drives Conference (IEMDC), 2011 IEEE International*, May 2011, pp. 1131–1136. doi: 10.1109/IEMDC.2011.5994760.

[59] P. A. Lynn, *Onshore and offshore wind energy: an introduction*. Chichester, West Sussex ; Hoboken, NJ: Wiley, 2012.

[60] J. P. S. Bala and M. C. P. Sandeberg, "DC connection of offshore wind power plants without platform," in *Paper presented at the 13th Wind Integration Workshop*, 2014, vol. 11, p. 13.

[61] "Compendium of all HVDC projects - Cigre." http://b4.cigre.org/Publications/Other-Documents/Compendium-of-all-HVDC-projects

[62] V. K. Sood, *HVDC and FACTS controllers: applications of static converters in power systems.* Boston: Kluwer Academic Publishers, 2004.

[63] "BritNed HVDC System - Cigre." http://b4.cigre.org/Publications/Other-Documents/Compendium-of-all-HVDC-projects/BritNed-HVDC-System

[64] J. Arrillaga, Y. H. Liu, and N. R. Watson, *Flexible power transmission: the HVDC options.* Chichester, England ; Hoboken, NJ: John Wiley, 2007.

[65] Randy Wachal and Manitoba HVDC Research Centre, "Voltage Source Converter (VSC) IEEE PES Winnipeg Tutorial," presented at the IEEE PES Winnipeg Tutorial, Winnipeg, Canada, Dec. 18, 2012.

[66] J. Zhao, K. Yeates, and Y. Han, "Analysis of high efficiency DC/DC converter processing partial input/output power," in *Control and Modeling for Power Electronics (COMPEL), 2013 IEEE 14th Workshop on*, 2013, pp. 1–8. Accessed: May 09, 2016. [Online]. Available: http://ieeexplore.ieee.org/xpls/abs_all.jsp?arnumber=6626440

[67] P. S. Shenoy, K. A. Kim, B. B. Johnson, and P. T. Krein, "Differential Power Processing for Increased Energy Production and Reliability of Photovoltaic Systems," *IEEE Transactions on Power Electronics*, vol. 28, no. 6, pp. 2968–2979, Jun. 2013, doi: 10.1109/TPEL.2012.2211082.

[68] C. Schaef and J. T. Stauth, "Efficient Voltage Regulation for Microprocessor Cores Stacked in Vertical Voltage Domains," *IEEE Transactions on Power Electronics*, vol. 31, no. 2, pp. 1795–1808, Feb. 2016, doi: 10.1109/TPEL.2015.2426572.

[69] C. Schaef, "Design and Control of High-Density DC-DC Converters for Cell Balancing and Low-Voltage Power Delivery Applications," Ph.D., Dartmouth College, United States -- New Hampshire, 2016. Accessed: May 24, 2017. [Online]. Available: http://search.proquest.com/docview/1827691014/abstract/86C683A8B8F8410DPQ/1

[70] H. Chen, H. Kim, R. Erickson, and D. Maksimović, "Electrified Automotive Powertrain Architecture Using Composite DC–DC Converters," *IEEE Transactions on Power Electronics*, vol. 32, no. 1, pp. 98–116, 2017.

[71] K. S. Hansen, R. J. Barthelmie, L. E. Jensen, and A. Sommer, "The impact of turbulence intensity and atmospheric stability on power deficits due to wind turbine wakes at Horns Rev wind farm: Power deficits in offshore wind farms," *Wind Energy*, vol. 15, no. 1, pp. 183–196, Jan. 2012, doi: 10.1002/we.512.

[72] M. H. Johnson and D. C. Aliprantis, "Analysis of Series-DC Offshore Wind Plants with Aerodynamic Wake Effects," *IEEE Transactions on Sustainable Energy*, vol. 8, no. 4, pp. 1706–1714, Oct. 2017, doi: 10.1109/TSTE.2017.2703879.

[73] N. Mohan, T. M. Undeland, and W. P. Robbins, *Power Electronics - Converters, Applications, and Design (3rd Edition)*. [Online]. Available: http://www.knovel.com/web/portal/browse/display?_EXT_KNOVEL_DISPLAY_bookid=3400

[74] S. M. Muyeen, Ed., *Wind Energy Conversion Systems*. London: Springer London, 2012. Accessed: Aug. 11, 2016. [Online]. Available: http://link.springer.com/10.1007/978-1-4471-2201-2

[75] B. Wu, Ed., *Power conversion and control of wind energy systems*. Piscataway, NJ : Hoboken, N.J: IEEE Press ; Wiley, 2011.

[76] Tor Inge Reigstad, "Direct Driven Permanent Magnet Synchronous Generators with Diode Rectifiers for Use in Offshore Wind Turbines," Norwegian University of Science and Technology, 2007. Accessed: Aug. 10, 2016. [Online]. Available: https://daim.idi.ntnu.no/masteroppgaver/003/3527/masteroppgave.pdf

[77] H. Li, Z. Chen, and H. Polinder, "Optimization of Multibrid Permanent-Magnet Wind Generator Systems," *IEEE Transactions on Energy Conversion*, vol. 24, no. 1, pp. 82–92, Mar. 2009, doi: 10.1109/TEC.2008.2005279.

[78] R. T. Naayagi, A. J. Forsyth, and R. Shuttleworth, "High-Power Bidirectional DC–DC Converter for Aerospace Applications," *IEEE Transactions on Power Electronics*, vol. 27, no. 11, pp. 4366–4379, Nov. 2012, doi: 10.1109/TPEL.2012.2184771.

[79] A. K. Jain and R. Ayyanar, "Pwm control of dual active bridge: Comprehensive analysis and experimental verification," *IEEE Transactions on Power Electronics*, vol. 26, no. 4, pp. 1215–1227, Apr. 2011, doi: 10.1109/TPEL.2010.2070519.

[80] A. D. Marzouk, S. Fournier-Bidoz, J. Yablecki, K. McLean, and O. Trescases, "Analysis of partial power processing distributed MPPT for a PV powered electric aircraft," in *2014 International Power Electronics Conference (IPEC-Hiroshima 2014 - ECCE ASIA)*, May 2014, pp. 3496–3502. doi: 10.1109/IPEC.2014.6869998.

[81] J. Jonkman, S. Butterfield, W. Musial, and G. Scott, "Definition of a 5-MW Reference Wind Turbine for Offshore System Development," NREL/TP-500-38060, 947422, Feb. 2009. doi: 10.2172/947422.

[82] L. Sethuraman and K. L. Dykes, "GeneratorSE: A Sizing Tool for Variable-Speed Wind Turbine Generators," NREL/TP--5000-66462, 1395455, Sep. 2017. doi: 10.2172/1395455.

[83] L. Sethuraman, M. Maness, and K. Dykes, "Optimized Generator Designs for the DTU 10-MW Offshore Wind Turbine using *GeneratorSE*," presented at the 35th Wind Energy Symposium, Grapevine, Texas, Jan. 2017. doi: 10.2514/6.2017-0922.

[84] J. D. Grunnet, M. Soltani, T. Knudsen, M. Kragelund, and T. Bak, "Aeolus Toolbox for Dynamics Wind Farm Model, Simulation and Control," p. 11.

[85] T. Bak *et al.*, "Baseline layout and design of a 0.8 GW reference wind farm in the North Sea: A reference wind farm," *Wind Energy*, vol. 20, no. 9, pp. 1665–1683, Sep. 2017, doi: 10.1002/we.2116.

[86] G. Guo *et al.*, "HB and FB MMC Based Onshore Converter in Series-Connected Offshore Wind Farm," *IEEE Transactions on Power Electronics*, vol. 35, no. 3, pp. 2646–2658, Mar. 2020, doi: 10.1109/TPEL.2019.2929689.

[87] Forsythe, G.E., Malcolm, M.A., and Moler, C.B., *Computer Methods for Mathematical Computations*. Prentice-Hall, 1976.

[88] V. Hussennether *et al.*, "Projects BorWin2 and HelWin1–large scale multilevel voltage-sourced converter technology for bundling of offshore windpower," Paris, France, 2012.

[89] "SimWindFarm Toolbox." http://www.ict-aeolus.eu/SimWindFarm/ (accessed Jul. 19, 2018).

[90] M. Dreidy, H. Mokhlis, and S. Mekhilef, "Inertia response and frequency control techniques for renewable energy sources: A review," *Renewable and Sustainable Energy Reviews*, vol. 69, pp. 144–155, Mar. 2017, doi: 10.1016/j.rser.2016.11.170.

[91] J. A. Mueller and J. W. Kimball, "An Improved Generalized Average Model of DC–DC Dual Active Bridge Converters," *IEEE Transactions on Power Electronics*, vol. 33, no. 11, pp. 9975–9988, Nov. 2018, doi: 10.1109/TPEL.2018.2797966.

[92] H. Zhang, D. Flórez, C. Saudemont, and F. Gruson, "Improved overvoltage limitation control approach of a DC series offshore wind farm based on MMC," in *2016 18th Mediterranean Electrotechnical Conference (MELECON)*, Apr. 2016, pp. 1–6. doi: 10.1109/MELCON.2016.7495355.

[93] Haibo Zhang, D. Flórez, C. Saudemont, and F. Gruson, "Control strategies of a dc based offshore wind farm with series connected collection grid," in *2016 IEEE*

International Energy Conference (ENERGYCON)*, Apr. 2016, pp. 1–6. doi: 10.1109/ENERGYCON.2016.7514062.

[94] J. Guo, X. Wang, Z. Zhang, H. Li, P. Lakshmanan, and J. Liang, "Energy curtailment analysis of offshore wind farms with DC series-parallel collection systems," in *2015 5th International Conference on Electric Utility Deregulation and Restructuring and Power Technologies (DRPT)*, Nov. 2015, pp. 2014–2019. doi: 10.1109/DRPT.2015.7432570.

[95] G. Shi, Z. Wang, M. Zhu, X. Cai, and L. Yao, "Variable speed control of series-connected DC wind turbines based on generalized dynamic model," in *2nd IET Renewable Power Generation Conference (RPG 2013)*, Sep. 2013, pp. 1–6. doi: 10.1049/cp.2013.1845.

[96] P. Lakshmanan, J. Guo, and J. Liang, "Energy curtailment of DC series–parallel connected offshore wind farms," *IET Renewable Power Generation*, vol. 12, no. 5, pp. 576–584, 2018, doi: 10.1049/iet-rpg.2017.0457.

[97] G. Shi, Jianwen Zhang, X. Cai, and M. Zhu, "Decoupling control of series-connected DC wind turbines with energy storage system for offshore DC wind farm," in *2016 IEEE 7th International Symposium on Power Electronics for Distributed Generation Systems (PEDG)*, Jun. 2016, pp. 1–6. doi: 10.1109/PEDG.2016.7527064.

[98] M. H. Rashid, *Power electronics handbook devices, circuits, and applications*. Burlington, MA: Butterworth-Heinemann, 2011. Accessed: May 11, 2015. [Online]. Available: http://app.knovel.com/web/toc.v/cid:kpPEHDCAE1/viewerType:toc/root_slug:power-electronics-handbook

[99] M. Pape and M. Kazerani, "An Offshore Wind Farm with DC Collection System Featuring Differential Power Processing," *IEEE Transactions on Energy Conversion*, Nov. 2019, doi: 10.1109/TEC.2019.2951331.

[100] M. Pape and M. Kazerani, "Turbine Startup and Shutdown in Wind Farms Featuring Partial Power Processing Converters," *IEEE Open Access Journal of Power and Energy*, vol. 7, pp. 254–264, 2020, doi: 10.1109/OAJPE.2020.3006352.

[101] G. Guo, K. Zha, J. Zhang, Z. Wang, F. Zhang, and J. Cao, "Grounding Fault in Series-Connection-Based Offshore Wind Farms: Fault Clearance," *IEEE Transactions on Power Electronics*, vol. 35, no. 9, pp. 9357–9367, Sep. 2020, doi: 10.1109/TPEL.2020.2971640.

[102] M. Pape and M. Kazerani, "On the Efficiency of Series-Connected Offshore DC Wind Farm Configurations," presented at the 2019 IEEE Energy Conversion Congress and Exposition (ECCE), Oct. 2019.

[103] A. D. Wright and L. J. Fingersh, "Advanced Control Design for Wind Turbines; Part I: Control Design, Implementation, and Initial Tests," NREL/TP-500-42437, 927269, Mar. 2008. doi: 10.2172/927269.

[104] J. M. Kos, J. P. Patrick, and K. I. Harner, "Multi-mode control system for wind turbines," US4193005A, Mar. 11, 1980 Accessed: Jul. 29, 2019. [Online]. Available: https://patents.google.com/patent/US4193005A/en

[105] M. H. Hansen and L. C. Henriksen, *Basic DTU Wind Energy controller*. DTU Wind Energy, 2013. Accessed: Apr. 30, 2020. [Online]. Available: https://orbit.dtu.dk/en/publications/basic-dtu-wind-energy-controller

[106] BVG Associates, "Wind farm costs - Guide to an offshore wind farm BVG Associates," *Guide to an offshore wind farm.* https://guidetoanoffshorewindfarm.com/wind-farm-costs (accessed Jan. 25, 2021).

[107] P. Djapic and G. Strbac, "Cost Benefit Methodology for Optimal Design of Offshore Transmission Systems," p. 86.

[108] B. Ragnarsson, G. Oddsson, R. Unnthorsson, and B. Hrafnkelsson, "Levelized Cost of Energy Analysis of a Wind Power Generation System at Búrfell in Iceland," *Energies*, vol. 8, no. 9, pp. 9464–9485, Sep. 2015, doi: 10.3390/en8099464.

[109] "BorWin 1 HVDC system - Cigre." http://b4.cigre.org/Publications/Other-Documents/Compendium-of-all-HVDC-projects/BorWin-1-HVDC-system

[110] W. Choi, K. M. Rho, and B. H. Cho, "Fundamental Duty Modulation of Dual-Active-Bridge Converter for Wide-Range Operation," *IEEE Transactions on Power Electronics*, vol. 31, no. 6, pp. 4048–4064, Jun. 2016, doi: 10.1109/TPEL.2015.2474135.

[111] F. Krismer and J. W. Kolar, "Accurate Power Loss Model Derivation of a High-Current Dual Active Bridge Converter for an Automotive Application," *IEEE Transactions on Industrial Electronics*, vol. 57, no. 3, pp. 881–891, Mar. 2010, doi: 10.1109/TIE.2009.2025284.

[112] G. Ortiz, J. Biela, and J.W. Kolar, "Optimized Design of Medium Frequency Transformers with High Isolation Requirements," Glendale, AZ, Nov. 2010, pp. 631–638. Accessed: Aug. 10, 2016. [Online]. Available: http://ieeexplore.ieee.org/ielx5/5661635/5674827/05675240.pdf?tp=&arnumber=5675240&isnumber=5674827

[113] National Electrical Manufacturers Association, "NEMA Premium Efficiency Transformer Program Guidelines - Program Description and Specification Document." May 01, 2010. Accessed: Sep. 26, 2017. [Online]. Available: https://www.nema.org/Policy/Energy/Efficiency/Documents/NEMA_Premium_Efficiency_Transformer_Product_Specifications.pdf

[114] IEEE Power Engineering Society, Substations Committee, and IEEE Standards Board, *IEEE recommended practice for determination of power losses in high-voltage direct-current (HVDC) converter stations*. New York, NY: Institute of Electrical and Electronics Engineers, 1992. Accessed: Aug. 23, 2017. [Online]. Available: http://books.google.com/books?id=5QRCAQAAIAAJ

[115] M. Pape and M. Kazerani, "A Generic Power Converter Sizing Framework for Series-Connected DC Offshore Wind Farms," *IEEE Transactions on Power Electronics*, pp. 1–1, 2021, doi: 10.1109/TPEL.2021.3106578.